National Institute of
Standards and Technology
U.S. Department of Commerce

NIST Technical Note 1552

Measurements to Support Public Safety Communications: Attenuation and Variability of 750 MHz Radio Wave Signals in Four Large Building Structures

William F. Young
Kate A. Remley
John Ladbury
Christopher L. Holloway
Chriss Grosvenor
Galen Koepke
Dennis Camell
Sander Floris
Wouter Numan
Andrea Garuti

NIST Technical Note 1552

Measurements to Support Public Safety Communications: Attenuation and Variability of 750 MHz Radio Wave Signals in Four Large Building Structures

William F. Young
Kate A. Remley
John Ladbury
Christopher L. Holloway
Chriss Grosvenor
Galen Koepke
Dennis Camell
Sander Floris
Wouter Numan
Andrea Garuti

Electromagnetics Division
National Institute of Standards and Technology
325 Broadway
Boulder, CO 80305

U.S. Department of Commerce
Gary Locke, Secretary

National Institute of Standards and Technology
Patrick D. Gallagher, Deputy Director

Certain commercial entities, equipment, or materials may be identified in this document in order to describe an experimental procedure or concept adequately. Such identification is not intended to imply recommendation or endorsement by the National Institute of Standards and Technology, nor is it intended to imply that the entities, materials, or equipment are necessarily the best available for the purpose.

National Institute of Standards and Technology Technical Note 1552
Natl. Inst. Stand. Technol. Tech. Note 1552, 133 pages (August 2009)
CODEN: NTNOEF

U.S. Government Printing Office
Washington: 2005

For sale by the Superintendent of Documents, U.S. Government Printing Office
Internet bookstore: gpo.gov Phone: 202-512-1800 Fax: 202-512-2250
Mail: Stop SSOP, Washington, DC 20402-0001

Contents

Executive Summary

This is the sixth in a series of NIST technical notes (TN) on propagation and detection of radio signals in large building structures (apartment complex, hotel, office buildings, sports stadium, shopping mall, etc). The first, second, and third NIST Tech Notes (NIST TN 1540, NIST TN 1541, and NIST TN 1542) described experiments related to radio propagation in a structure before, during, and after implosion. The next two Tech Notes (NIST TN 1545 and NIST TN 1546) focused exclusively on RF propagation into large buildings, with no implosion results. These reports are intended to give first responders and system designers a better understanding of what to expect from the radio-propagation environment in disaster situations. The overall goal of this project is to create a large, public-domain data set describing the attenuation and variability of radio signals in various building types in the public safety frequency bands.

Because the Federal Communications Commission (FCC) is in the process of auctioning spectrum between 764 MHz and 776 MHz for a new public-safety band, additional measurements were carried out in the 750 MHz frequency band in four different large building structures: a convention center, a high-rise office building, an apartment building, and a laboratory/office building. Three different types of signal measurements included (1) spectrum analyzer radio mapping, (2) narrowband communications receiver radio mapping, and (3) broadband synthetic-pulse measurements.

The first two measurement techniques using radio mapping provide the received signal strength at a fixed location outside the structure from a transmitter that is carried through the structure while emitting an unmodulated, 750 MHz radio signal within the structure. The synthetic pulse system provides stepped-frequency measurements of the received signal across a wide frequency band (100 MHz to 18 GHz for the measurements reported here). The phase of each received frequency component is synchronized with the excitation by the use of an optical fiber cable. Thus, we are able to reconstruct a short-pulse, time-domain waveform in post processing. The short pulse enables the study of the multipath in a given environment. Figures of merit such as the RMS delay spread may be calculated and used to quantify the time it takes for multipath reflections to decay below a given threshold level.

Similar median and standard deviation values are observed across most of the measurements in both the spectrum analyzer and receiver systems. For the spectrum analyzer, the median values for all four buildings calculated on data normalized to a direct line-of-sight path ranged from -25.1 dB to -98.5 dB, and the corresponding standard deviation values ranged from 6.8 dB to 30.1 dB. With the narrowband receiver, the median values ranged from -27.9 dB to -93.0 dB, and the standard deviation ranged from 9.0 dB to 29.1 dB. From the synthetic pulse measurements, the RMS delay spread results ranged from 15 ns to 450 ns at various test locations within the four buildings. In these measurements, the calculation of the RMS delay spread was not significantly affected by either (a) the directionality of antennas used in acquiring the data, or (b) the frequency bandwidth used in signal processing. The RMS delay values for measurements made in large open floor plan buildings were typically two to five times that of measurements in buildings with relatively narrow corridors.

The measured results presented here provide key parameters that describe the wireless propagation environment in representative responder environments. Measurement uncertainties

are not reported; however, end users of these data are interested primarily in large-scale behavior on the order of tens of decibels. Including instrumentation repeatability on the order of ±1 dB, expected for these measurements, is of little value in this case. We anticipate that improved channel descriptions provided by these measurements will be useful for assessing current and future wireless technology in emergency scenarios, for standards development, and for qualifying wireless equipment in environments such as those studied here.

Measurements to Support Public Safety Communications: Attenuation and Variability of 750 MHz Radio Wave Signals in Four Large Building Structures

William Young, Kate A. Remley, John Ladbury, Christopher L. Holloway,
Galen Koepke, Dennis Camell, Sander Floris, Wouter Numan, and Andrea Garuti

Electromagnetics Division
National Institute of Standards and Technology
325 Broadway, Boulder, CO 80305

In this report, we investigate radio communication problems faced by emergency responders (firefighters, police, and emergency medical personnel) in disaster situations. A fundamental challenge to radio communications into and out of large buildings is the strong attenuation of radio signals caused by losses and scattering in the building materials and structure, as well as the large amount of additional signal variability due to multipath that occurs throughout these large structures. We conducted measurements in four large building structures in an effort to quantify radio-signal attenuation and variability in scenarios encountered by emergency response organizations. We performed three different types of measurements. For the first two types of measurements, we carried RF transmitters throughout the structures and placed two different types of receiving systems outside the structures. One receiver type was based on a commercial, off-the-shelf spectrum analyzer, and the other on a NIST-developed narrowband communications receiver system having a high dynamic range. The transmitters were tuned to approximately 750 MHz. The third type of measurement tested the time-domain response of the channel at particular locations within the buildings using a synthetic-pulse measurement system. These measurements utilized the vector network analyzer with its output port tethered to the receive antenna by a fiber-optic cable to allow for reconstruction of the time-domain response of the propagation channel. This report summarizes the experiments performed in four large building structures. We describe the experiments, detail the measurement systems, show results from the data we collected, and discuss some of the propagation effects we observed.

Key words: attenuation; building penetration; building shielding; emergency responders; multipath; excess path loss; public-safety; radio communications; radio propagation experiments; RMS delay spread; signal variability; weak-signal detection; wireless system.

1. Introduction

When emergency responders enter large structures (apartment and office buildings, sports stadiums, stores, malls, hotels, convention centers, warehouses, etc.) radio communication to individuals on the outside is often impaired. Mobile-radio and cell-phone signal strength is reduced due to attenuation caused by propagation through the building materials and scattering by the building structural members [1-8]. Also, a large amount of signal variability may be encountered due to multipath reflections throughout the structures, which can cause signal degradation in communication systems.

Here, we report on a project conducted by the National Institute of Standards and Technology (NIST) to investigate the communications problems faced by emergency responders (firefighters, police, and emergency medical personnel) in disaster situations involving large building structures. The project was sponsored by the Department of Justice Community Oriented Policing Services (COPS) program. As part of this work, we are investigating the propagation and coupling of radio waves into large building structures in the 750 MHz frequency band. This band is currently of interest because the FCC is in the process of allocating spectrum between 764 MHz and 776 MHz for a nationwide, next-generation, interoperable broadband network for use by the public-safety community.

The experiments reported here were performed in four different large building structures and are the results of measurements of the reduction and variability of radio signal strength caused by propagation through the structures. These structures include a convention center, an apartment building, a 57-story office building, and an office corridor. This study includes data gathered using three different measurement techniques, each of which will be discussed below.

2. Signal Measurement Methods

Three different measurement techniques were used to capture the behavior of signals penetrating into structures in the 750 MHz frequency band from both time- and frequency-domain viewpoints. Use of various types of measurement provides more comprehensive insight into signal behavior in a given environment because some effects, such as the time it takes for multipath reflections to die out, are more pronounced in the time domain than in the frequency domain. While measurement uncertainties are not reported, end users of these data are interested primarily in large-scale behavior on the order of tens of decibels. Including uncertainties on the order of ±1 dB, expected for these measurements, is of little value when we are studying quantities that can vary by tens of decibels when changing by a fraction of a wavelength.

2.1. Radio Mapping Using a Spectrum Analyzer

The experiments performed here are referred to as "radio mapping." These experiments involved carrying transmitters (or radios) tuned to approximately 750 MHz throughout the four structures while recording the received signal at a fixed site located outside the building. A reference level was used to normalize the received power levels for these data. It consisted of a direct, unobstructed line-of-sight signal-strength measurement with the transmitters external to the different structures and in front of the receiving antennas. The separation distance between the transmitter and receiver antennas varied depending on the receive site location and the building, and these differences are reflected in the different reference levels. The purpose of the radio-mapping measurements was to investigate how signals at 750 MHz couple into the structures, and to determine the field-strength variability throughout the structures. A detailed description of the transmitters we used is provided in Section *2.1.1 Transmitters*, and a description of the measurement system and antennas are given in Section *2.1.2 Receiving Antenna and Measurement System*. The main procedures and components of the radio-mapping receive systems are shown in Figure 1. (See Appendix I)

2.1.1 Transmitters

The design requirements for the transmitters used in the experiments discussed here were that they should (1) transmit at 750 MHz, (2) operate continuously for several hours, and (3) be portable. To accomplish this, a commercially available off-the-shelf radio system was used. The radios could transmit continuously for 12 to 18 hours. Permission was granted to transmit from licensees at the frequency of interest, and the National Telecommunications and Information Administration (NTIA) frequency coordinator was also made aware of our transmissions.

2.1.2 Receiving Antenna and Measurement System

Each receive site used an omnidirectional discone antenna at a height between 2 and 3 meters. In addition, the receive sites contained a spectrum analyzer, a narrowband receiver, computers, and associated cabling. Not shown are the power generator and uninterruptible power supply (UPS) for powering the receive site.

As shown in Figure 1(c), the measurement system consisted of a portable spectrum analyzer and a laptop computer. The data collection process was automated by use of a graphical programming language. This software was designed to control the analyzer, and collect, process, and save data at the maximum throughput of the equipment. The software controlled the spectrum analyzer via an IEEE-488 interface bus.

The software was written to maximize throughput of the data collection process and to run for an undefined time interval. This was achieved by running parallel processes of collecting, processing, and saving the data for post-collection processing. The data were continuously read from the spectrum analyzer and stored in data buffers. These buffers were read and processed for each signal and displayed for operator viewing. The processed data were then stored in additional buffers to be re-sorted and saved to a file on disk.

The sampling rate of the complete measurement sequence was the major factor in how much spatial resolution we had during radio-mapping experiments (we also had some flexibility in our walking speed) and the time resolution for recording the signals. Software and parameter settings allowed experiment sampling rates of between 3 to 5 samples per second. The resolution bandwidth (RBW) is the key parameter in balancing the dynamic range versus the time between samples. These experiments used an RBW setting of approximately 500 Hz, which corresponded to an average spectrum analyzer noise floor in the range of -101 to -103 dBm. The data from the spectrum analyzer trace were saved in binary format to disk; they were then processed to extract the signals at the desired frequency. These results were put into a spreadsheet file and saved with other measurement information.

2.1.3 Spectrum Analyzer Data Processing

The spectrum analyzers collected the raw received power P^{rec}, but the subsequent processing was performed on the normalized received power P^{norm}. Only the samples collected during the actual walk-through were used; *i.e.,* the N samples were collected while the prescribed path was covered. The normalized power was calculated as

$$P^{norm}(\text{dB}) = P^{rec}(\text{dBm}) - P^{ref}(\text{dBm}), \tag{1}$$

where P^{ref} is the average of several samples obtained from the reference line-of-sight measurement.

The mean and standard deviation were found from

$$\mu = \frac{1}{N}\sum_{i=1}^{N} P_i^{norm} \ (\text{mW}), \tag{2}$$

and

$$s = \sqrt{\frac{1}{N-1}\sum_{i=1}^{N}\left(P_i^{norm}(\text{dB}) - \mu(\text{dB})\right)^2}\ (\text{dB}), \tag{3}$$

respectively. The median is the value that lies in the middle of the measured values. The calculation was as follows. First, the collected power samples were ordered by magnitude

$$\textit{Ordered power samples} = P_1^{norm} \le P_2^{norm} \ldots\ldots \le P_m^{norm} \le P_{m+1}^{norm} \le P_{m+2}^{norm} \ldots\ldots \le P_{N-1}^{norm} \le P_N^{norm}, \tag{4}$$

where N is the total number of samples, and m is the middle value if N is odd or m and $m+1$ are the middle two values if N is even. Then, the median value is

$$M = P_m^{norm}\ , \text{if } N \text{ is odd, and } M = [P_m^{norm} + P_{m+1}^{norm}] \div 2 \text{ if } N \text{ is even.} \tag{5}$$

The collected data were plotted as normalized power level versus the sample number. Note that the reference level was not always the strongest measured signal level. Also, in a few cases, a line-of-sight reference was not available, and an average of near-maximum values was utilized as the reference value instead. This difference in reference level does not affect the standard deviation of the received-signal level, but does impact the median and the mean.

Histograms were created by use of a bin width of 1 dB, based on normalized received-signal power levels. The empirical cumulative density function (CDF) was calculated from the same 1 dB bin widths in the following manner:

$$CDF(n) = \frac{\sum_{i=1}^{n} N_i}{N}, \tag{6}$$

where N_i is the sample count in bin i, n is the current bin, and N is the total number of samples. The normalized received-signal power levels were left in units of dB for the purposes of obtaining bin counts for the histograms.

Median, mean, and standard deviation statistics were all calculated based on the normalized values of the measured data. In the present work, the mean values were calculated based on the linear representation of the signal-power (*i.e.*, milliwatts as opposed to dBm) and then converted to a logarithmic value, while the standard deviation was calculated directly on the logarithmic quantities. This approach is commonly used as evident in the literature; for example [9-15]. In addition, use of the median values rather than the mean is illustrated in [10], [14], and [15]. Use of the median values helps prevent skewing of the centrality measure by outlying results. All resulting quantities are reported in decibels. Note that the median decibel value is the same regardless of whether it was calculated on the linear values and then converted to a decibel representation, or calculated directly on the decibel values.

2.2. Radio Mapping Using a Narrowband Communications Receiver

We also collected radio-mapping data using a narrowband communications receiver. This instrument, when combined with NIST-developed post-processing techniques, provides a high-dynamic-range measurement system that is affordable for most public safety organizations. Part of our intent was to demonstrate a user-friendly system that could be utilized by public-safety organizations to assess their own unique propagation environments. These data were collected at the same time the spectrum analyzer measurements described above were conducted. We carried the radio transmitter throughout the structures while recording the received signal at a fixed receive site, as illustrated in Figure 1(a)

The use and calibration of the communications receiver is described in more detail in other publications, (for example [16]), but is briefly summarized here for convenience. The system, shown in block diagram form in Figure 2(a), is based on a commercially available communications receiver and a personal computer (PC) sound card. The receiver is set to its "upper sideband" mode and is tuned to a frequency slightly below the carrier. In this way, the receiver acts as a frequency downconverter (Figure 2(b)), transforming the RF signal to baseband (audio) frequencies. The baseband signal is digitized by use of the sound card and is then post-processed and graphically displayed, letting the operator know whether a radio signal is present and what the level of that signal is.

We may observe the upper and lower sidebands of the down-converted signal by setting the receiver's center frequency to approximately the middle of its intermediate-frequency (IF) passband. For example, a signal with a 100 MHz carrier frequency may be measured by a receiver with a 3 kHz passband by tuning the receiver to 99.9985 MHz. In this case, the receiver will display the 100 MHz signal at 1.5 kHz (see Figure 2(c)).

The communications receiver has an automatic-gain-control (AGC) circuit whose function is to control the receiver gain to produce a constant-output-level signal regardless of the input power. The AGC circuit ensures the receiver circuitry operates in its optimal range. For the receiver we used, the AGC is active only for signals above a certain power threshold, and does not modify weak signals (on the order of received powers less than -90 dBm).

The purpose of the AGC circuit is to ensure that the receiver will demodulate at as high of a signal level as possible without overdriving the front end. It does this by altering the received-signal level to fit the best range for the demodulator. However, for received-power measurements the signal-level information is exactly what we are trying to determine. Hence, we need to undo the effects of the AGC modification of the signal level. To extract the signal-level information from the AGC-modified received signal, we monitor the DC voltage level that corresponds to the feedback of the AGC circuit. This voltage is directly related to the received-signal power and may be used to compensate for the AGC. We measure the DC voltage at the AGC jack on the back panel of the receiver with a digital multimeter having a recording feature. By synchronizing the recorded signal with the recorded AGC levels, we may determine the received signal's level during post-processing.

Once the post-processing steps are carried out, the average received-signal power for each location in a building may be measured. Note that the received power depends on the antenna and cabling used with the receiver. However, these effects may be calibrated out to display system-independent electric field level, enabling easy comparison of measurements from different measurement systems. In the measurements described here, we used an omnidirectional, discone antenna for frequencies below 1 GHz.

The communications receiver allows us to determine the range of received-power values that can be expected for a given structure. In the following section, we instead report on the received-signal level relative to a reference line-of-sight measurement, as described in the previous section. Similar to the spectrum analyzer data collected in earlier NIST Technical Notes [5, 7, 17, 18], these data are then processed in terms of mean, median, and standard deviation to provide channel models for network simulations. Because data are collected continuously, signal levels can easily be associated with features in the propagation environment. One advantage of the communications receiver over the spectrum analyzer is its increased dynamic range; that is, we can detect weaker signals with this system. Also, our receiver system has a lower cost compared to that of a spectrum analyzer.

2.3. Wideband Excess-Path-Loss Measurements and Time-Delay Spread

2.3.1 VNA-based measurement system

In addition to single-frequency radio-mapping measurements, we studied excess path loss over a wide frequency band at selected locations within each structure with the use of a vector network analyzer (VNA). Wideband excess path loss measurements provide measurements of received signal strength relative to the expected direct-path, free-space signal for a wide frequency band of 25 MHz to 18 GHz. Our wideband measurements provide a channel transfer function $H(f)$, and our excess-path-loss is then $H(f)^2/H_r(f)^2$, where $H_r(f)$ is the free-space reference. While this ratio provides the typical notion of excess-path-loss at a particular frequency, the VNA measurements provide a much richer data set; that is, they include both magnitude and phase information.

For the measurements reported here, we also present a subset of these measurements covering frequencies from 700 MHz to 800 MHz. The excess-path-loss measurements complement the narrowband, continuously recorded received power measured with the spectrum analyzer and

communications receiver discussed above by providing the received power over a wide range of frequencies but at only a few locations. Time-delay spread was calculated from the excess path loss data in post processing. Root-mean-square (RMS) delay spread is a figure of merit that gives an indication of the level of multipath interference encountered during the signal transmission.

For the wideband measurements, we used a synthetic-pulse, ultrawideband system based on a VNA [19]. Figure 3 is a diagram of the measurement system. Here the system is shown collecting a line-of-sight reference measurement. In practice, the transmitting and receiving antennas may be separated by significant distances, although they must remain tethered together by the fiber-optic link. Even though directional horn antennas are shown in Figure 3, omnidirectional antennas were also used in our measurements, offering insight into antenna systems most often used in public-safety applications.

In the synthetic-pulse system, the VNA acts as both transmitter and receiver. The transmitting section of the VNA steps over a wide range of frequencies a single frequency at a time. The transmitted signal is amplified and fed to a transmitting antenna, as shown in Figure 3. The received signal is picked up over the air by the receiving antenna and sent back to the VNA via a fiber-optic cable. The fiber-optic cable minimizes the loss and phase change that would be associated with RF coaxial cables between the receiving antenna and the transmitting antenna. We can then reconstruct the time-domain characteristics of the received signal in post-processing. Because the wideband transmitted signal corresponds to a short-duration pulse in the time domain, this system lets us measure the transmitted signal, modified by the propagation path, including losses and multipath reflections that the short-duration pulse experiences as it travels from the transmitter to the receiver. One advantage of this system is that it provides a high dynamic range relative to true time-domain-based measurement instruments.

To make the measurement, the vector network analyzer is first calibrated by use of standard techniques, where known impedance standards are measured. The calibration corrects for the systematic errors in the response of the fiber-optic system, amplifiers, and any other electronics used in the measurement. Then, a reference measurement is conducted where the transmitting and receiving antennas are placed to minimize reflections from the surrounding environment. This reference measurement allows us to verify that the system is operating correctly and allows us to determine the far-field response of the antennas and the cables that connect them to the measurement system. We compare this reference with the frequency response of the antennas measured separately in the laboratory environment at NIST. The antenna response is deconvolved in a post-processing step.

Once the measurements have been made, an additional post-processing step is carried out on the raw VNA measurements to provide clean frequency-domain and time-domain representations. Our optical links add a large amplitude oscillation to the measured signal, most likely due to the reflection off a fiber face. Because this oscillation occurs at a low frequency, we are able to suppress it by applying a high-pass filter, as shown in Figure 4.

Note that we use the phrase “excess path loss” in the context of vector-network-analyzer (VNA)-based measurements. Technically, we are measuring received signal relative to the transmitted signal, not path loss. Graphs of path loss would have positive ordinates and increase with

distance. However, the phrase "excess path loss" has a specific meaning in the measurement community and will be used throughout this report.

2.3.2 Excess path loss

Our wideband measurements provide a channel transfer function $H(f)$, where $H(f)$ typically is derived from the measured transmission parameter $S_{21}(f)$. To find the frequency-dependent path loss between the transmit and receive antennas, we first compute $|H(f)|^2/|H_r(f)|^2$, where $H_r(f)$ is a free-space reference made at a known distance d_r from the transmit antenna. The use of a ratio to find the path loss enables us to calibrate out the antenna response of the system.

Excess path loss is typically understood to be the loss seen to exceed that measured in a free-space environment [20]. To find the excess path loss, we reduce the total path loss by the expected free-space path loss over the overall separation distance d between the transmitting and receiving antennas. To do this, we divide the measurement of $|H(f)|^2$ by $(4\pi d/\lambda)^2$. Equivalently, we can multiply $|H(f)|^2/|H_r(f)|^2$ by $(d_R/d)^2$. The distance d may be measured or estimated from maps, depending on the environment. As stated earlier, this provides the loss in excess of that which would be measured at the same distance in free space. We note that communication engineers typically think of excess path loss as a single frequency or narrowband measurement. However, the VNA measurements provide a much richer data set because they include both magnitude and phase information over a broad frequency range.

As an example, Figure 5 shows the time-domain response for a reference measurement using a pair of dual-ridged-guide antennas separated by 3 m. In Figure 5(a), the reference measurement, transformed to the time domain, is shown with all environmental effects. The reference measurement is gated (windowed) from 20 ns to 32 ns to isolate the antenna response, which was determined previously in a separate measurement. The corresponding frequency-domain response in Figure 5(b) shows a noisier trace when environmental effects are included, compared with a smoother trace for isolated antennas. The gated response is what we would see if the antenna were measured in a free-space environment, free from environmental reflections.

2.3.3 RMS delay spread

Root-mean-square (RMS) delay spread is calculated from the power-delay profile of a measured signal [21-23]. Figure 6 shows the power-delay profile for a typical building propagation measurement. The peak level usually occurs when the signal arrives at the receiving antenna, although sometimes we see the signal build up gradually to the peak value and then fall off (the latter behavior is indicative of a reverberation environment). A common rule of thumb is to calculate the RMS delay spread by use of signals at least 10 dB above the noise floor of the measurement. For typical measurements, we define the maximum dynamic range to be about 40 dB below the peak value. However, for the measurement shown in Figure 6, we extended the window down to 70 dB below the peak value, because the RMS delay spread does not change appreciably due to the almost constant slope of the power decay curve. Note that the dynamic range value may change for low signal levels. The following equation is used to define the RMS delay spread, σ_τ:

$$RMS = \sigma_\tau = \sqrt{\overline{\tau^2} - \left(\overline{\tau}\right)^2}. \quad (5)$$

In (2), $\overline{\tau}$ is defined as the average of the power-delay profile in the defined dynamic range, and $\overline{\tau^2}$ is the variance of the power-delay profile.

2.3.4 Measurement set-up

For the measurements reported in this document, the VNA-based synthetic pulse system was set up with the following parameters. The initial output power was set to -15 dBm to -13 dBm, across all frequencies, but do not compensate for the frequency dependence of components such as cables and antennas. The gain of the amplifier and the optical link and the system losses ensured that the power level at the receiving port was not more than 0 dBm. An intermediate-frequency (IF) averaging bandwidth of around 1 kHz was used to average the received signal. We typically used 6401 or 16001 points per frequency band, depending on the frequency band. For these measurements, the high-band measurements (750 MHz to 18 GHz, using directional dual ridge guide (DRG) antennas) were taken by measuring 48003 points for a total of three bands. Only one band was required for the low-frequency measurements (25 MHz to 1.4 GHz with omnidirectional dicone antennas and 6401 points). The dwell time was approximately 25 μs per point.

3. Building Structure Descriptions and Experimental Set-up

This section briefly describes the four different large building structures characterized in these experiments and details the experimental set-up. These structures include a convention center, an apartment building, a laboratory building with multiple office corridors, and a 57-story office building. This study includes data gathered with the three different measurement techniques described above.

3.1 Colorado Convention Center, Denver, CO

The first structure was the Colorado Convention Center. This massive three-level structure is constructed of reinforced concrete, steel, and standard interior finish materials. The exterior of the building is a combination of glass, metal, and concrete. Figure 7 and Figure 8 show both internal and external photos of the convention center. As shown in Figure 9, the convention has a basement and two above-ground levels. An auditorium was located on the Speer Boulevard side of the second level. The third level consists of a large open space that can be subdivided by moveable walls. During the experiment, the space was open and nearly empty.

Our receive sites were located at the street level, which is level two. The three receive sites are depicted on Figure 9, denoted as RX1, RX2, and RX3, respectively. All three locations were located between 10 m to 15 m from the building at the closest point. Placement of these receive sites was intended to simulate the location of emergency response vehicles during a response scenario.

3.2 Republic Plaza, Denver, CO

The Republic Plaza is a 57-story office building in downtown Denver. The construction materials are a typical combination of concrete and steel. The interior building materials are a combination of metal framing, drywall, and trim, with stone finishes in the lobby. The exterior is a combination of glass and metal. Figure 10 and Figure 11 illustrate the exterior and interior of the building, respectively. In Figure 12, floor plans for several levels are shown.

In this experiment, the three receive sites, depicted in Figure 13 and Figure 14, varied substantially in distance from the building. Receive site 1 was located on the 17th Street side, approximately 10 m from the building; receive site 2 was located on the 16th Street side, approximately 25 m from the building; and finally, receive site 3 was located on the roof of a parking garage approximately 215 m southwest on Tremont Plaza. These locations were intended to simulate the locations of command vehicles in an emergency response scenario.

Light blue numbers enclosed by squares in Figure 15 show the locations within the building used in the synthetic pulse tests. Those locations that correspond to a radio-mapping test location shown in Figure 12 are indicated as well.

3.3 Apartment Building, Boulder, CO

This building was the 11-story Horizon West apartment building in Boulder, CO (Figure 16). The building is constructed of reinforced concrete, steel, and brick with standard interior finish materials. The building was fully furnished and occupied during the experiments. Measurements were performed during daytime hours and, as a result, people were moving throughout the building during the experiments. Figure 17 displays some internal photos of the apartment complex building.

For the radio-mapping experiments, two fixed receive sites (see Figure 18(a)) were assembled on the east side and north side of the apartment building, approximately 60 m and 80 m from the apartment building. During this experiment, the transmitters were carried throughout the building. Measurements were performed with the receive antennas polarized in the vertical direction. As the received signal was recorded, the location of the transmitters in the apartment building was also recorded. The locations of the synthetic pulse measurements are shown in Figure 18(b). These measurements were acquired approximately every 5 m, as indicated in the figure, on floors two and seven of the building.

3.4 NIST Laboratory, Boulder, CO

This building is the main building (referred to as the Radio Building) at the NIST laboratories in Boulder, CO. The building is constructed of reinforced concrete and is basically a four-story building. However, the building is built on a hillside, and consequently, some locations in the building are below ground level. Measurements were made on the 3rd floor hallway called "Wing 4", with the radio-mapping continuing in to "Wing 3" on the 3rd floor, and "Wing 5" on the

fourth floor. The measurements were performed during daytime hours and, as a result, people were moving throughout the building during the experiments.

For the radio-mapping experiments, two fixed receiving sites were assembled on the south side of the laboratory building (see Figure 19 and Figure 20). The receive site at Wing 4 was located on the loading dock, while the receive site at Wing 6 was approximately 10 m from the building. During these experiments, the transmitters were carried throughout the laboratory. Measurements were performed with the receiving antennas polarized in the vertical direction. As the received signals were recorded, the location of the transmitters in the buildings was also recorded.

Note that in Figure 20 there are two separate paths that were covered during the radio-mapping data collection process. Path one is reference location→A→B→C→D→C→B→A→reference location and path 2 is reference location→A→B→C2→B→A→reference location. The section between the reference location and position B is covered twice in both paths. Figure 21 shows the locations of the synthetic pulse measurements.

4. Experimental Results

In this section, the measured data (see Appendix II) are presented from several perspectives. Each subsection discusses a different set of building structure measurements. Plots of the radio-mapping data, normalized to a line-of-site (LOS) reference level, are provided for the frequency of 750 MHz, and the appropriate figures containing the data are indicated in the subsection discussions. Plots of the radio-mapping data statistics are also included. Discrete locations, where the synthetic-pulse measurements were collected, are marked on the appropriate figures. We provide excess path loss data covering the frequencies from 700 MHz to 800 MHz as well as the RMS delay spread associated with each location.

Descriptions of the experimental setups for the various sites were provided earlier in Section 2. Any unique features at a site that appear to impact the collected data are pointed out in the appropriate subsection. The common acronyms and abbreviations used in the labeling of the radio-mapping figures and statistical plots are provided in Table 1 below.

Table 1. Abbreviations used in Statistic Tables and Data Figures.

Acronym or Abbreviation	*Meaning*
Apmt.	apartment
Approx.	approximate
DRG	dual ridged guide horn
Fl., FL, fl.	floor
Freq.	frequency
LOS	line-of-sight
L*x*	level *x* or floor *x*, where *x* is a number
N.E.	northeast
N.W.	northwest
Ref.	reference signal level
RMS	root mean square

Std. dev.	standard deviation
S.E.	southeast
S.W.	southwest
Vert.	vertical

4.1 Colorado Convention Center: Measurement Results

The first set of results is from the Colorado Convention Center. All three types of measurements were performed. Due to high attenuation of the received signals caused by this structure, both the spectrum analyzer data and the synthetic pulse data were affected. The statistics from the spectrum analyzer data were skewed by data points below the noise floor of the instrument and only a few locations in the synthetic pulse tests provided enough signal strength to compute a meaningful RMS delay spread.

4.1.1. Radio Mapping

The spectrum analyzer radio mapping results for the Colorado Convention Center are shown in Figure 22 through Figure 24, and the narrowband receiver radio mapping results are shown in Figure 26 through Figure 28. In all six plots, the line-of-sight reference signal is clearly seen by the distinct largest peaks in each plot. The features of the results from the two different measurement systems track well at each of the receive sites. The narrowband receiver results cover a broader range of signal levels. We see that spectrum analyzer results are at the noise floor across much of the collected data. However, the narrowband receiver data provides useful results down to approximately 15 dB below the noise floor of the spectrum analyzer system.

Figure 25 and Figure 29 show histograms and empirical CDFs from the Colorado Convention Center for data from the spectrum analyzer and narrowband receiver systems, respectively. One of the most notable features is the step function behavior of the spectrum analyzer CDFs due to the amount of time the signal was below the noise floor level for that measurement system. The results from the narrowband receiver are probably a more accurate representation of the propagation effects due to the increased dynamic range. The high bin count on two of three narrowband receiver histograms is due to the hard noise floor limit imposed during the data processing. In other words, the received values below a certain level are all given the same value. This affects the median value but has little effect on the mean. Note that we need to include these points because they represent deep fades.

4.1.2 Synthetic Pulse System

The VNA measurements were carried out at the positions indicated in Figure 9, with the VNA located at receive site 2 (RX2). The VNA results are limited in number due to the significant signal attenuation experienced while moving into the center of the building. Two different antenna configurations were used for the measurements; a directional dual ridged guide horn (DRG) to DRG and a DRG to omnidirectional "tophat" antenna. We also considered two different frequency bands in data processing: 700 MHz to 800 MHz and 700 MHz to 18 GHz. The excess path loss plots for these four antenna and frequency band combinations are shown in Figures 30 through 33.

We computed the RMS delay spread from the 700 MHz to 800 MHz excess path loss data. When the dynamic range falls below a certain threshold, the accuracy of the computed RMS delay spread value decreases. (See Figure 6 for an explanation of the dynamic range.) The RMS delay spread is nearly the same across the four combinations of measurements.

In Figure 34, we see the RMS delay spread plotted for each test position, where the positions illustrated in Figure 9 are located progressively deeper into the Convention Center. Past position six, the dynamic range was insufficient to allow an accurate calculation of the RMS delay spread. Positions one through four were measurements made in a large, open, two-story lobby of the convention center. Here, we see RMS delay spreads of between 100 ns and 150 ns. These values increase sharply (up to a maximum of 200 ns) once the receiver turns the corner and proceeds down a large hallway.

4.2 Republic Plaza Measurement Results

The second set of measurement results is from the 57-story Republic Plaza Building in Denver. All three types of measurements were performed. Because there was less attenuation, we were able to calculate the RMS delay spread at more positions than we could in the Colorado Convention Center.

4.2.1. Radio Mapping

The spectrum analyzer radio mapping results for the Republic Plaza Building are shown in Figure 35 through Figure 37, and the narrowband receiver radio mapping results are shown in Figure 39 through Figure 41. In the plots for receive sites two and three, the line-of-sight is clearly seen by the distinct largest peaks in each plot. The basic structure of the two types of measurements track well at each of the receive sites, and the additional free space path loss for receive site three is evident in the approximately 18 dB reduction in the reference value as compared to values obtained at receive sites one and two. As in the Convention Center measurements, the narrowband receiver results cover a broader signal range; however, the most notable difference in the signal range covered by spectrum analyzer versus the narrowband receiver occurs at site three. This is due to the fact that site three was located much further from the building than either site one or two.

Figure 38 and Figure 42 show the histograms and empirical CDFs of the radio mapping measurements from the Republic Plaza for the spectrum analyzer and narrowband receiver systems, respectively. The basic shapes of the empirical CDFs are quite similar for the first two sites, (see Figure 38 (a), (b) and Figure 42 (a), (b)). The spectrum analyzer empirical CDF for site three exhibits a much more rapid rise due to the high number of data points at the noise floor of the measurement system. The histograms for the narrowband receiver all demonstrate a hard noise floor by the high count in the last bin. As discussed in the Colorado Convention Center section, hard noise floor does not significantly affect the mean value, but the data are important because they represent very deep fades in the signal level.

4.2.2 Synthetic Pulse System

Synthetic pulse measurements were collected at positions marked in Figure 15, with the VNA located at receive site 1 (RX1) in Figure 14. We collected excess path loss measurements over the frequency bands 200 MHz to 180 MHz and 700 MHz to 18 GHz. For the lower-frequency measurements we used omnidirectional discone antennas, and for the higher-frequency measurements we used DRG antennas.

We also calculated the RMS delay spread from the excess path loss data. Twenty-one positions within the building were tested, and eighteen of those positions had sufficient dynamic range to provide useful results. Figures 43 to Figure 54 show the excess path loss, and Figure 55 shows the calculated RMS delay spread. In cases where the dynamic range fell below 20 dB, no RMS delay spread was calculated.

In some cases, the 700 MHz to 800 MHz frequency band data did not exhibit a dynamic range greater than 20 dB. To estimate the RMS delay spread over this frequency band, we calculated the RMS delay spread for frequency bands where we did have more than 20 dB of dynamic range and compared these to what we calculated between 700 MHz and 800 MHz. These frequency bands were 200 MHz to 1.8 GHz, and 200 MHz to 600 MHz. We also included the RMS delay spread in the 900 MHz ISM band, with calculation limits between 865 MHz and 965 MHz. As shown in Figure 55, the computed RMS delay spread values for the four frequency bands track quite well across the eighteen positions, and suggests that results for the other two frequency bands provide good estimates of the RMS delay spread for the 700 MHz to 800 MHz band.

Figure 55 shows that the RMS delay spread is lowest at the landing of each floor, where a window was located. The delay spread does moderately increase as the height increases (from around 50 ns on floor 1 to around 150 ns on the highest floor). However, when the measurements were made deeper within the building on floors 5 and 10 (positions 9, 10, and 16), the RMS delay spread increased significantly (to between 300 and 450 ns, depending on the location and the frequency band used to calculate the RMS delay spread).

4.3 Boulder, CO Apartment Building Results

The third set of results is from the 11-story Horizon West apartment building in Boulder, Colorado. This building has been used in other experiments, with results for radio mapping in other frequency bands found in [18] and synthetic-pulse measurements found in [8].

4.3.1. Radio Mapping

The radio-mapping experiment included sixty-three locations throughout the building, with a brief description of these locations provided in Table 4. The spectrum analyzer radio mapping results for the apartment building are shown in Figure 56 and Figure 57, and the narrowband receiver radio mapping results are shown in Figure 59 and Figure 60. Both sets of figures illustrate a similar structure, with peaks at the same positions. Note that some difference in locations is attributable to the manual process by which the positions are recorded during the

experiment. In both cases the signal is well above the noise floor, which is evident in the histograms shown in Figure 58 and Figure 61. The empirical CDFs are quite similar and are consistent with a Gaussian shaped probability density function.

The overall spread, minimum to maximum, of the measured signals is approximately 60 dB for both receive sites and both measurement systems. Also, the median and mean values are at least 15 dB closer than the two other building measurements, primarily because the received signals are well above the noise floor. Even when the transmitters were in the elevator, (locations 61 to 62 on the radio-mapping plots), the received signal did not experience a deep fade.

The difference in relative proximity to the building for receive site one and two at Horizon West is evident by the difference in the reference levels of approximately 14 dB for both measurement systems. Generally, the Horizon West apartment building represented a fairly benign propagation environment, as the measured signals were typically well above the noise floor.

4.3.2 Synthetic Pulse System

Synthetic pulse measurements for this building were carried out previously, and the results, reproduced from TN 1546 [8], can be found in Figures 62 through 65. The RMS delay spread is summarized in Figure 66. While these results are not calculated specifically across the 700 MHz to 800 MHz band, as demonstrated by the earlier results, the expected behavior should be quite similar even when considering a much wider bandwidth, especially because the signal energy is greatly reduced at the higher frequencies.

The RMS delay spread values at the apartment building are all in a range below 50 ns. This is in contrast to those from the other two buildings, which were more massive and had longer propagation delays between reflections.

4.4 NIST Boulder Laboratory Results

The fourth set of data is from the NIST Laboratory in Boulder, CO. In the radio mapping experiments, the transmitters were carried over two different paths, shown in Figure 20. Path I started at the reference location, and proceeded to position D before returning to the reference location. Location C2 was not included in this path. Path II again started at the reference location, proceeded to position C2, and then returned to the reference location. Locations C and D were not covered in this second path. Unlike the other three structures, data were collected for a repeated walk over each path. Thus, the combination of two collection sites, two walking paths, and a repeat measurement for each path created four independent data sets for both the spectrum analyzer and narrowband receiver measurement setups. The repeated walk provides an indication of the repeatability. The statistics are computed on the data collected between the location A points marked in the figures. These points are clearly marked by the on/off transition in the radio-mapping plots. The reference value is taken as the maximum value across all the collected data, so for site one, this maximum occurs near location A, and for site 2, the maximum occurs at the reference location indicated in Figure 20. In both cases, the transmitter has line-of-sight communications with the receive site, which is consistent with the experimental setup and data-processing approach used for the other three buildings.

4.4.1. Radio Mapping

The spectrum analyzer results collected at the Wing 4 (site 1) and Wing 6 (site 2) receive locations are shown in Figure 67 and Figure 68, respectively, with the repeated Path I walk results shown for sites 1 and 2 shown in Figure 70 and Figure 71 respectively. The histogram and empirical CDF plots corresponding to these two walks are shown in Figure 69 and Figure 72, respectively. The power profile results in Figure 67 and 70 are quite similar, as are the profile results in Figure 68 and Figure 71. In addition, the shape of the histograms and empirical CDFs in Figure 69(a) and (b) compare well to those in Figure 72(a) and (b). However, the calculated statistics indicate differences for the receive site one case, with the first walk-through resulting in a median value that is 11.8 dB lower than the repeated walk-through.

The difference between these repeat walk-throughs is not due to the repeatability of the instrumentation: it occurs because of small-scale fading, a phenomenon caused by constructive and destructive interfering signal reflections from environmental features such as walls, floors, and metallic objects. Small-signal fading can introduce signal level variations of several decibels even for measurements made nominally along the same path because it is very position dependent. However, the large-scale path loss dependence of the path (if the small-scale fading was smoothed out) represented by the statistics presented here remains consistent. The mean and the standard deviation are 3.1 dB and 1.3 dB lower for the first walk-through, respectively. Note that the reference level is within 0.1 dB for the two walks, so the statistics are not being skewed by normalization with respect to the reference level. The site two cases exhibit a median difference of 1.7 dB between the two walks of the first path, and difference of 0.9 dB and 0.2 dB for the mean and standard deviation, respectively. The reference level differs by 1.2 dB.

Path II spectrum analyzer power profiles for the first walk for sites one and two are given in Figure 73 and Figure 74, respectively, and the repeat walk results are shown in Figure 76 and Figure 77 for sites one and two, respectively. The corresponding histogram and empirical PDF plots for the two walks are shown in Figure 75 and Figure 78, respectively. The site one profiles (Figure 73 and Figure 76), indicate some small differences at the first pass though location B, and the histogram and empirical CDF plots (Figure 75(a) and Figure 78(a)) show some 20 differences as well. The mean value is 2.4 dB lower for the first walk, but the median is 1.8 dB lower for the second walk. The standard deviation is 1.7 dB less for the first walk, and the reference level is 3.1 dB lower for the second walk. The site two profiles for the two walks (Figure 76 and Figure 77) are quite similar, and the histogram and empirical CDF plots (Figure 75(b) and Figure 78(b)) exhibit similar shapes. The difference in median, mean, standard deviation, and reference level values is 0.8 dB, 2.5 dB, 1.5 dB and 0.2 dB respectively. As with the Path I results, the site 2 results track closely between repeated walks.

Figure 79 and Figure 80 show the received power profile for the narrowband receiver at sites one and two, respectively, for the first path (Path I) and the first walk. Figure 82 and Figure 83 show the narrowband receiver results at sites one and two, respectively, for the repeated walk of Path I. The corresponding histogram and empirical CDF plots for the two walks are shown in Figure 81 and Figure 84. All the corresponding power profile, histogram, and empirical CDF plots for the two walks of Path I are quite similar. A noticeable difference occurs in the statistics for site one, where the median, mean and standard deviation differ by 7.4 dB, 7.1 dB, and 1.0 dB,

respectively (see Figure 81(a) and Figure 84(a)). However, the reference level at site 1 is almost identical for the two walks of Path I. This behavior is consistent with the spectrum analyzer Path I results discussed earlier in this section. Site 2 statistics indicate a difference of 0.8 dB, 2.5 dB, 0.2 dB, and 1.5 dB in the median, mean, standard deviation, and reference levels (see Figure 81(b) and Figure 84(b)). These relatively small differences are consistent with the spectrum analyzer results discussed previously.

Path II narrowband profiles of data collected at sites one and two for the first walk are given in Figure 85 and Figure 86, respectively, and the profiles for the second walk of Path II are given in Figure 88 and Figure 89, respectively. The corresponding histogram and empirical CDF plots for the two walks of Path II are shown in Figure 87 and Figure 90. All the corresponding narrowband received power profiles match well between repeated walks, (for example, compare Figures 85 to 88, and Figures 86 to 89). An important feature in all four of these plots is that the signal level is typically above the noise floor. This is illustrated clearly in the histogram and empirical CDF plots of Figure 87 and Figure 90. While the general shape of the corresponding histogram and empirical CDF results in Figure 87(a) and Figure 90(a) are quite similar, the mean and standard deviation values differ by 5.9 dB and 3.0 dB, respectively. The median and reference levels differ by 1.9 dB and 0.4 dB, respectively, in Figure 87(a) and Figure 90(a). Histogram and empirical CDF results for receive site two (Figure 87(b) and Figure 90(b)) are similar in shape, and the differences in median, mean, standard deviation, and reference levels are 3.4 dB, 1.2 dB, 1.5 dB, and 0 dB, respectively.

4.4.2 Synthetic Pulse System

We also carried out measurements in the Wing 4 corridor with the VNA-based synthetic-pulse measurement system described in Section 2.3. Measurements were made at points approximately every 15.25 meters (50 feet) along the corridor as shown in Figure 21. The transmitting antenna was located either at site one at the end of Wing 4 or at site two, outside the building by the end of Wing 6, as shown earlier in Figure 19 and Figure 20. The receiving antenna was moved along the corridor to the locations marked in Figure 21. In this report, we discuss the building penetration results; i.e., the transmitting antenna is located at site two. Additional results with the transmitting antenna at site one are found in [8].

We collected data covering two frequency bands. For the lower-frequency band (25 MHz to 1.3 GHz), we used omnidirectional antennas, as would be used by most emergency response companies. For the higher-frequency band (750 MHz to 18 GHz) we used both omnidirectional antennas and a set of directional horn antennas. Since this report is focused on 750 MHz, we present the complete lower frequency band here (Figure 91 through Figure 97), while the upper frequency band data are available in [8]. However, we include a plot that compares the omnidirectional results for both the lower and upper bands (Figure 98).

In Figure 91, the top plot shows the excess path loss with the receiver located at position 1 in Figure 21. The received signal is greater than the system noise across the frequency band, and thus allows computation of a RMS delay spread. In contrast, note that by positions 9 and 10, (Figure 95), the received signal is less than the system noise across much of the frequency band.

Thus, only the first eight positions exhibit sufficient power across the frequency band to calculate the RMS delay spread.

The RMS delay spread calculated from the VNA measurements with the transmitter at site two is summarized in Figure 98. Two different measurement configurations are shown covering different frequency ranges, both with omnidirectional antennas. The lower frequency band indicates a range of 43 ns - 85 ns, while the upper frequency band shows a range of 31 ns - 79 ns. The greatest difference between the two frequency bands (approximately 25 ns) occurs at position 4.

5. Summary of Results and Conclusion

Here we summarize the results from all four buildings to provide a straightforward comparison. Table 2 lists the computed statistics for the spectrum analyzer and narrowband receiver data. Figures 99 through 101 provide graphical representations of these data. The index column in Table 2 is used in the figures that follow, where several aspects of the data are compared. Note that index number pairs of 9 and 10, 11 and 12, 13 and 14, and 15 and 16 represent repeated walks over the same path. In addition, these four pairs are all from the NIST laboratory building.

Table 2. Aggregate statistics from the radio-mapping experiments for the spectrum analyzer (SA#) and narrowband radio receiver (R#) tests.

Experiment	Index	Median (dB)	Mean (dB)	Std. Dev. (dB)	Ref. (dBm)
Spectrum Analyzer Tests					
Colorado Convention Center SA1	1	-52.2	-22.3	9.0	-30.9
Colorado Convention Center SA2	2	-57.4	-23.2	10.7	-26.5
Colorado Convention Center SA3	3	-44.2	-23.4	6.8	-39.4
Republic Plaza SA1	4	-65.2	-23.2	20.0	-33.7
Republic Plaza SA2	5	-63.1	-20.3	20.0	-32.3
Republic Plaza SA3	6	-46.5	-18.2	11.8	-50.2
Horizon West SA1	7	-29.5	-17.7	11.0	-34.5
Horizon West SA2	8	-25.1	-18.3	9.9	-49.0
NIST Laboratory SA1, Path I, Walk 1	9	-98.5	-19.8	28.8	-11.5
NIST Laboratory SA1, Path I, Walk 2	10	-86.7	-16.7	30.1	-11.6
NIST Laboratory SA2, Path I, Walk 1	11	-61.5	-39.6	9.5	-40.7
NIST Laboratory SA2, Path I, Walk 2	12	-63.2	-38.2	11.3	-41.9
NIST Laboratory SA1, Path II, Walk 1	13	-62.8	-18.4	25.2	-11.6
NIST Laboratory SA1, Path II, Walk 2	14	-64.6	-16.0	26.9	-14.7
NIST Laboratory SA2, Path II, Walk 1	15	-61.1	-39.8	10.9	-41.6
NIST Laboratory SA2, Path II, Walk 2	16	-61.9	-37.3	12.4	-41.8
Narrowband Receiver Tests					
Colorado Convention Center R1	1	-75.0	-22.6	21.0	-26.0
Colorado Convention Center R2	2	-77.7	-25.1	19.8	-22.1
Colorado Convention Center R3	3	-68.2	-26.1	20.2	-37.2
Republic Plaza R1	4	-68.3	-26.0	20.3	-29.3
Republic Plaza R2	5	-60.0	-18.9	21.5	-32.7
Republic Plaza R3	6	-49.3	-19.9	17.8	-49.8
Horizon West R1	7	-33.2	-20.6	10.8	-31.1
Horizon West R2	8	-27.9	-19.3	9.0	-45.2
NIST Laboratory R1, Path I, Walk 1	9	-93.0	-17.4	29.1	-19.4
NIST Laboratory R1, Path I, Walk 2	10	-85.6	-24.5	28.1	-19.4
NIST Laboratory R2, Path I, Walk 1	11	-71.5	-39.9	16.5	-34.8
NIST Laboratory R2, Path I, Walk 2	12	-70.7	-42.4	16.3	-33.3
NIST Laboratory R1, Path II, Walk 1	13	-64.0	-21.8	23.9	-19.8
NIST Laboratory R1, Path II, Walk 2	14	-65.9	-15.9	26.9	-19.4
NIST Laboratory R2, Path II, Walk 1	15	-62.2	-39.1	15.2	-33.0
NIST Laboratory R2, Path II, Walk 2	16	-65.6	-37.8	16.7	-33.0

Figure 99 plots the standard deviation for the two radio-mapping systems versus all the receive sites. Excluding the Colorado Convention Center results, the standard deviation values are within 7 dB for the spectrum analyzer and narrowband measurements when compared on a site-by-site basis. In addition, excluding the results from receive site 3 at Republic Plaza and the first results for Path I, receive site 2 at the NIST Laboratory, leaves a maximum difference of 5 dB in the standard deviation between the two systems. Perhaps more importantly, in Figure 100, we see a large difference between the median and mean values. The Horizon West median and mean are

within 12.6 dB for both sites. However, the Colorado Convention Center and the Republic Plaza results show a difference between the mean and the median ranging from 20.8 dB to 52.6 dB. The NIST Boulder Laboratory shows differences in the median and mean ranging from 21.3 dB to 78.7 dB. These wide ranges illustrate the difference between calculating statistics using logarithmic quantities (the median was selected as the middle value in dB) and the mean (which was calculated as the mean of the normalized linear power and then converted to dB). The former gives a better indication of the differences in average received power for the different sites and different receiver types. Note that the median does not change whether computed on the logarithmic or linear power quantities.

The mean received signal strengths shown in Figure 100 indicate similar values between measurement systems and across all sites, with the only significant difference occurring at the NIST building, site 2. This is due the dominance of the values near 0 dB (*i.e.*, the normalized reference level) on the calculation of the mean using linear values. A few values near 0 dB can skew the mean due to the weight of those values when the mean is computed. Excluding the NIST building, the maximum site-by-site difference for the spectrum analyzer is 2.9 dB (Horizon West, site 1). The mean values of the measurements taken at the NIST building, site 2, are approximately 20 dB lower than the mean results for the NIST building, site one. In addition, the mean values of the measurements taken at NIST, site 2, are 15 dB to 20 dB lower than the mean of all other receive sites for the three other buildings. This is due to the fact that the processed data for the NIST building, site 2, only included data that were approximately 20 dB below the reference value (normalized to 0 dB). From a comparison standpoint, the NIST building, site 1, results (*i.e.,* experiment index numbers 9, 10, 13, and 14) demonstrate mean behavior similar to that of the other three buildings.

Figure 101 plots the normalized median value added to the reference value that was used to normalize the data for each site and building combination (The reference value is measured when the transmitter is located at the reference location.) The results shown in Figure 101approximate the average power we would expect to receive when using a system with similar performance characteristics (receiver sensitivity and antenna systems) and location at the respective receive sites; for example, an emergency response vehicle located at the receive sites. All the statistics are computed by use of data normalized by the corresponding reference value. The dynamic range of the spectrum analyzer measurement system was extended for cases 4 through 16 by narrowing the search bandwidth. Due to the similarity in dynamic ranges, the difference between the two measurement systems is now less than 6 dB for cases 4 through 16.

The results presented in this report support a few observations. First, in comparing the two measurement techniques used in the radio mapping, we observe similar statistical results when the measured signal is significantly above the noise floor. For example, the statistics are least similar at the Colorado Convention Center and most similar for Horizon West. At the Colorado Convention Center, we see the spectrum analyzer results influenced by the increased number of samples in the noise as compared to the radio receiver. With respect to the uniqueness of the structures, the mean value does not indicate significant differences between buildings, or even the receive site locations at a particular building. The median values suggest greater difference in building behavior, and between the receive sites at a particular building. However, the median for the narrowband receive data may be skewed by the calibration issue described in Section

4.1.1., and by the hard noise floor. A smaller standard deviation value indicates less signal variability.

Aggregate results for the synthetic-pulse are provided in Table 3 below and Figure 102. Table 3 and Figure 102 shows that the calculation of the RMS delay spread is not significantly affected by either (a) the pair of antennas used in capturing the data, or (b) the frequency band used in the processing. Both of these factors allow more flexibility in the measurement process.

As mentioned in Section 4, we can directly trace the changes in the RMS delay spread to physical features in the structures. An interesting overall observation is that the RMS delay spread was two to five times larger in the convention center and the skyscraper, as compared to the apartment and the NIST laboratory/office buildings. The skyscraper and the convention center are both physically larger buildings than the apartment and NIST buildings. Also, for both the apartment and the NIST laboratory/office building, most of the measurements were made in a hallway or corridor, while many of the measurements for the skyscraper and the convention center were made in open areas.

Table 3. Aggregate RMS delay spread values and statistics; all values are in nanoseconds (ns).

Building	Colorado Convention Center				Republic Plaza				Horizon West		NIST Lab	
Comments	DRG-Tophat Antennas		DRG-DRG Antennas						Flr. 2	Flr. 7		
Index for Figure plot →	1	2	3	4	5	6	7	8	9	10	11	12
	Frequency bands used in RMS calculation											
Position Index (Location in building)	700-800 MHz	700-18000 MHz	700-800 MHz	700-18000 MHz	200-600 MHz	700-800 MHz	200-18000 MHz	865-965 MHz	1000-18000 MHz	1000-18000 MHz	25 -1300 MHz	750 - 18000 MHz
0									24.1	32.4		
1	70.4	94.7	72.3	88.3	62.0	65.2	64.7	70.1	21.4	23.7	44.2	47.9
2	67.8	86.6	90.2	100.1	56.8	63.5	56.7	60.6	16.7	24.3	44.2	32.7
3	104.5	113.3	123.4	94.6	66.9	76.9	72.2	103.4	15.3	14.5	53.7	64.2
4	147.2	170.4	145.0	158.7	89.8	134.9	96.9	136.0	24.9	35.9	51.0	76.2
5	194.0				89.6	108.3	97.0	113.8	48.2	44.2	73.6	76.9
6					74.6	110.4	74.6	107.7	30.7	37.4	75.3	78.7
7					73.9	140.3	79.6	148.1	36.3	40.8	71.4	64.7
8					96.1	143.5	94.4	165.6	31.2	38.8	84.8	63.6
9					326.0	416.7	344.7	446.5	30.4	30.5		
10					384.1	235.9	376.6	405.6	31.7	31.0		
11					148.5	184.0	146.4	206.9	39.4	34.8		
12					153.6	244.4	140.6	232.6	38.0	36.8		
13					131.6	209.8	128.1	222.3	20.8			
14					172.3	235.2	182.8	246.3				
15					181.7	292.6	171.3	277.0				
16					303.6	409.4	285.4	350.6				
17					198.5	288.7	198.7	303.0				
18					158.2	215.2	174.8	254.9				
Mean	116.8	116.3	107.7	110.4	153.8	198.6	154.8	213.9	29.2	32.7	62.3	63.1
Median	104.5	104.0	106.8	97.3	140.0	196.9	134.4	214.6	30.6	34.8	62.6	64.5
Minimum	67.8	86.6	72.3	88.3	56.8	63.5	56.7	60.6	15.3	14.5	44.2	32.7
Maximum	194.0	170.4	145.0	158.7	384.1	416.7	376.6	446.5	48.2	44.2	84.8	78.7

Disclaimer: Mention of any company names serves only for identification, and does not constitute or imply endorsement of such a company or of its products.

This work was sponsored by the U.S. Department of Justice through the Public Safety Communications Research Lab of NIST. We thank members of the technical staff of the Electromagnetics Division 818, who collected the measurements, and Dennis Friday, Mike Kelley, Perry Wilson, and Dereck Orr for programmatic support.

6. References

[1] Statement of Requirements: Background on Public Safety Wireless Communications, The SAFECOM Program, Department of Homeland Security, Vol. 1, March 10, 2004.

[2] M. Worrell and A. MacFarlane, Phoenix Fire Department Radio System Safety Project, Phoenix Fire Dept. Final Report, Oct. 8, 2004, http://www.ci.phoenix.az.us/FIRE/radioreport.pdf

[3] 9/11 Commission Report, National Commission on Terrorist Attacks Upon the United States, 2004.

[4] Final Report for September 11, 2001 New York World Trade Center terrorist attack, Wireless Emergency Response Team (WERT), Oct. 2001.

[5] C.L. Holloway, G. Koepke, D. Camell, K.A. Remley, D.F. Williams, S. Schima, S. Canales, and D.T. Tamura, "Propagation and Detection of Radio Signals Before, During and After the Implosion of a Thirteen Story Apartment Building," NIST Technical Note 1540, Boulder, CO, May 2005.

[6] C.L. Holloway, G. Koepke, D. Camell, K.A. Remley, and D.F. Williams, "Radio Propagation Measurements During a Building Collapse: Applications for First Responders," Proc. Intl. Symp. Advanced Radio Tech., Boulder, CO, March 2005, pp. 61-63.

[7] C.L. Holloway, G. Koepke, D. Camell, K.A. Remley, D.F. Williams, S. Schima, and D.T. Tamura, "Propagation and Detection of Radio Signals Before, During and After the Implosion of a Large Sports Stadium (Veterans' Stadium in Philadelphia)," NIST Technical Note 1541, Boulder, CO, October 2005.

[8] K. A. Remley, G. Koepke, C.L. Holloway, C, Grosvenor, D. Camell, J. Ladbury, R. T. Johnk, D. Novotny, W. F. Young, G Hough, M. C. McKinley Y. Becquet, J Korsnes, "Measurements to Support Broadband Modulated-Signal Radio Transmissions for the Public-Safety Sector, " NIST Technical Note 1546, Boulder CO, April 2008.

[9] L.P. Rice, "Radio transmission into buildings at 35 and 150 mc," Bell Syst. Tech. J., pp. 197-210, Jan. 1959.

[10] E. Walker, "Penetration of radio signals into building in the cellular radio environment," Bell Syst. Tech. J., 62(9), Nov. 1983.

[11] D. Molkdar, "Review on radio propagation into and within buildings," IEE Proceeding-H, 38(1): 61-73; Feb. 1991.

[12] W.J. Tanis and G.J. Pilato, "Building penetration characteristics of 880 MHz and 1922 MHz radio waves." Proc. 43th IEEE Veh. Technol. Conf., Secaucus, NJ, 18-20 May 1993, pp. 206-209.

[13] L.H. Loew, Y. Lo, M.G. Lafin, and E.E. Pol. "Building penetration measurements from low-height base stations at 912, 1920, and 5990 MHz," NTIA Report 95-325, National Telecommunications and Information Administration, Sept. 1995.

[14] A. Davidson and C. Hill, "Measurement of building penetration into medium buildings at 900 and 1500 MHz," IEEE Trans. Veh. Technol., 46(1): 161-168; Feb. 1997.

[15] E. F. T. Martijn and M. H. A. J. Herben, "Characterization of Radio Wave Propagation Into Buildings at 1800 MHz," IEEE Ant. and Wireless Prop. Letters, Vol. 2, 2003.

[16] M. Rütschlin, K. A. Remley, R. T. Johnk, D. F. Williams, G. Koepke, C. Holloway, A. MacFarlane, and M. Worrell, "Measurement of weak signals using a communications receiver system." Proc. Intl. Symp. Advanced Radio Tech., Boulder, CO, March 2005. pp. 199-204.

[17] C.L. Holloway, G. Koepke, D. Camell, K.A. Remley, D.F. Williams, S. Schima, M. McKinely, and R.T. Johnk, "Propagation and Detection of Radio Signals Before, During and After the Implosion of a Large Convention Center," NIST Technical Note 1542, Boulder, CO, June 2006.

[18] C.L. Holloway, W. Young, G. Koepke, D. Camell, Y. Becquet, K.A. Remley, "Attenuation, Coupling, and Variability of Radio Wave Signals Into and Throughout Twelve Large Building Structures," NIST Technical Note 1545, Boulder, CO, Aug 2008.

[19] B. Davis, C. Grosvenor, R.T. Johnk, D. Novotny, J. Baker-Jarvis, M. Janezic, "Complex permittivity of planar building materials measured with an ultra-wideband free-field antenna measurement system." Natl. Inst. Stand. Technol. J. Res., 112(1):67-73, Jan.-Feb., 2007.

[20] M. Riback, J. Medbo, J. Berg, F. Harryson, H. Asplund, "Carrier frequency effects on path loss," Proc. 63rd IEEE Vehic. Technol. Conf., Vol. 6, pp. 2717-2721, 2006.

[21] J.C.-I. Chuang, "The effects of time delay spread on portable radio communications channels with digital modulation." IEEE J. Selected Areas in Comm., SAC-5(5): 879-889, June 1987.

[22] Y. Oda, R. Tsuchihashi, K. Tsuenekawa, M. Hata, "Measured path loss and multipath propagation characteristics in UHF and microwave frequency bands for urban mobile communications," Proc. 53rd IEEE Vehic. Technol. Conf., Vol. 1, pp. 337-341, May 2001.

[23] J.A. Wepman, J.R. Hoffman, L.H. Loew, "Impulse Response Measurements in the 1850-1990 MHz Band in Large Outdoor Cells". NTIA Report 94-309, June 1994.

Appendix I: Experiment Setups and Locations

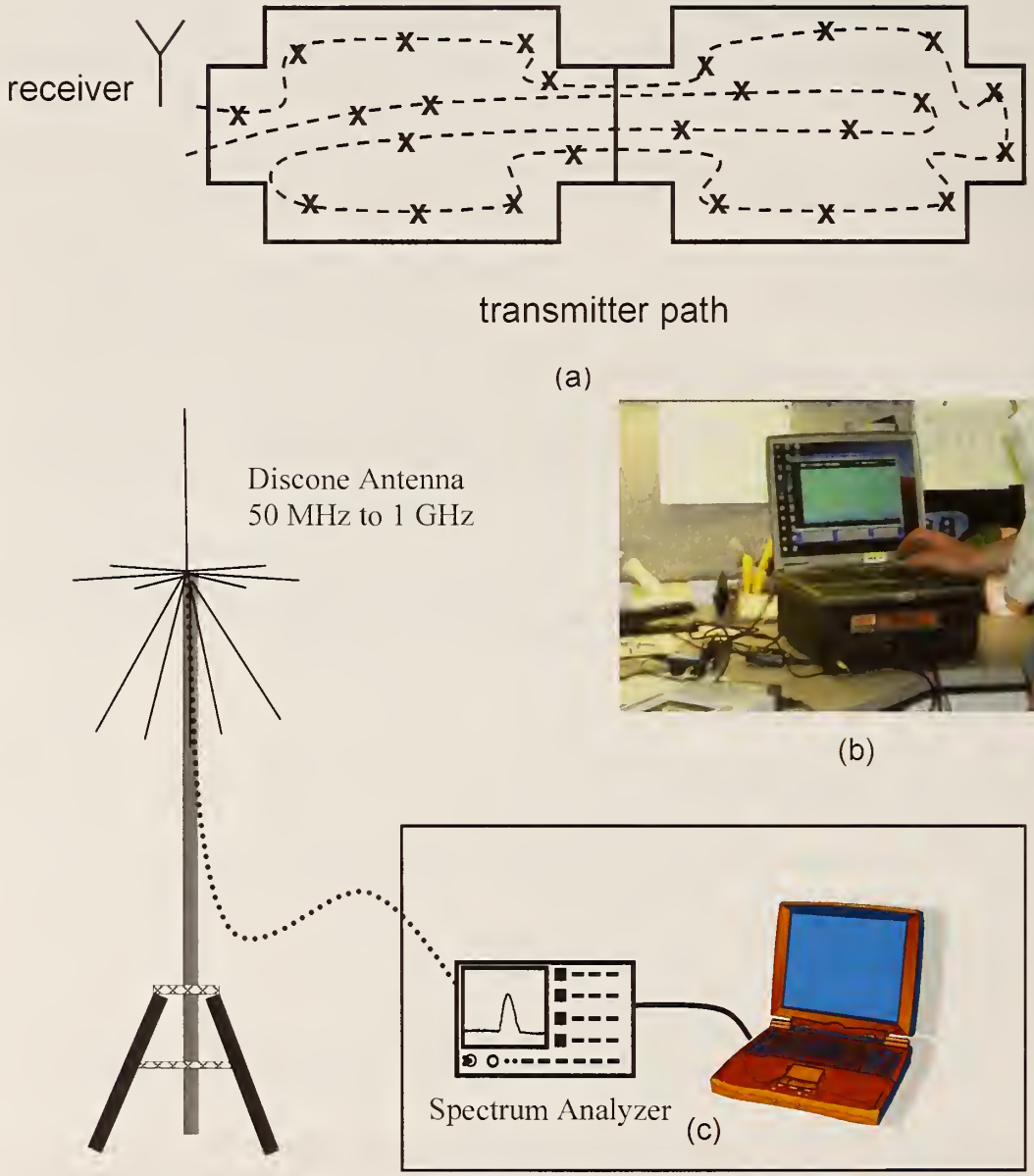

Figure 1. Illustration of the radio-mapping measurements. (a) A radio transmitter was carried throughout the building on a continuous path, and the signal strength was recorded by the receiver. (b) For one set of radio mapping experiments, the receiver consisted of a commercially available communications receiver, followed by post-processing steps to determine the received-signal level. (c) A spectrum analyzer and laptop made up the other data collection method. A separate receive antenna was used for the two data collection setups.

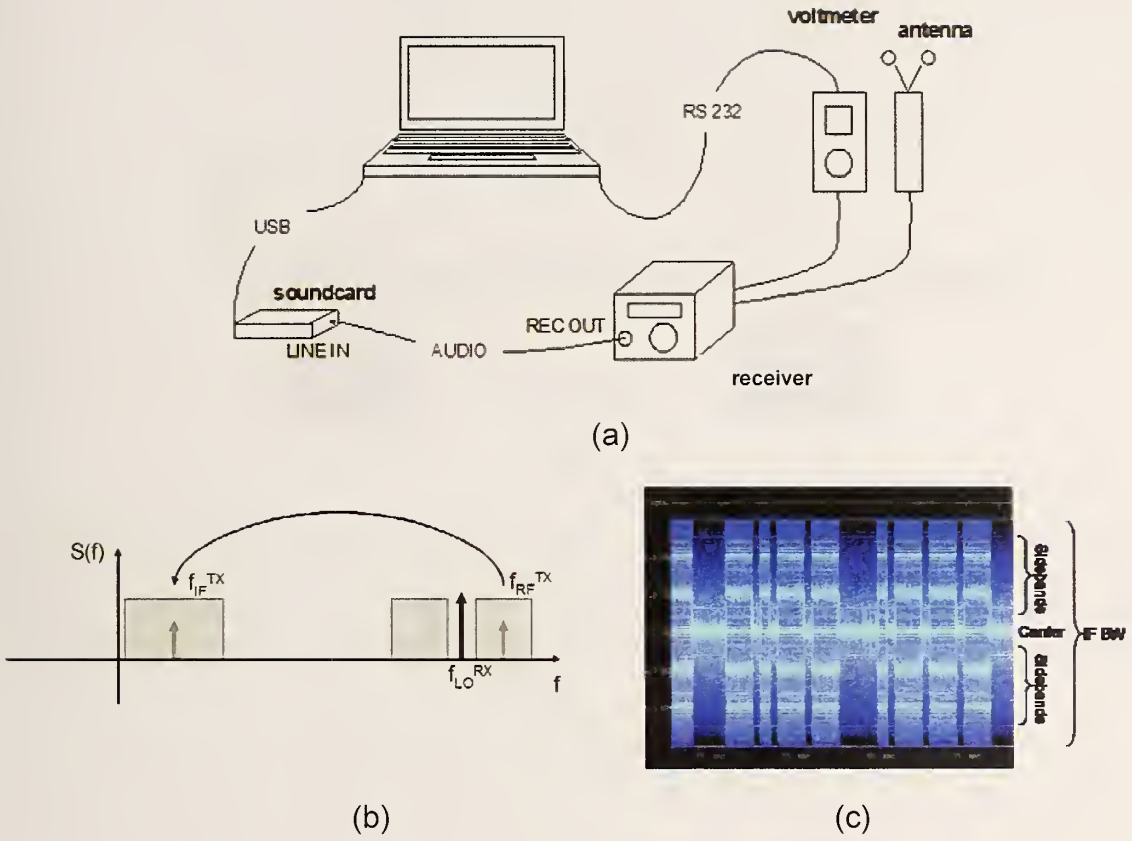

Figure 2. (a) Set-up used to enable a communications receiver to display received signal strength. The receiver down-converts the signal to baseband frequencies, as shown in (b), and the sound card digitizes the baseband signal. A DC voltmeter monitors the automatic-gain-control setting on the receiver. The AGC data are used in post-processing to determine the signal's actual level. Graphic (c) shows a recorded, down-converted signal with time on the *x*-axis and frequency on the *y*-axis. The stripe at the center corresponds to the carrier frequency, and the bands on either side correspond to the FM sidebands. In this case the received signal is in Morse code.

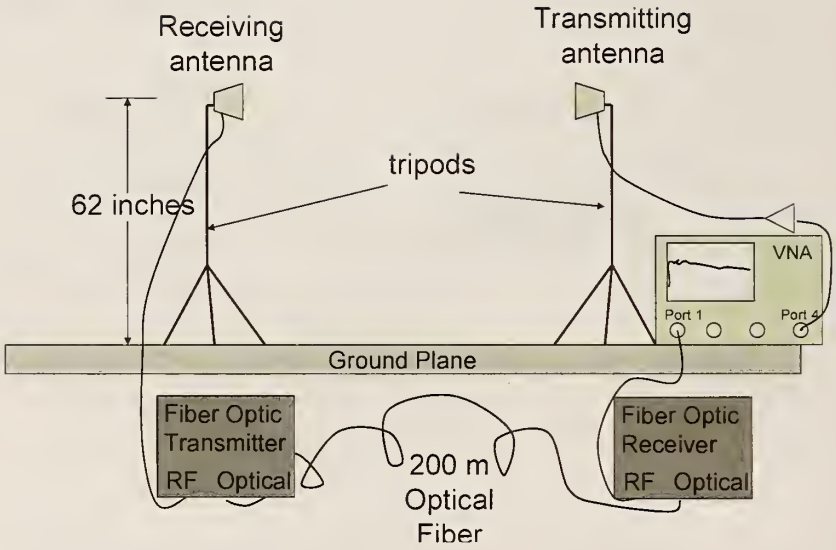

Figure 3. Synthetic-pulse measurement system based on a vector network analyzer. Frequency-domain measurements, synchronized by the optical fiber link, are transformed to the time domain in post-processing. This enables determination of excess path loss, time-delay spread, and other figures of merit important in characterizing broadband modulated-signal transmissions.

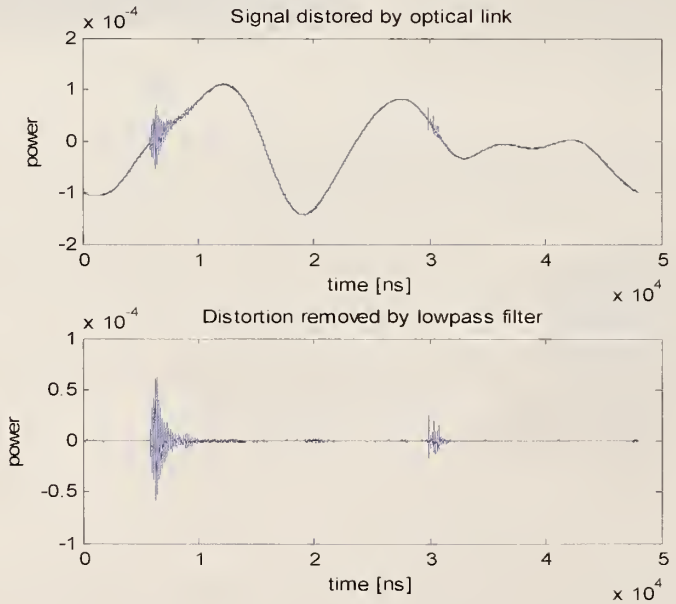

Figure 4. Low-frequency oscillations introduced by the optical link (top) are removed by use of a high-pass filter in post-processing (bottom). This enables us to clearly discern the measured data; here an initial pulse is received at approximately 5 ns, followed by a reflected pulse at approximately 30 ns.

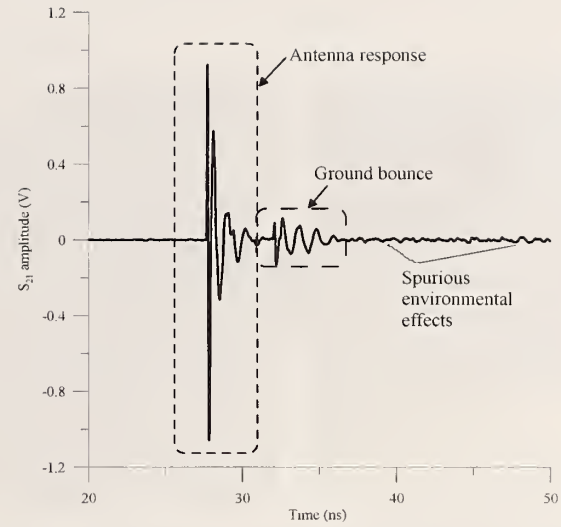

(a)

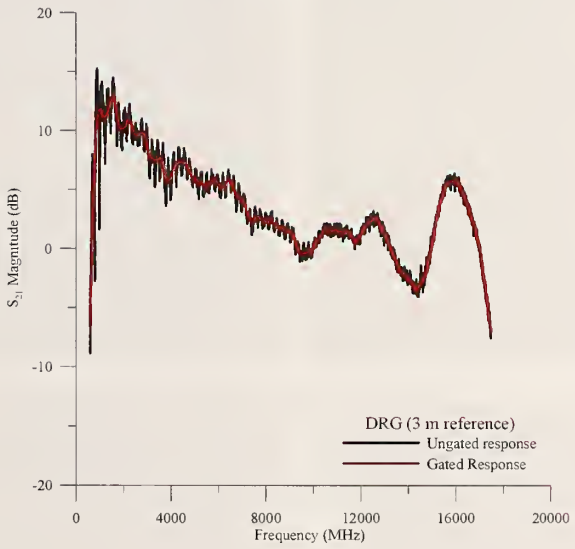

(b)

Figure 5. (a) Time-domain waveform for a dual ridge guide (DRG) horn antenna 3 m reference measurement. The waveform shows the antenna response, the ground-bounce response and the spurious environmental effects. (b) The frequency-domain response for both the ungated response (noisy black trace), which includes all environmental effects, and the gated response (smoother red trace), which includes only the antenna response.

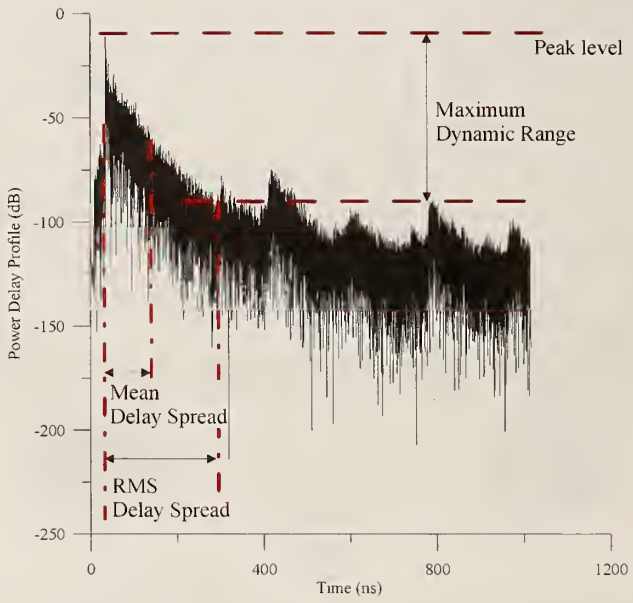

Figure 6. Power-delay profile for a building propagation measurement. The important parameters for a measured propagation signal are the peak level, the maximum dynamic range, the mean delay spread, and the RMS delay spread.

Figure 7. Photographs of the Colorado Convention Center.

Figure 8. Photographs of the Colorado Convention Center (cont.).

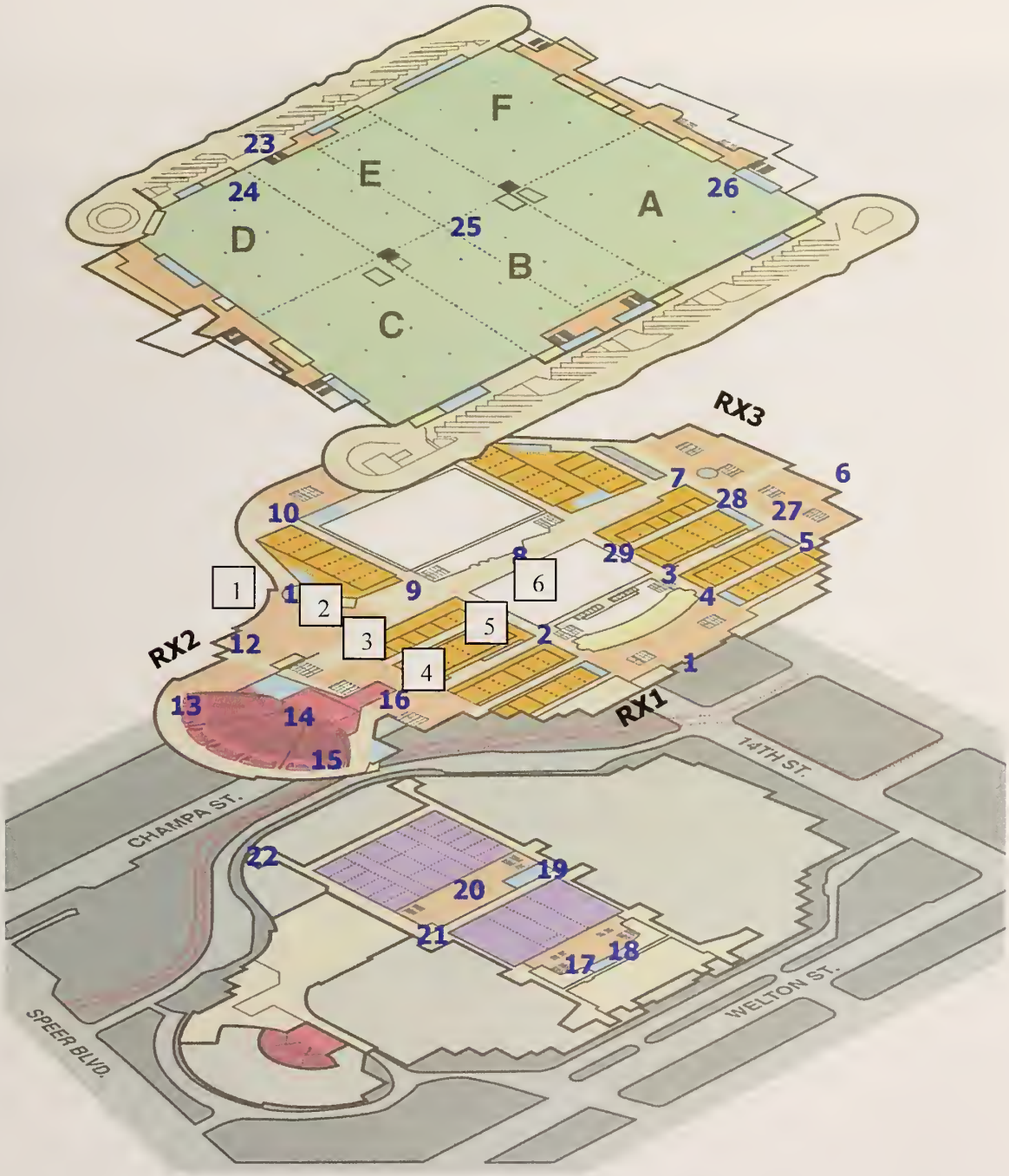

Figure 9. Layout of the Colorado Convention Center including the radio-mapping path. Numbers in boxes represent synthetic pulse measurement locations; the non-enclosed numbers denote positions indicated on the spectrum analyzer and narrowband receiver measurements.

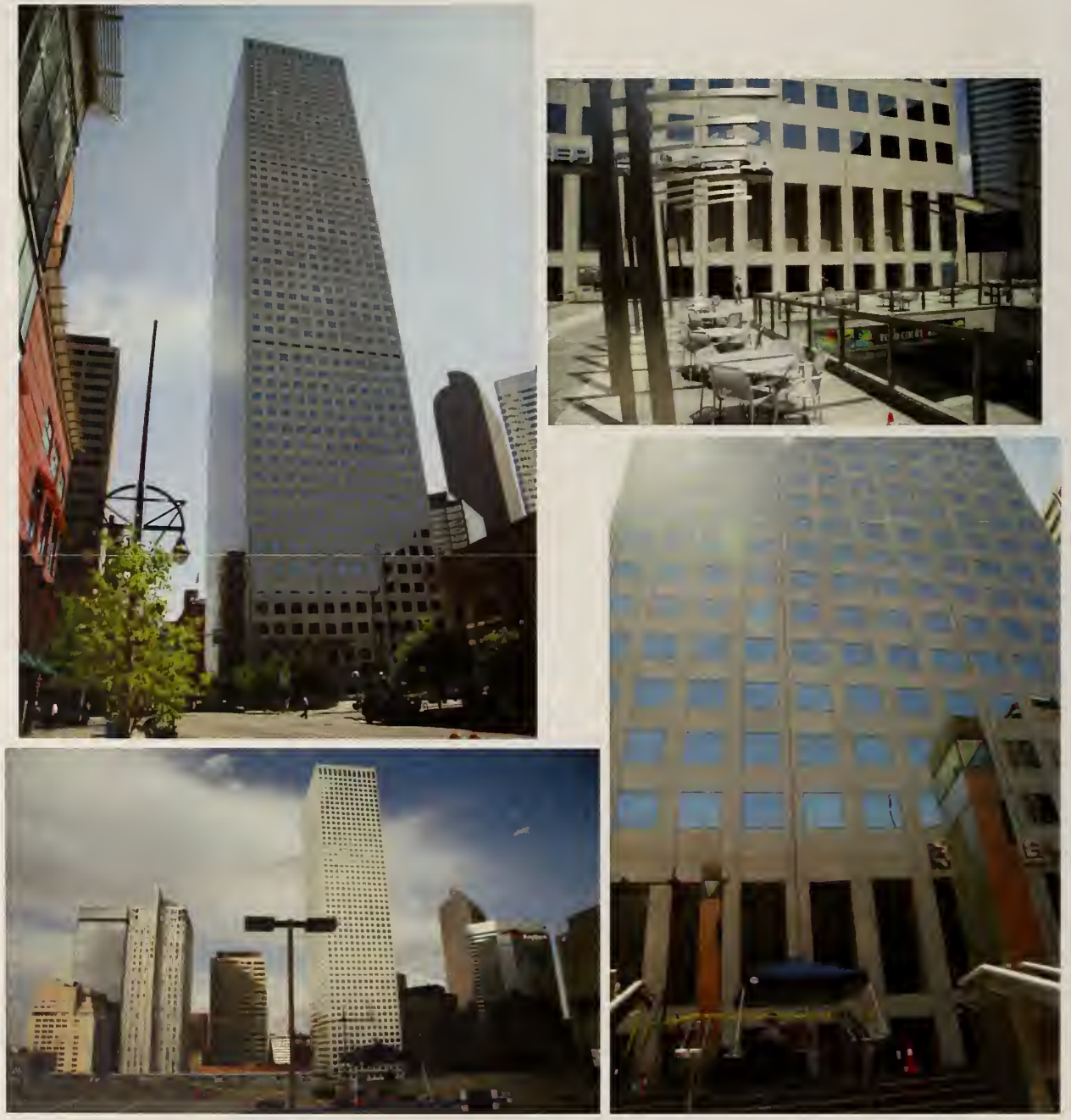

Figure 10. Photographs of the Republic Plaza Building.

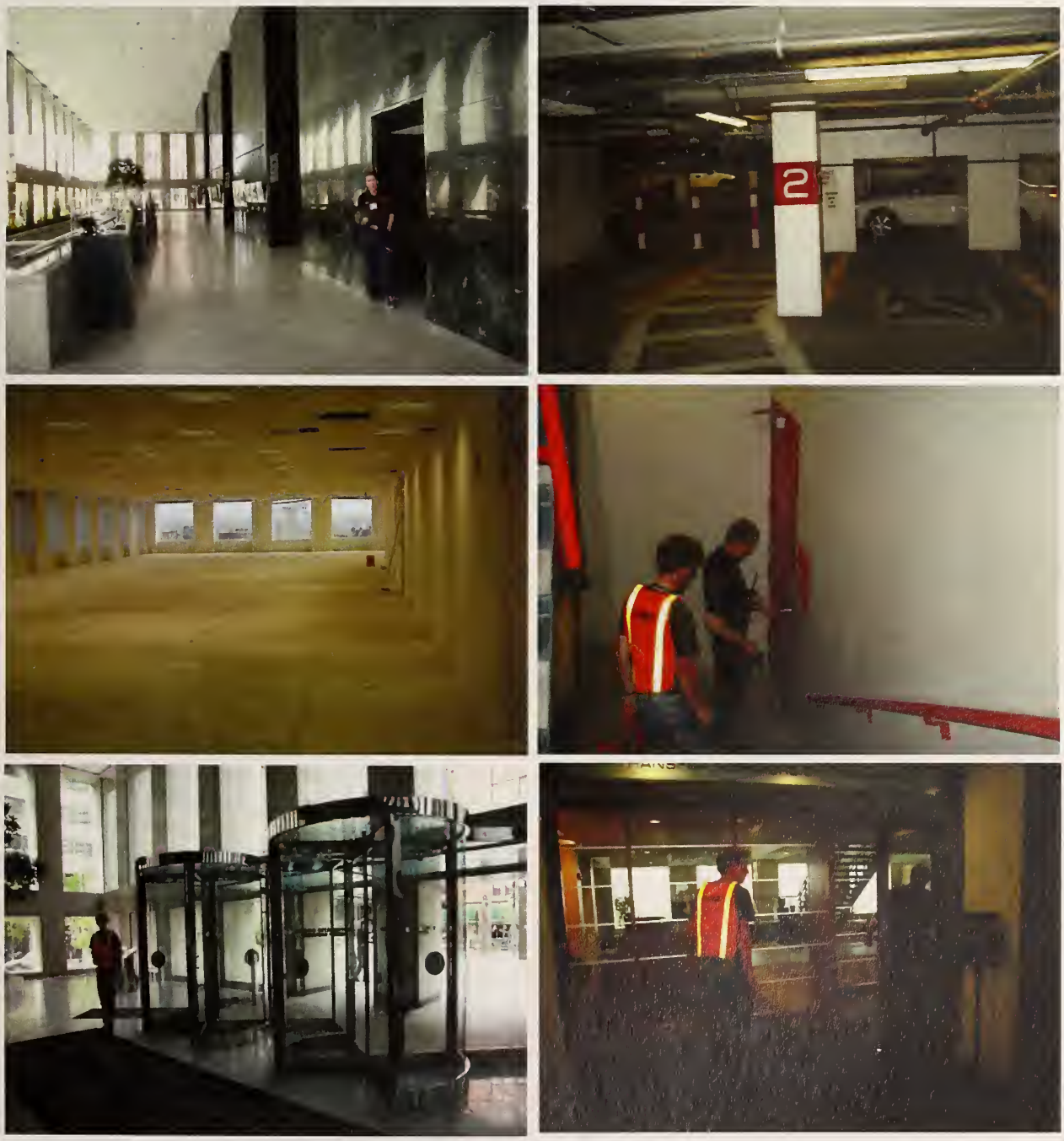

Figure 11. Photographs inside the Republic Plaza Building.

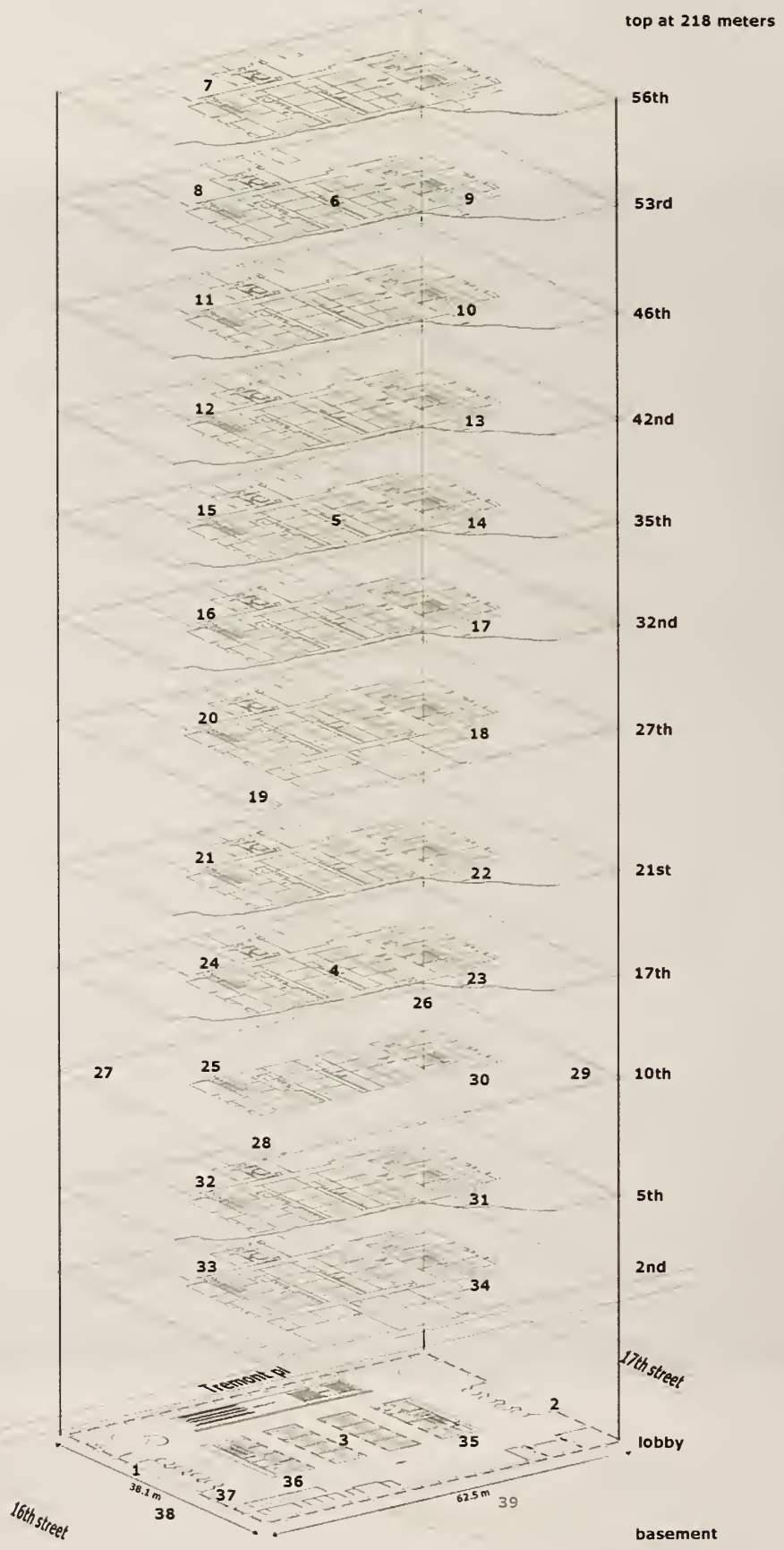

Figure 12. Layout of the Republic Plaza Building and radio-mapping path.

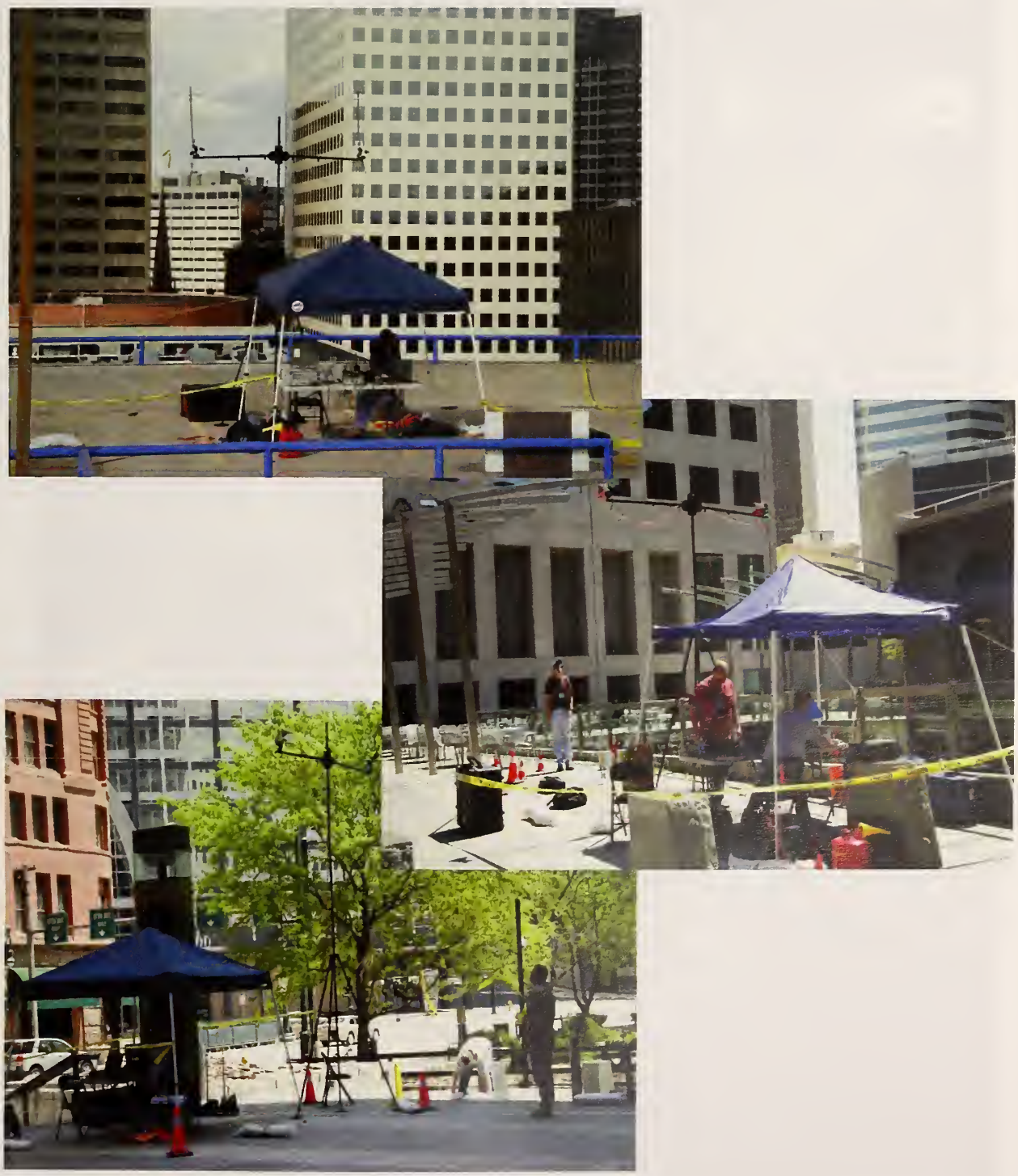

Figure 13. Photographs of the three receive sites at the Republic Plaza Building.

Figure 14. Location of receive sites at the Republic Plaza Building.

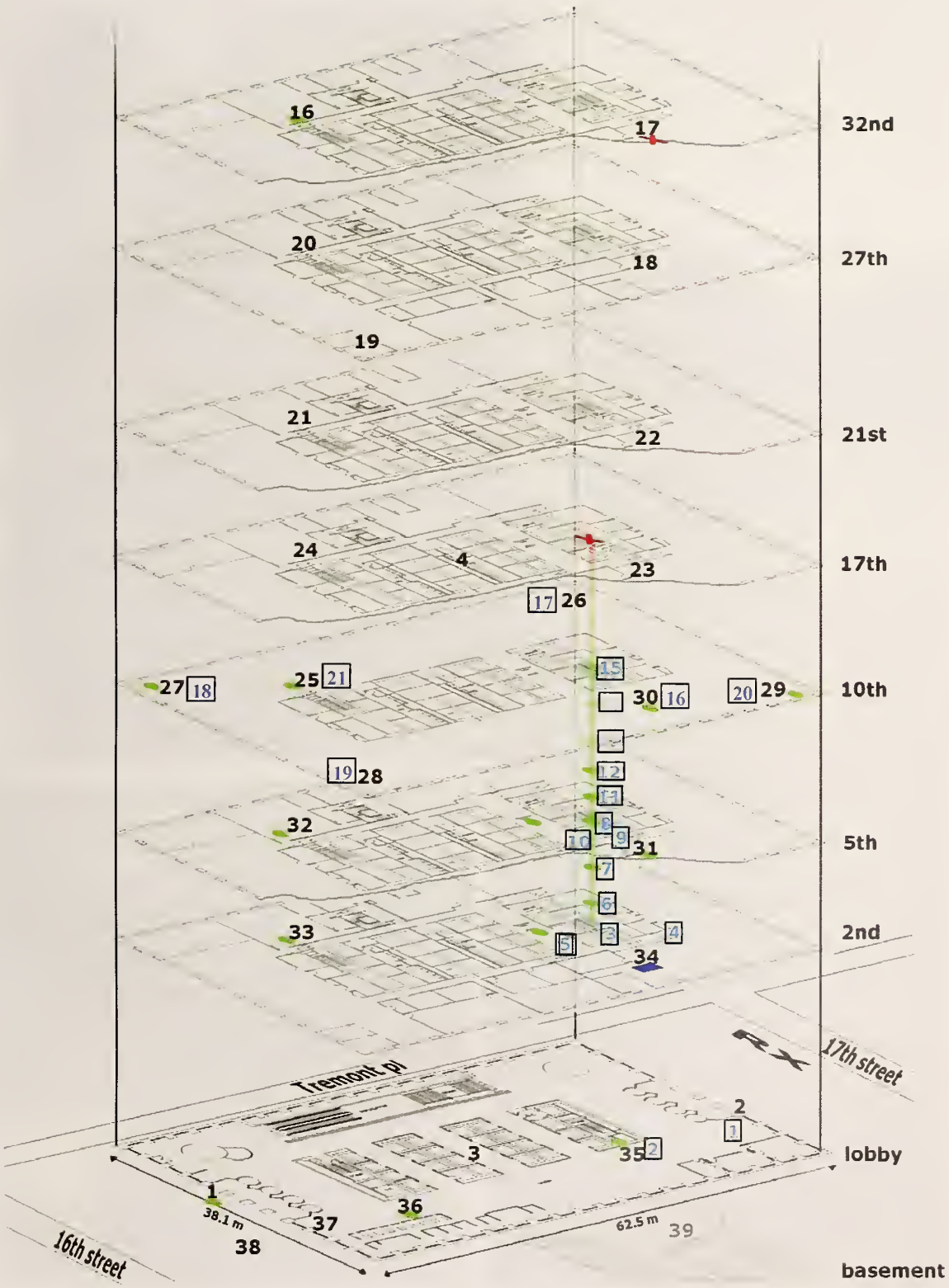

Figure 15. Synthetic pulse test points in Republic Plaza. The test locations are the blue numbers in the black boxes; the unboxed numbers are radio-mapping locations as in Figure 12.

Figure 16. Photographs of the Horizon West apartment building in Boulder, CO.

Figure 17. Photographs inside the Horizon West apartment building in Boulder, CO.

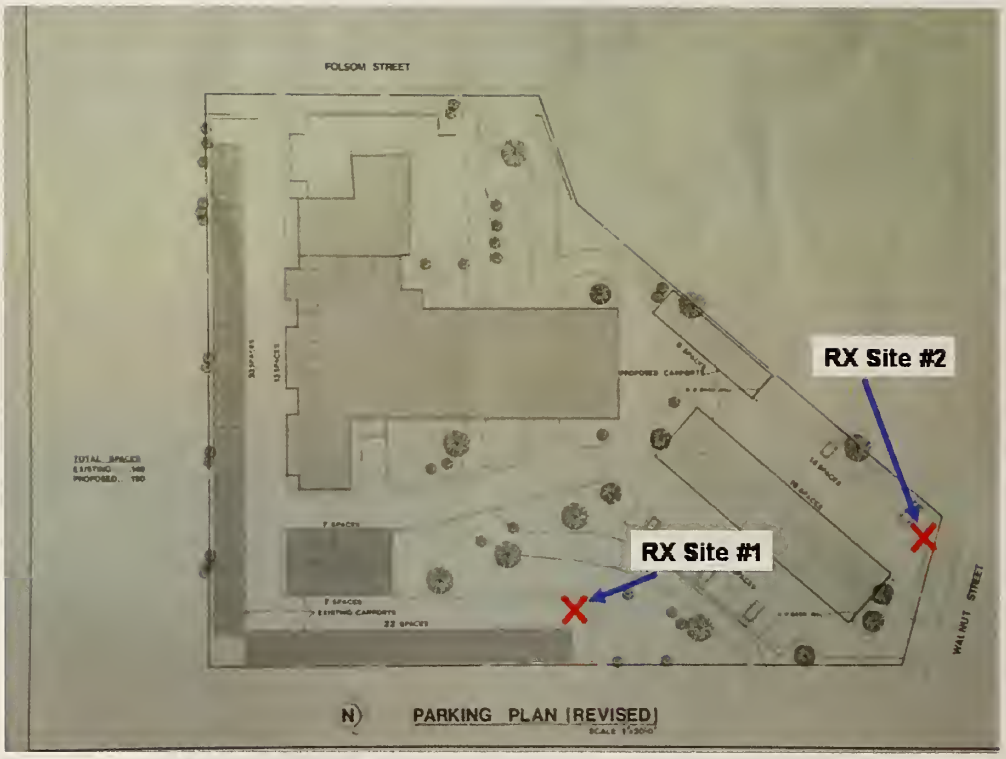

(a)

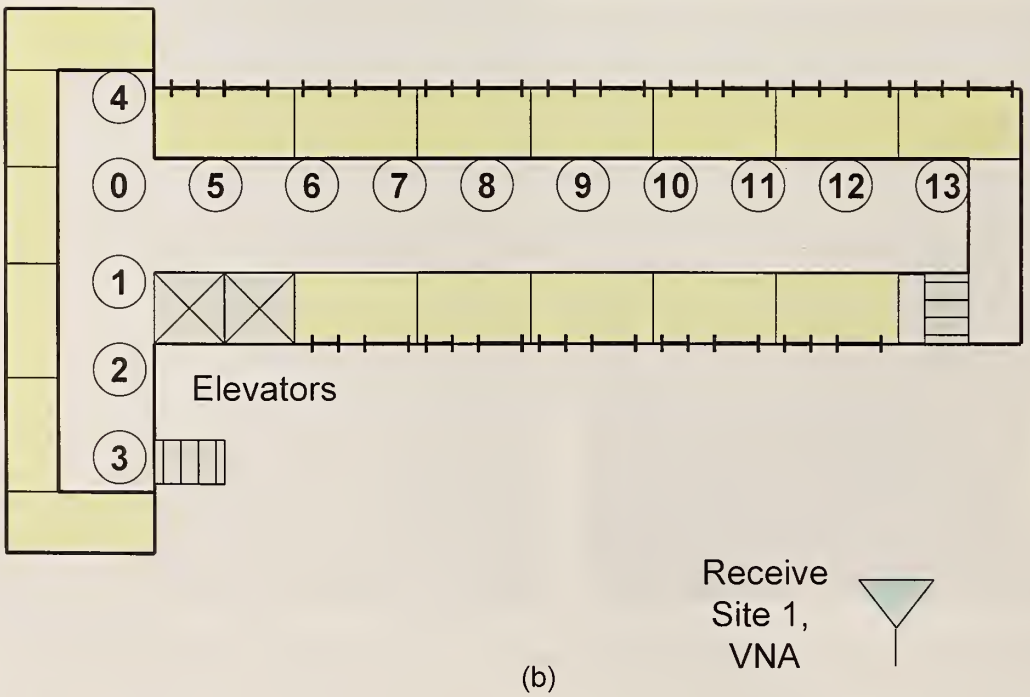

(b)

Figure 18. Receiver locations for the Horizon West apartment building. (a) Locations for radio-mapping tests. (b) Locations for synthetic pulse system measurements.

Figure 19. The receiver setups for the NIST's laboratories in Boulder, CO.

Figure 20. Receiver location and layout for the Boulder, CO laboratories.

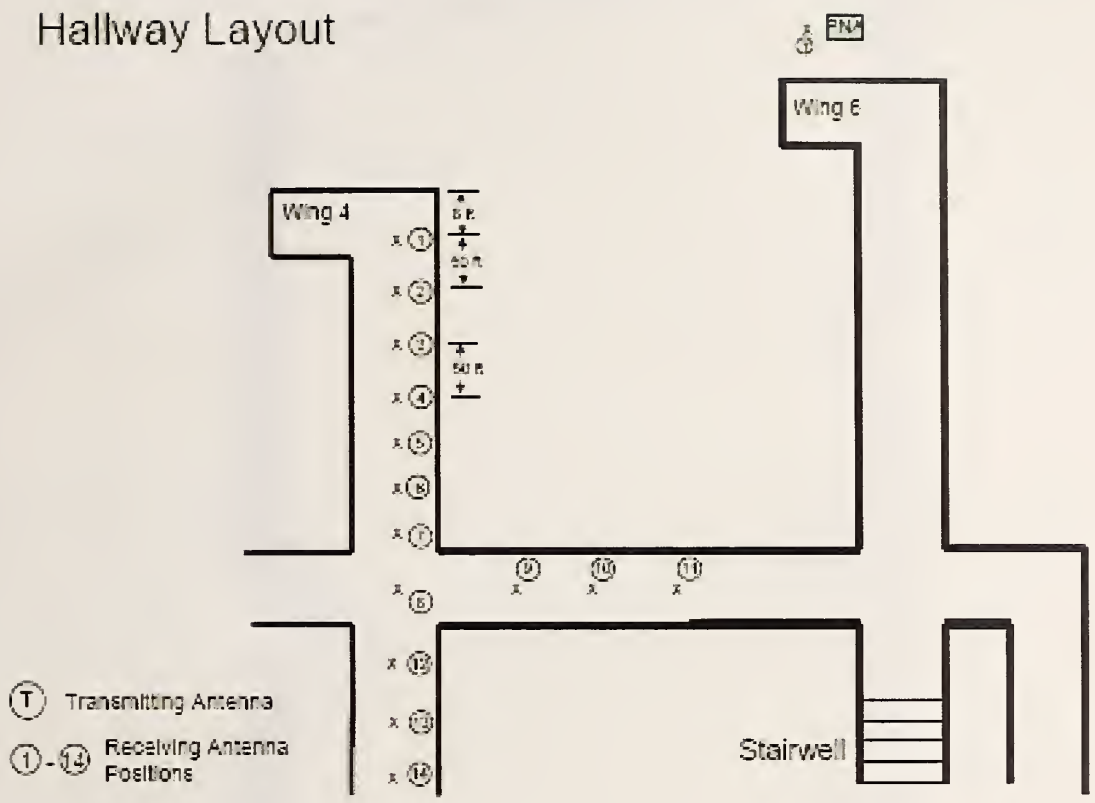

Figure 21. Synthetic pulse building penetration measurements were carried out at specific test locations indicated on the outline. The Wing 4 corridor is lined with offices having windows to the outside, thus indoor-to-outdoor coupling can be expected.

Appendix II: Measurement Results

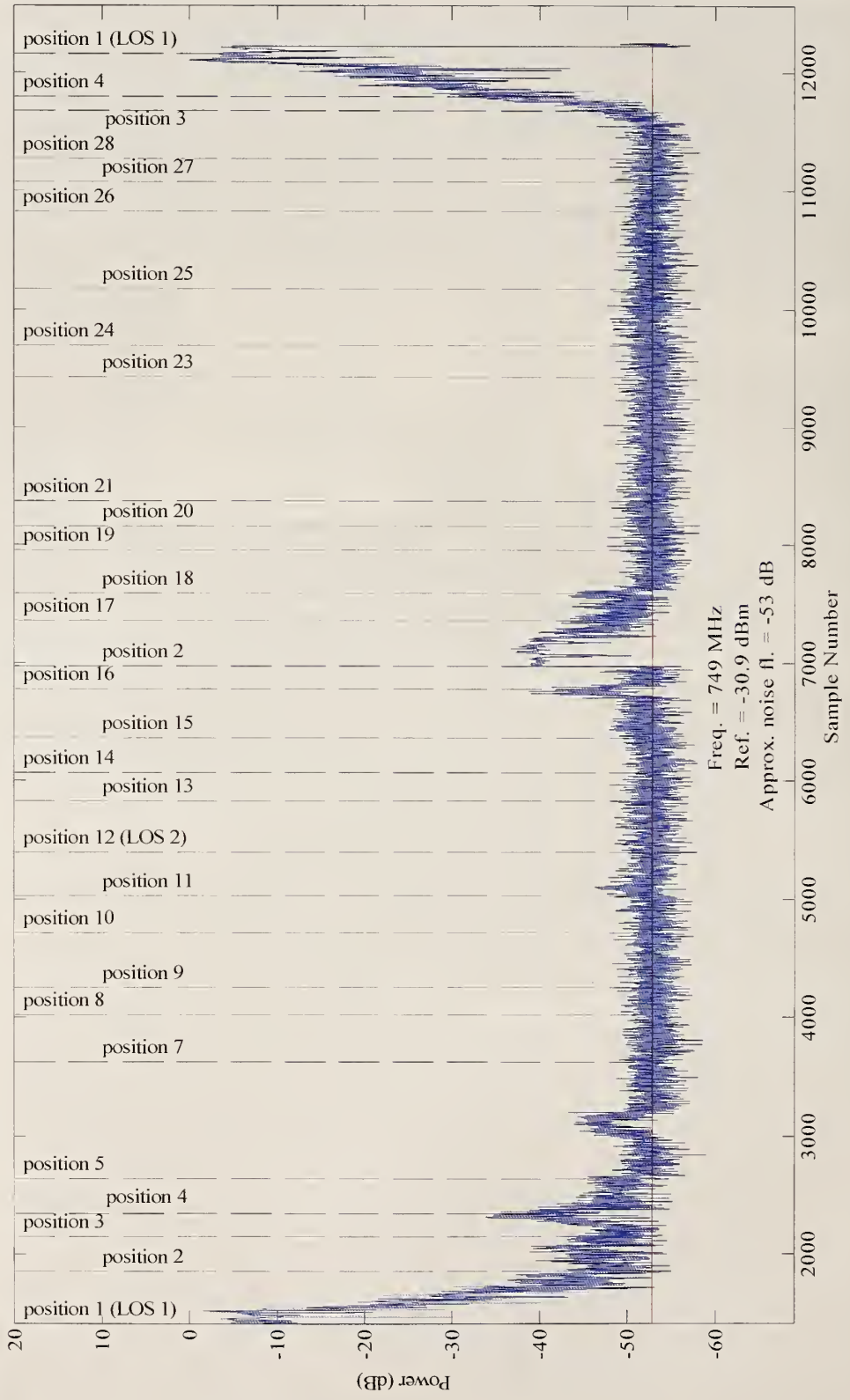

Figure 22. Colorado Convention Center, receive site 1. Normalized received-signal data from the spectrum analyzer as the 749 MHz transmitter is carried through the building.

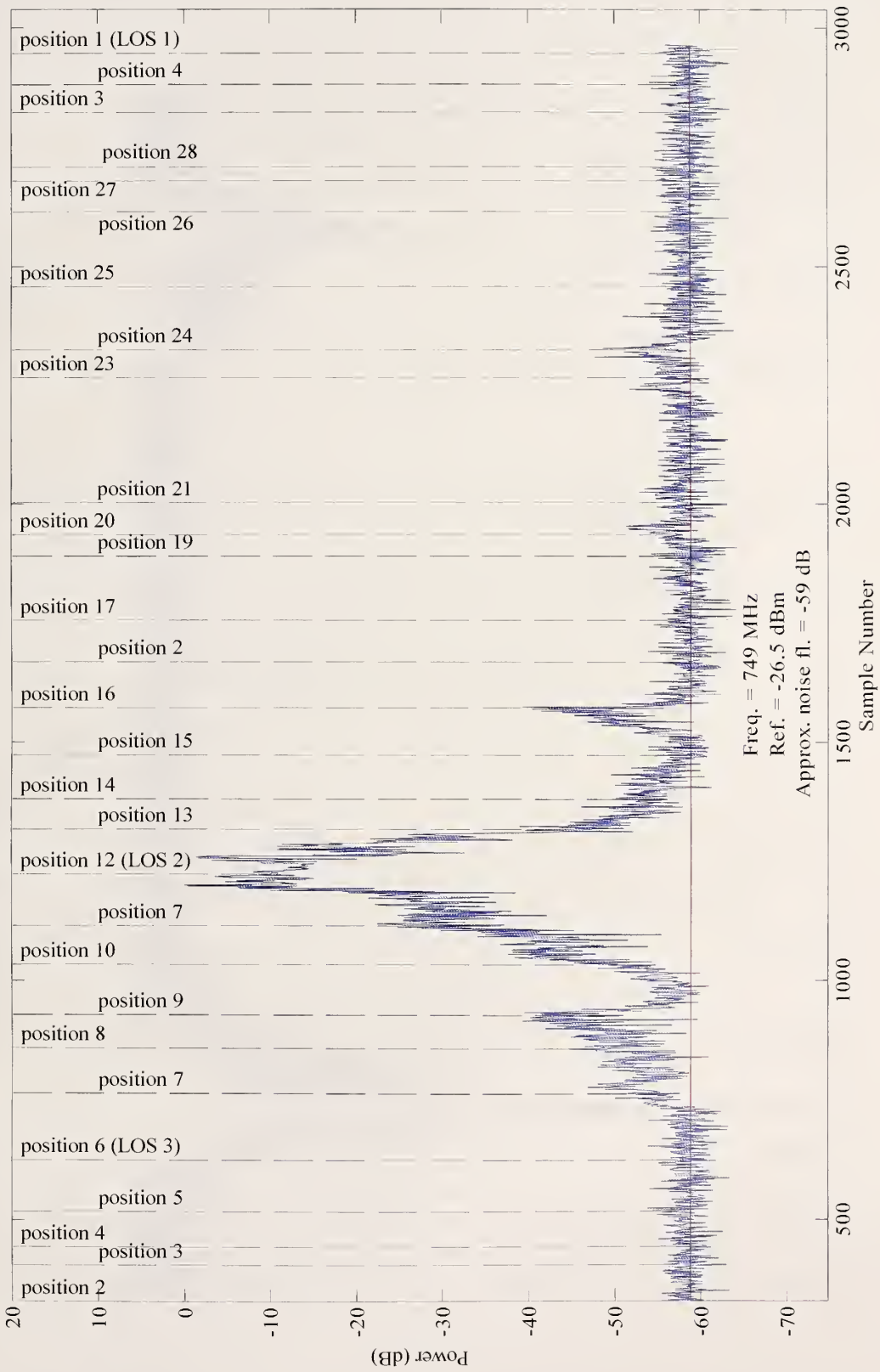

Figure 23. Colorado Convention Center, receive site 2. Normalized received-signal data from the spectrum analyzer as the 749 MHz transmitter is carried through the building.

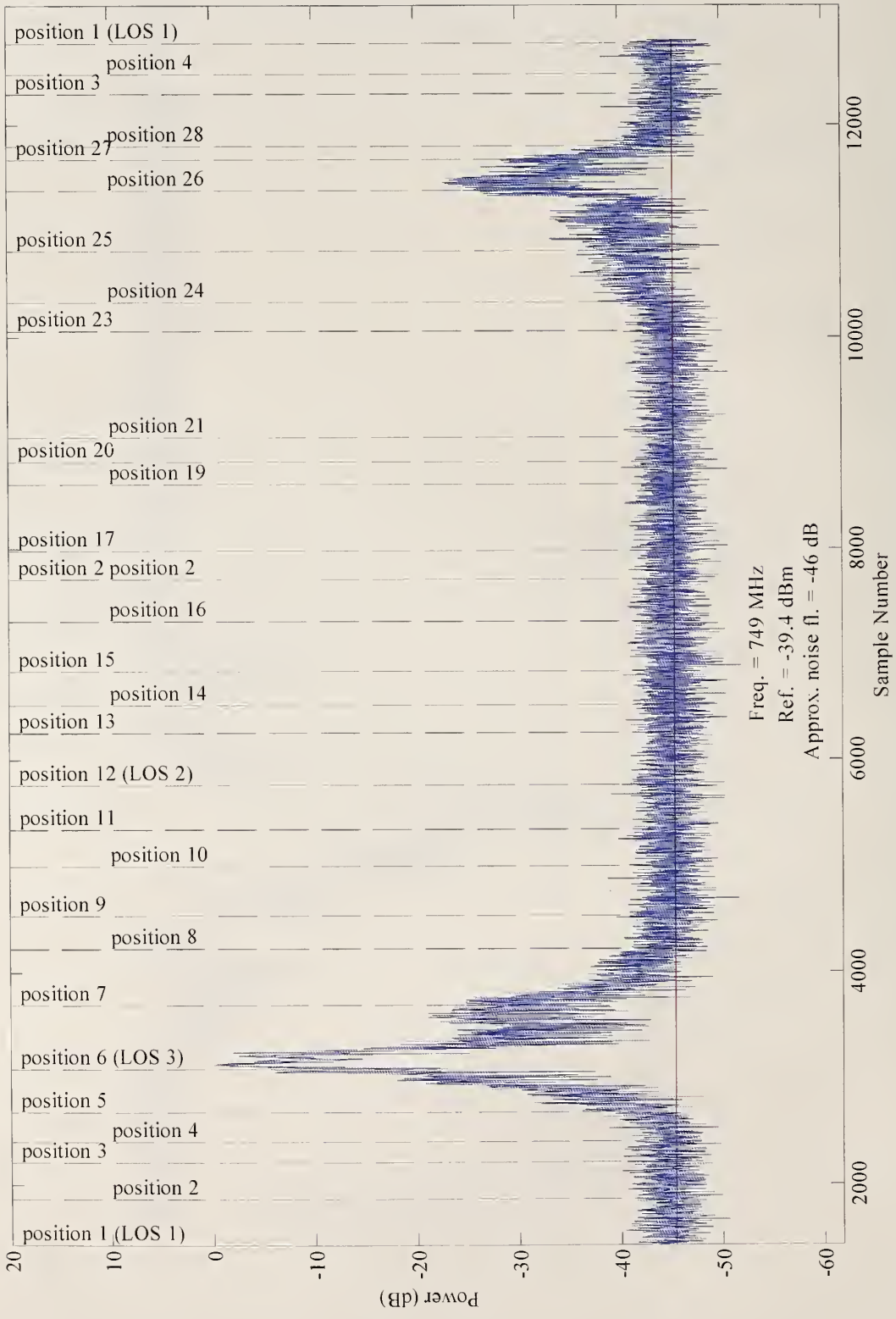

Figure 24. Colorado Convention Center, receive site 3. Normalized received-signal data from the spectrum analyzer as the 749 MHz transmitter is carried through the building.

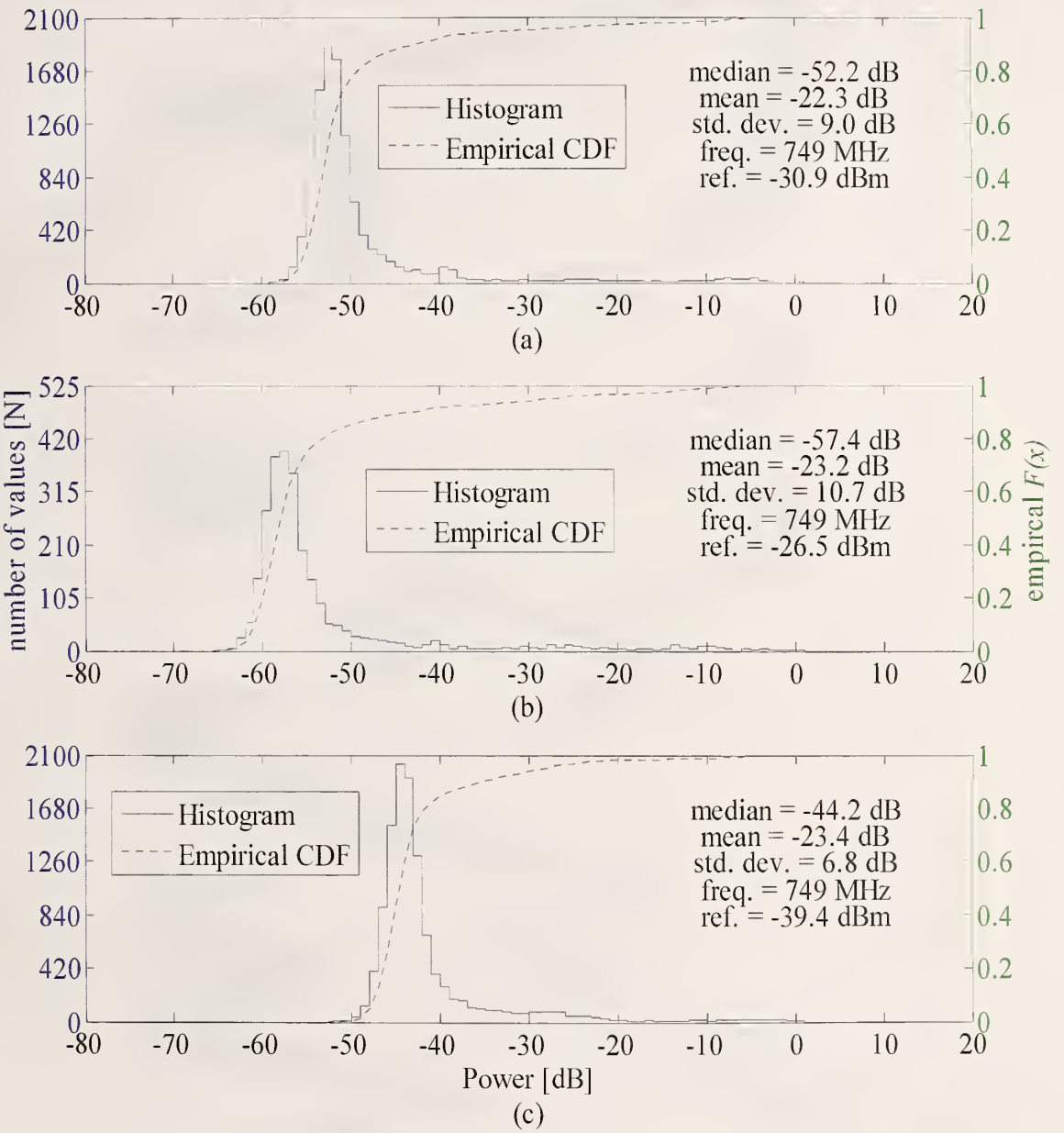

Figure 25. Histogram and empirical CDF of the received signal power from the spectrum analyzer at the Colorado Convention Center for (a) receive site one, (b) receive site two, and (c) receive site three. Note that histogram count scale is different for receive site two, plot (b).

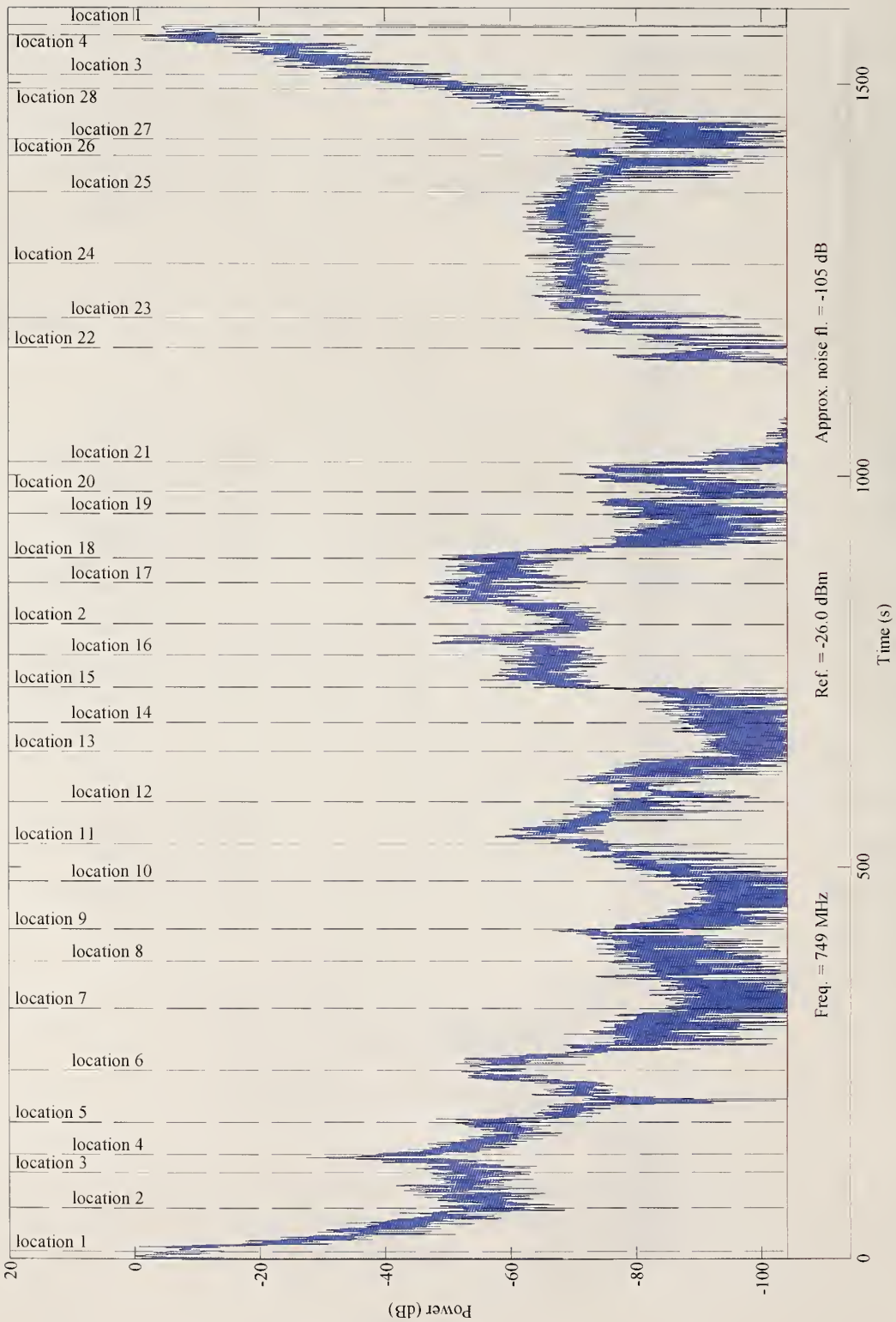

Figure 26. Colorado Convention Center narrowband receiver results for receive site 1.

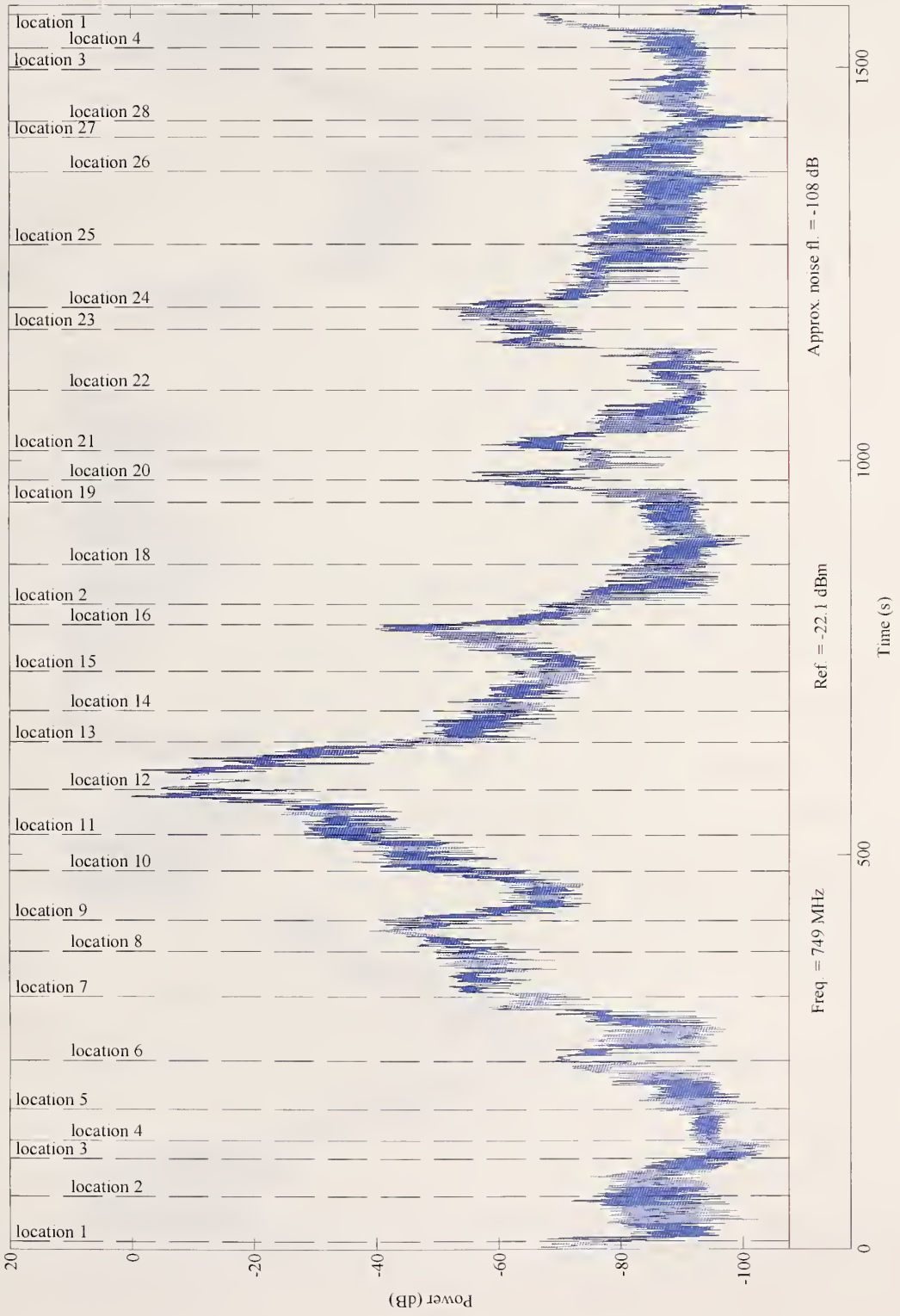

Figure 27. Colorado Convention Center narrowband receiver results for receive site 2.

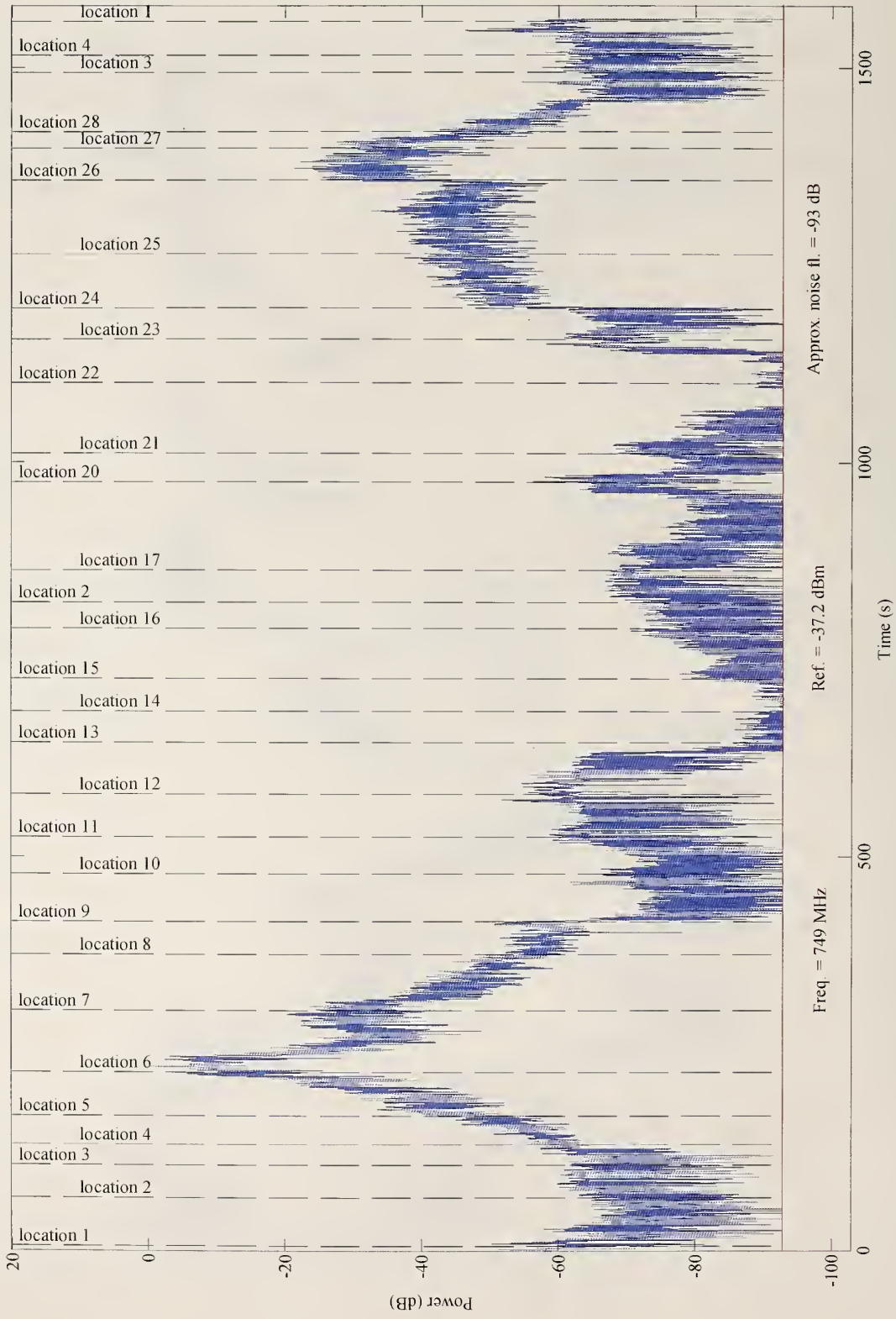

Figure 28. Colorado Convention Center narrowband receiver results for receive site 3.

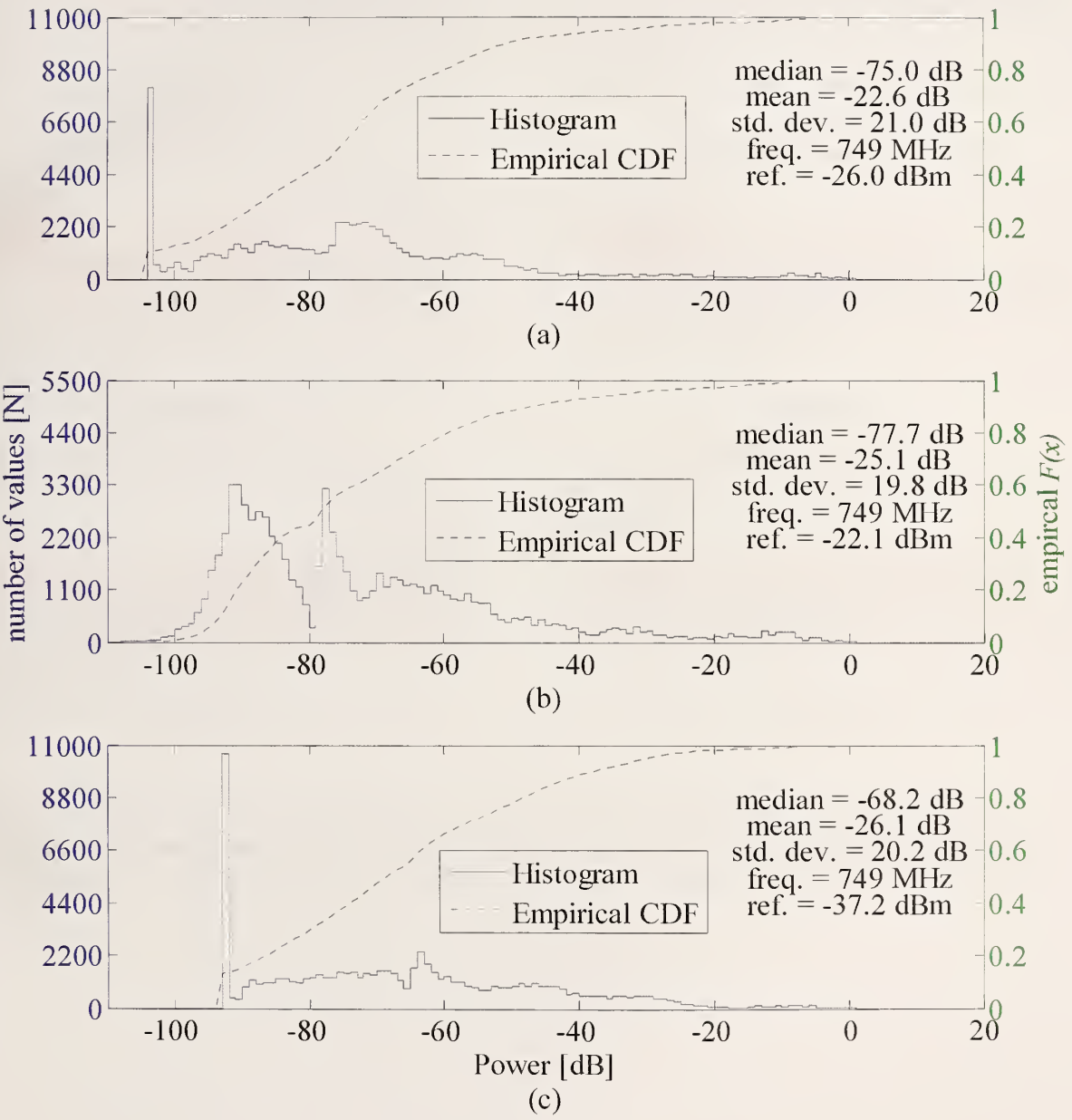

Figure 29. Histogram and empirical CDF of the narrowband receiver signal power at the Colorado Convention Center for (a) receive site one, (b) receive site two. and (c) receive site three. Note that histogram count scale is different for the receive site two, plot (b).

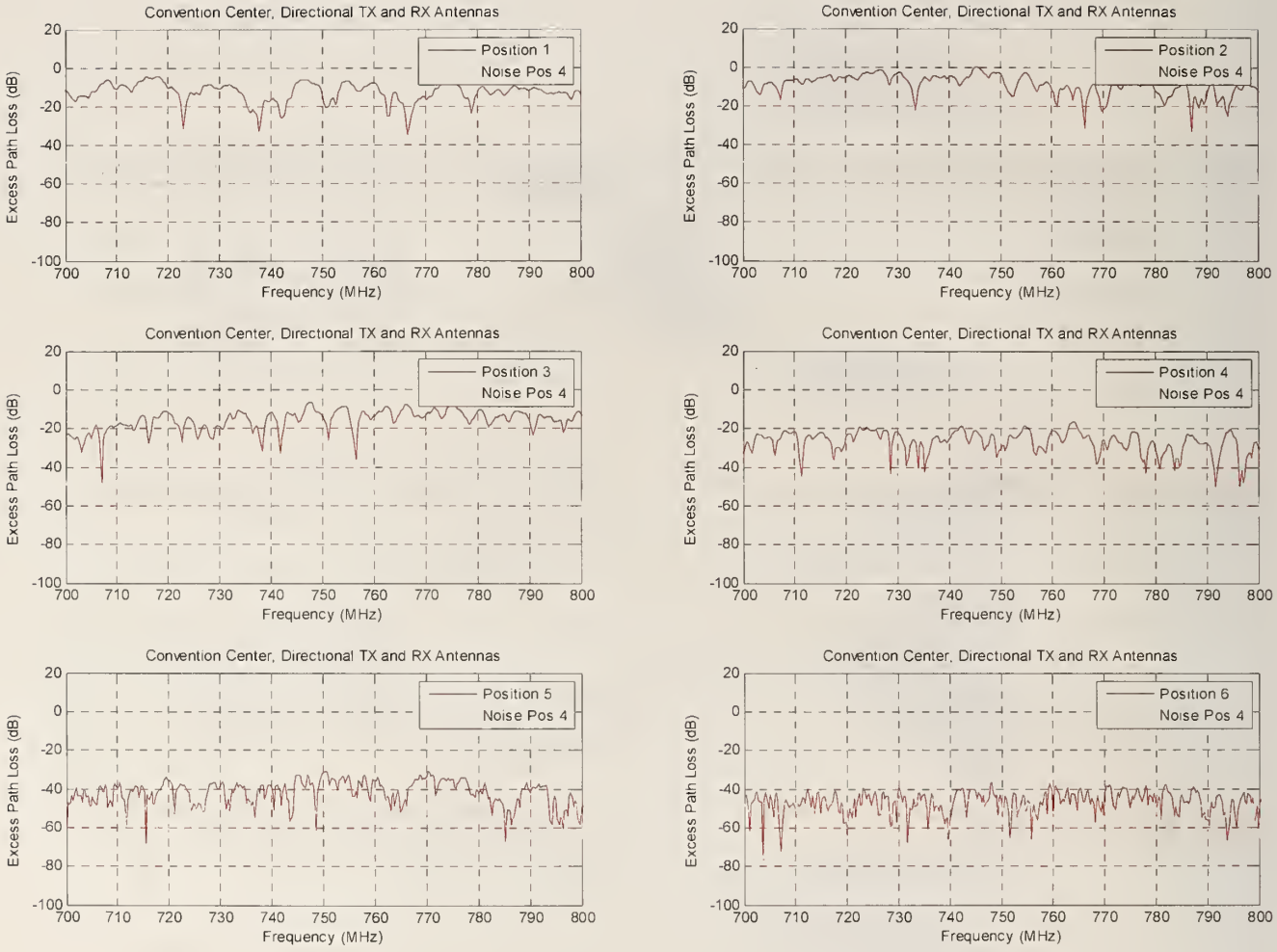

Figure 30. Excess path loss measurements at the Colorado Convention Center for the 700 MHz to 800 MHz frequency band. Directional transmit and receive antennas were used.

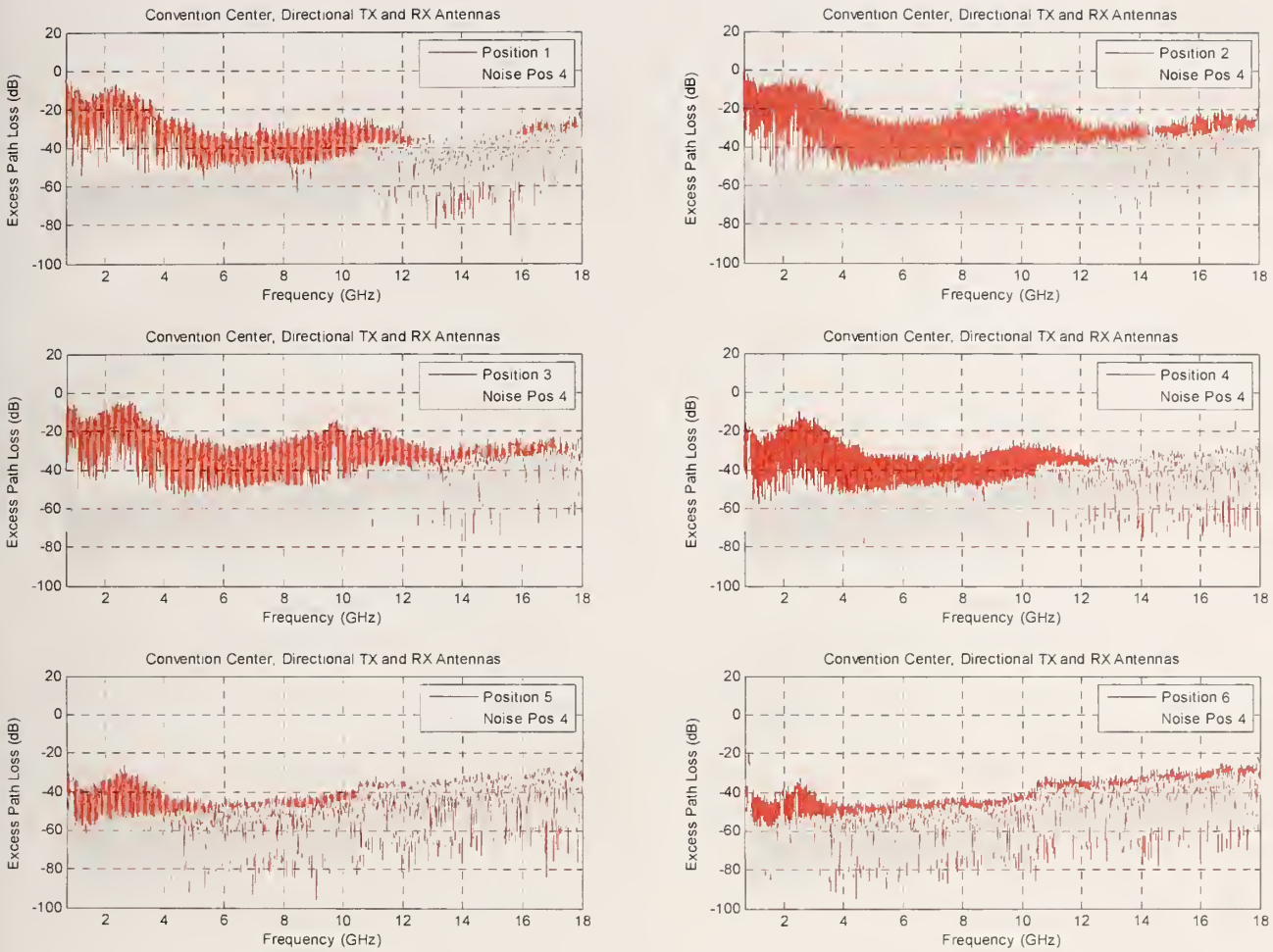

Figure 31. Excess path loss measurements at the Colorado Convention Center for the 700 MHz to 18 GHz frequency band. Directional transmit and receive antennas were used.

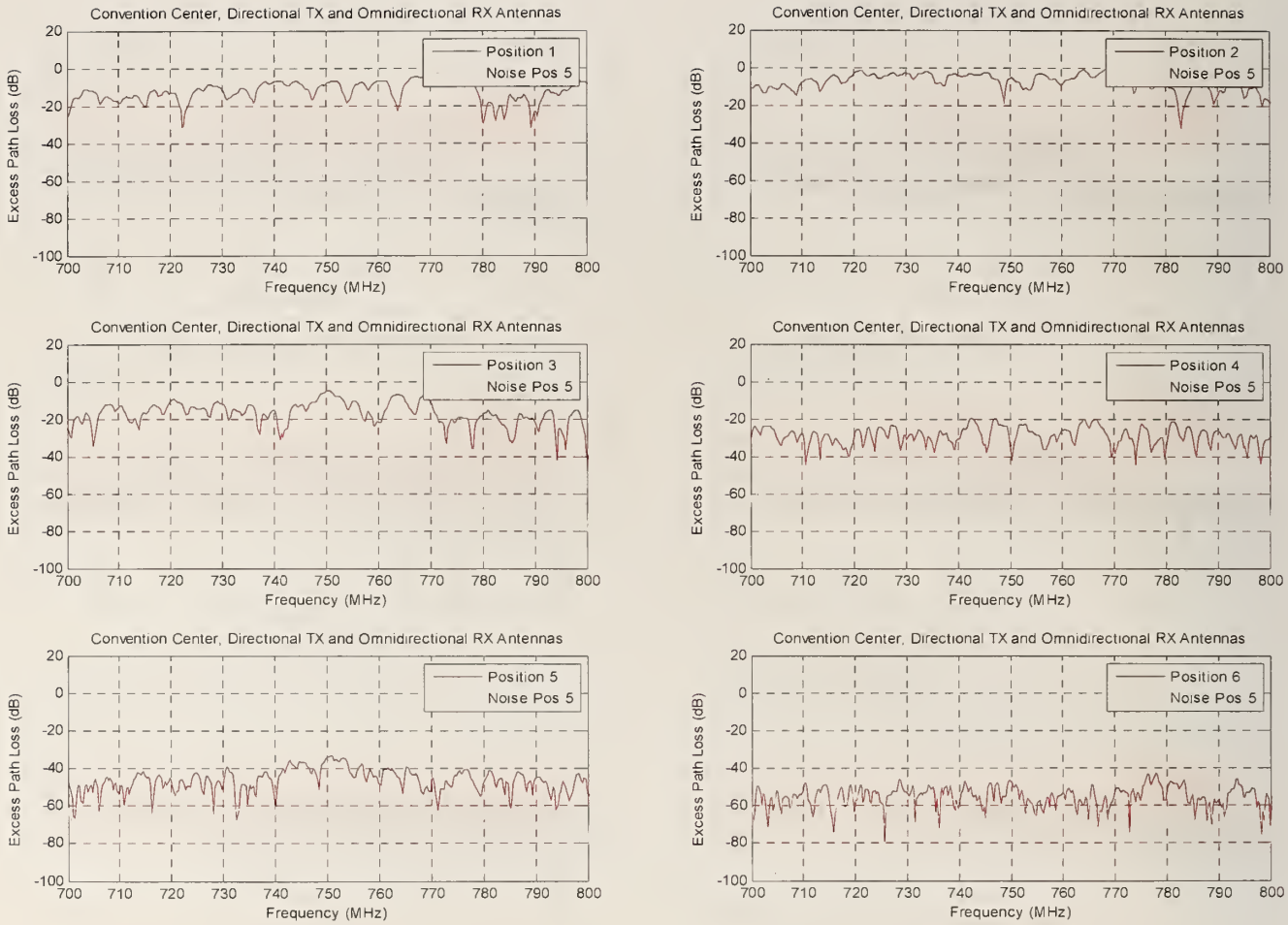

Figure 32. Excess path loss measurements at the Colorado Convention Center for the 700 to 800 MHz frequency band. Directional transmit antenna and omnidirectional receive antennas were used.

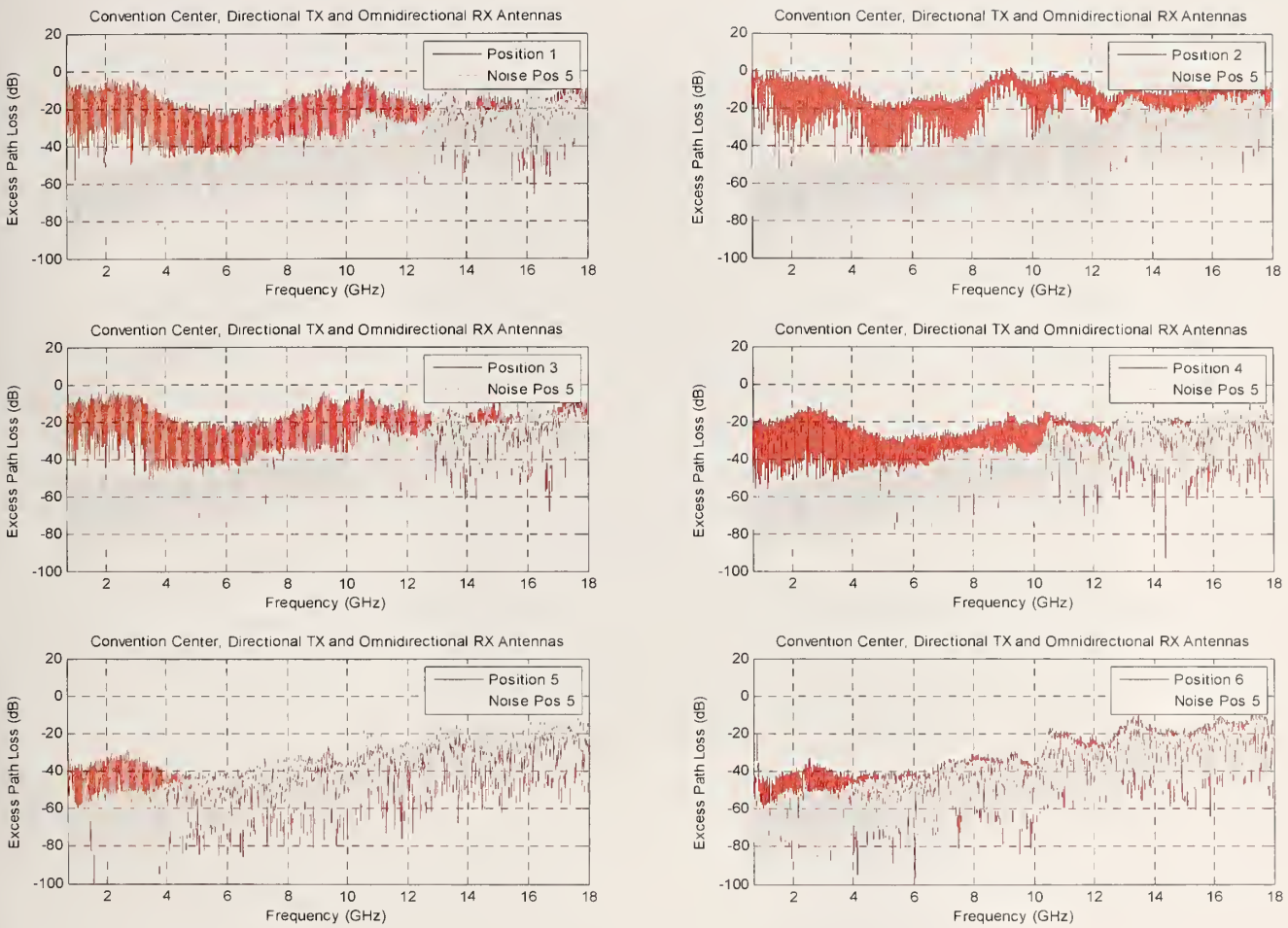

Figure 33. Excess path loss measurements at the Colorado Convention Center for the 700 MHz to 18 GHz frequency band. Directional transmit antenna and omnidirectional receive antennas were used.

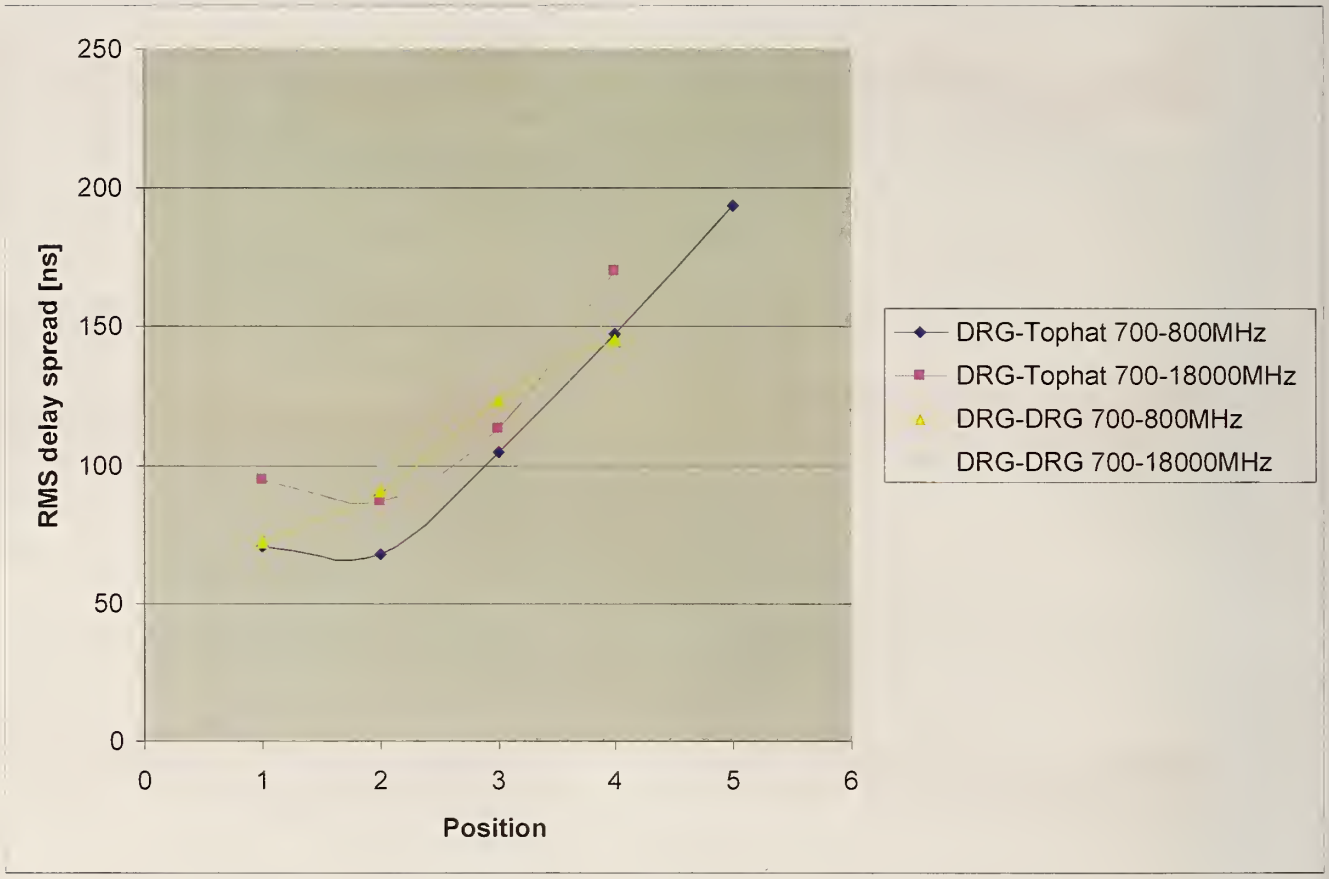

Figure 34. Colorado Convention Center RMS delay spread versus position for two antenna configurations and two different frequency bands. "DRG" refers to dual ridge guide horn. and is a directional antenna. "Tophat" refers to an omnidirectional receive antenna.

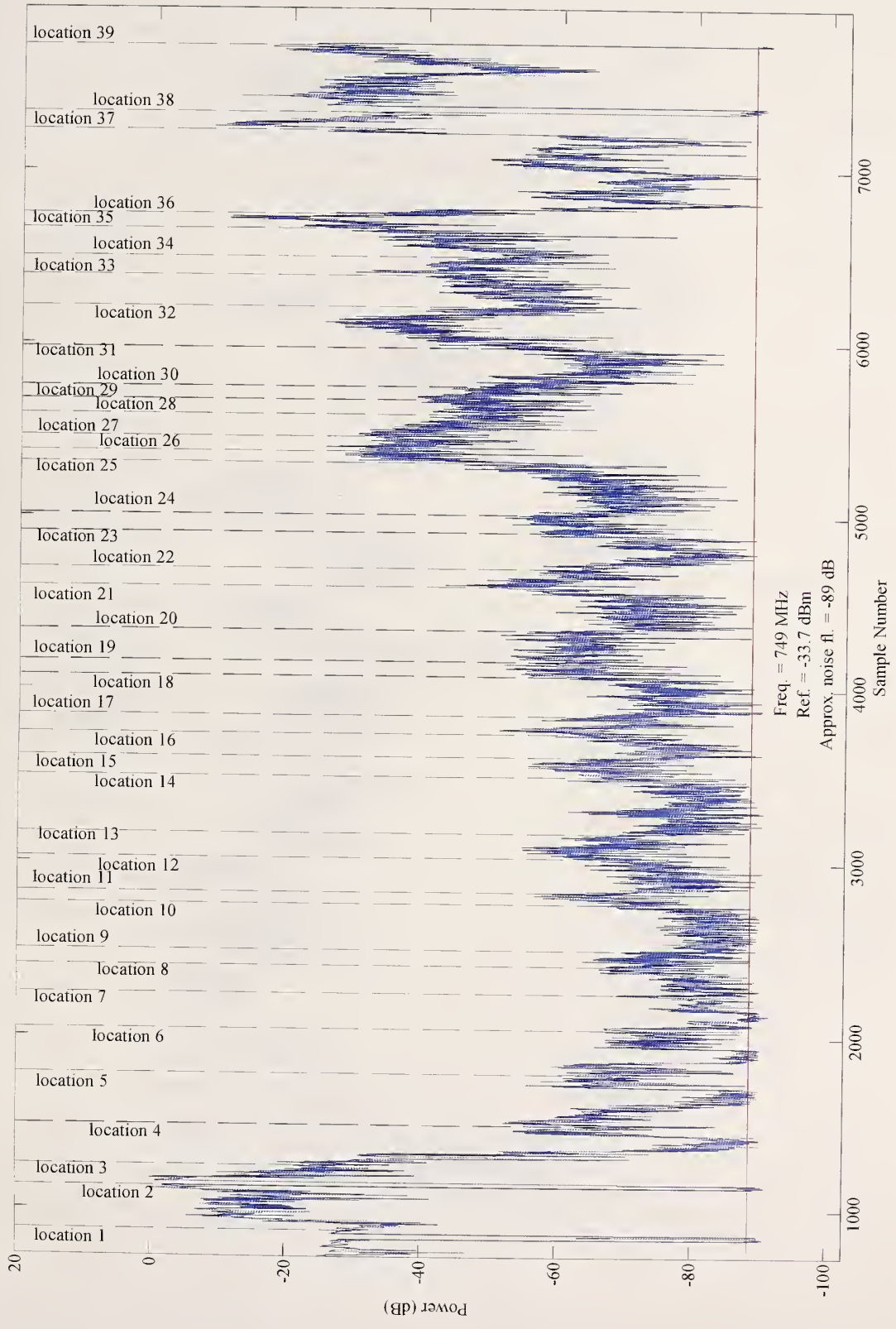

Figure 35. Republic Plaza, receive site 1. Normalized received signal power from the spectrum analyzer as the 749 MHz transmitter is carried through the building.

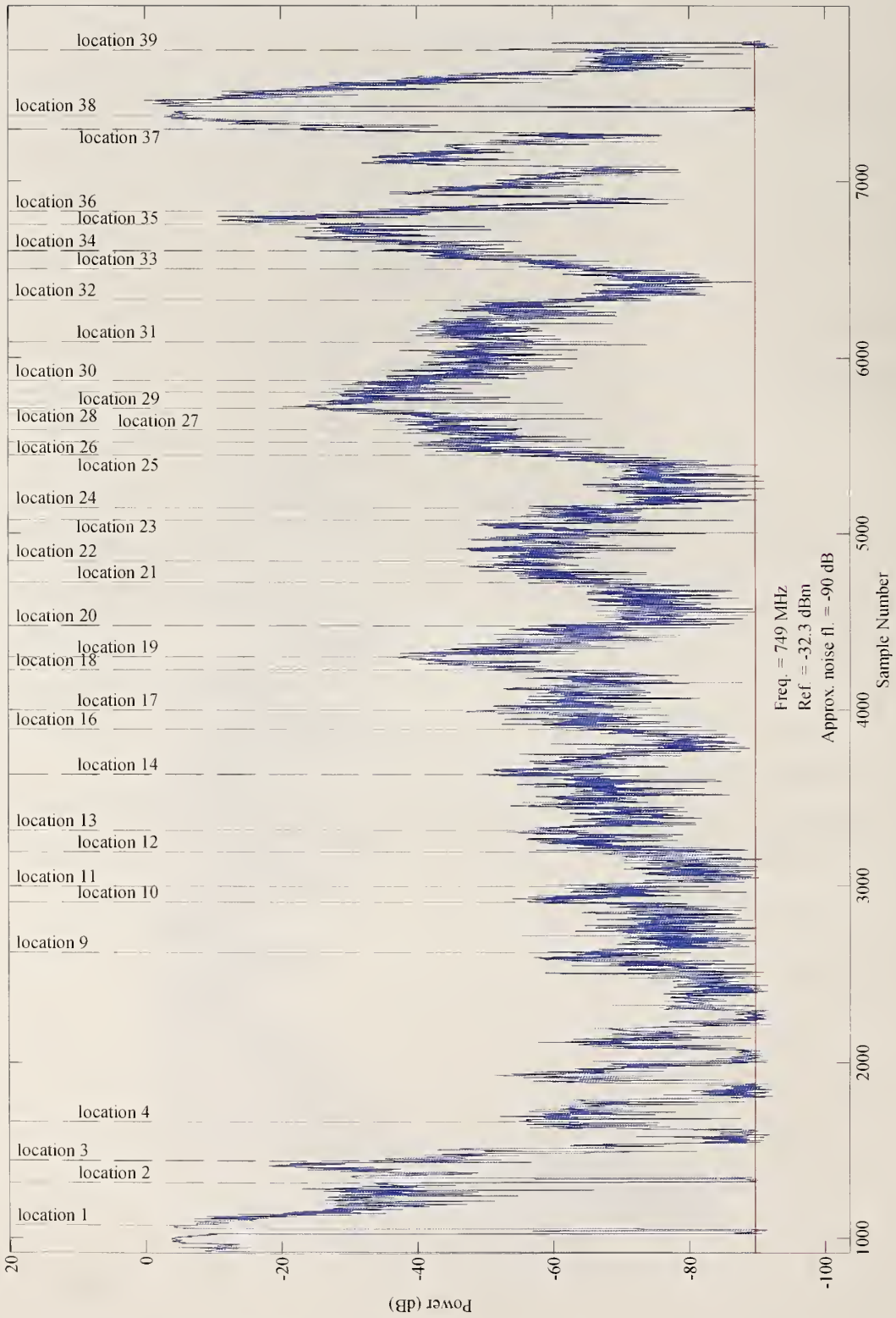

Figure 36. Republic Plaza, receive site 2. Normalized received signal power from the spectrum analyzer as the 749 MHz transmitter is carried through the building.

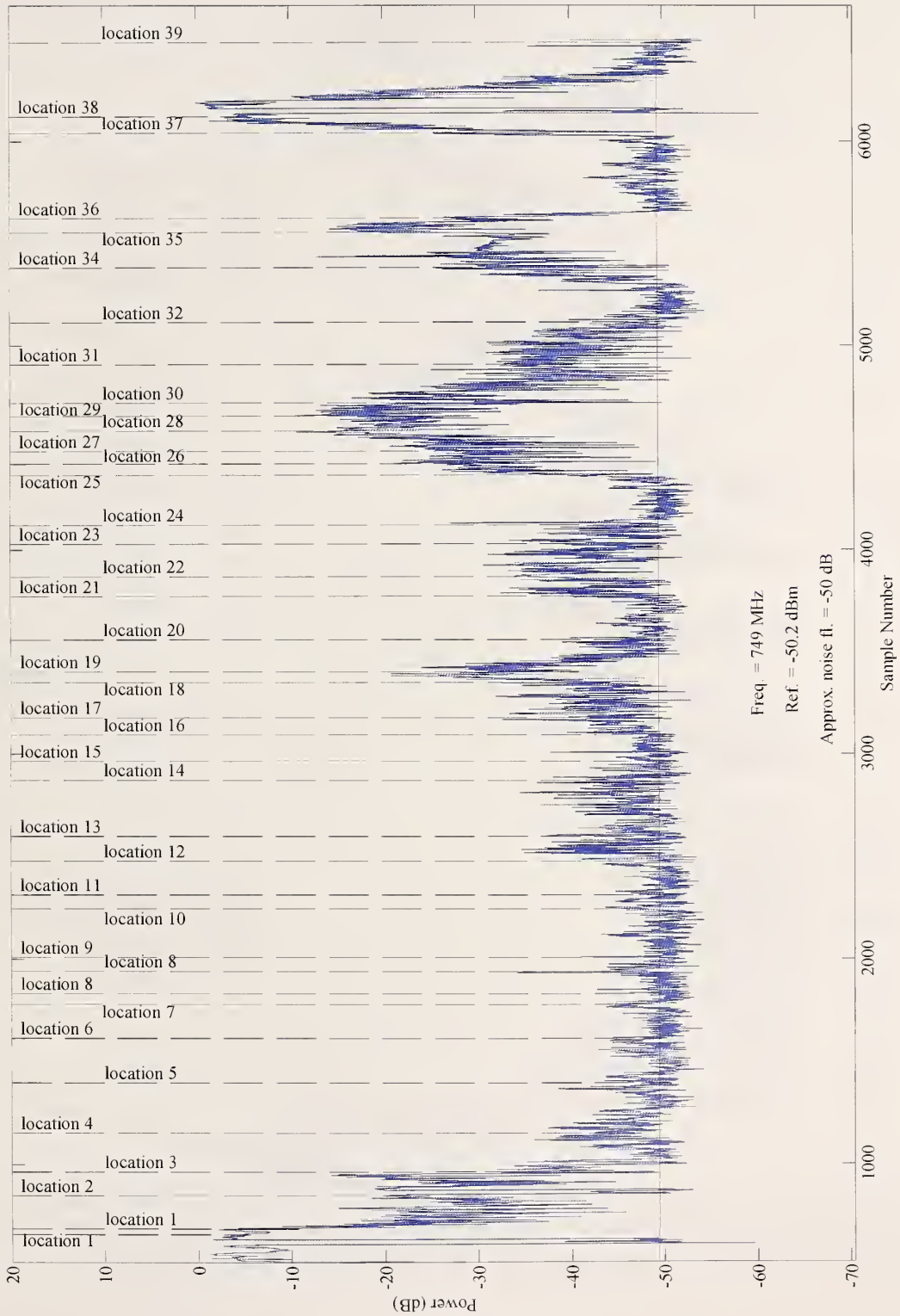

Figure 37. Republic Plaza, receive site 3. Normalized received signal power from the spectrum analyzer as the 749 MHz transmitter is carried through the building.

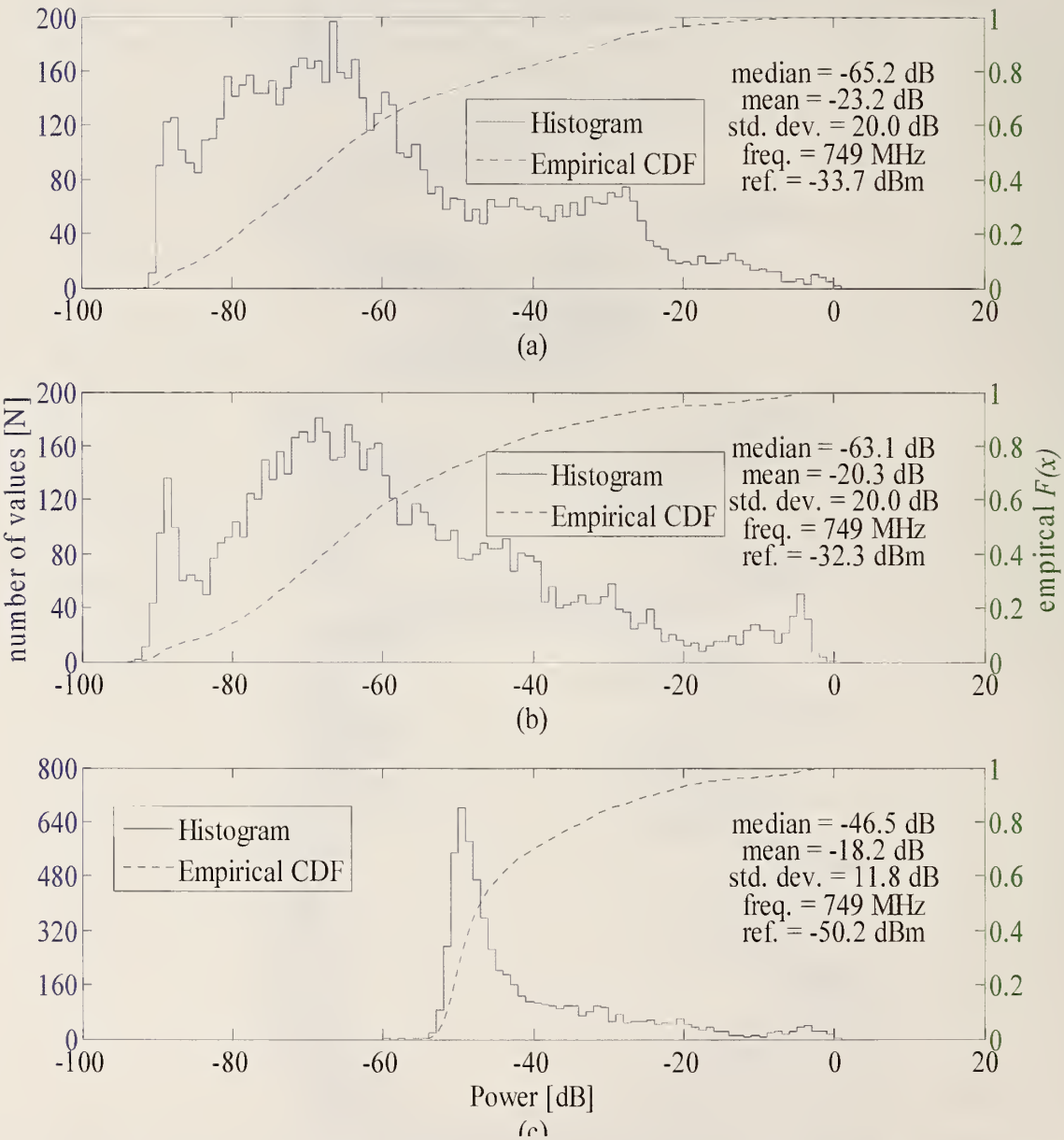

Figure 38. Histogram and empirical CDF of the received spectrum analyzer signal power at Republic Plaza for (a) receive site one, (b) receive site two, and (c) receive site three. Note that histogram count and the power scales are different for the receive site three, plot (c).

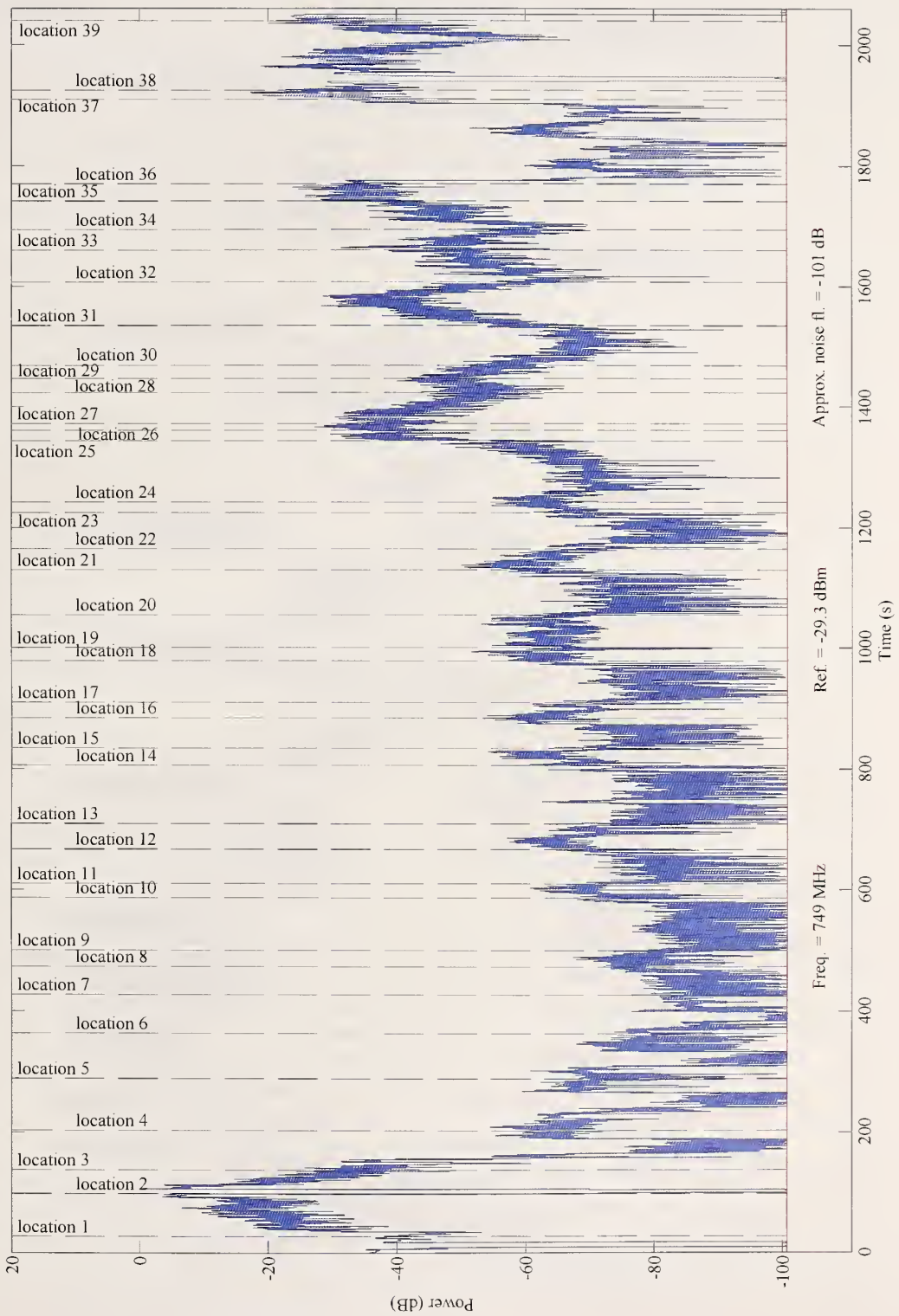

Figure 39. Republic Plaza, receive site 1. Normalized narrowband receiver signal power as 749 MHz transmitter is carried through the building.

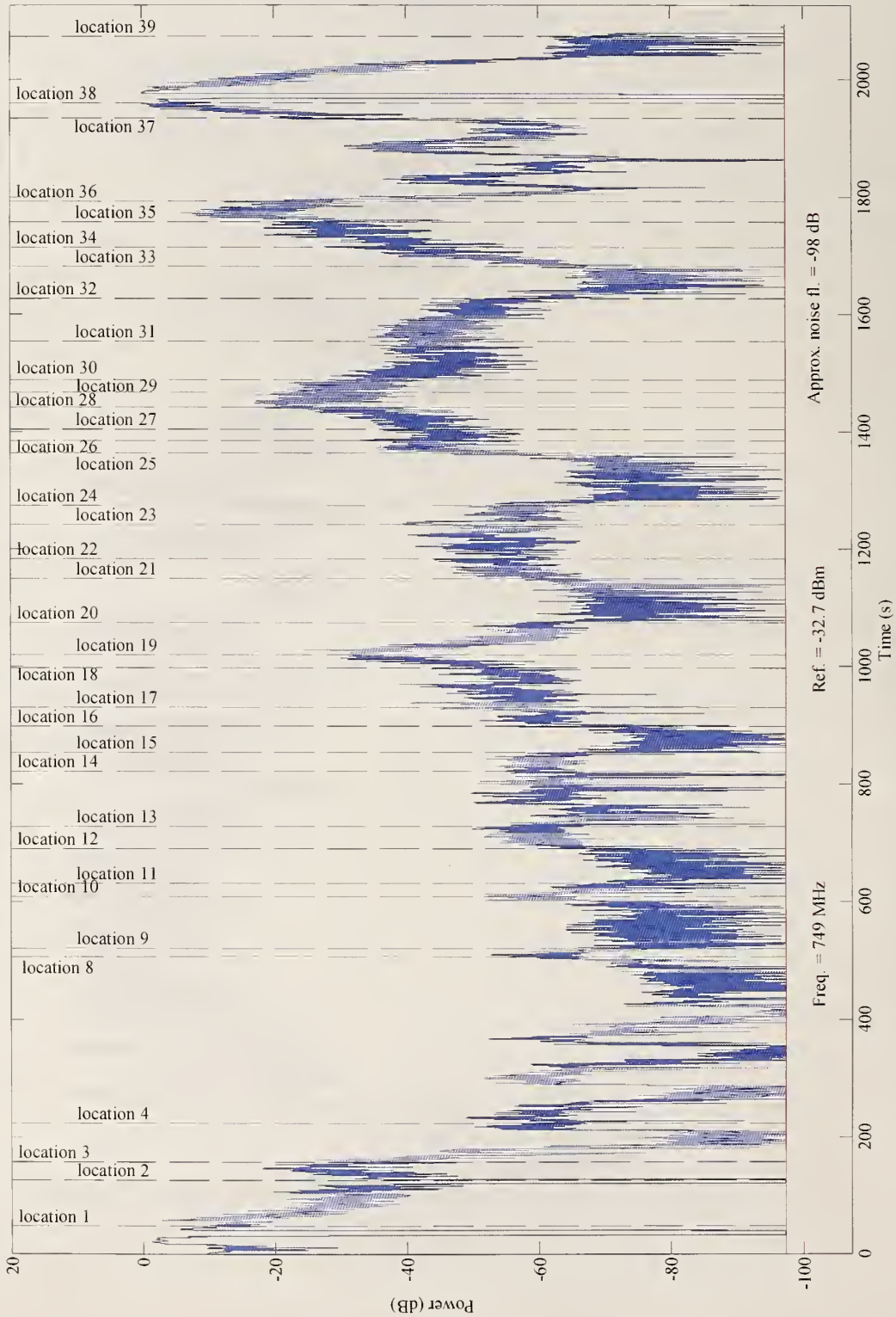

Figure 40. Republic Plaza, receive site 2. Normalized narrowband receiver signal power as 749 MHz transmitter is carried through the building.

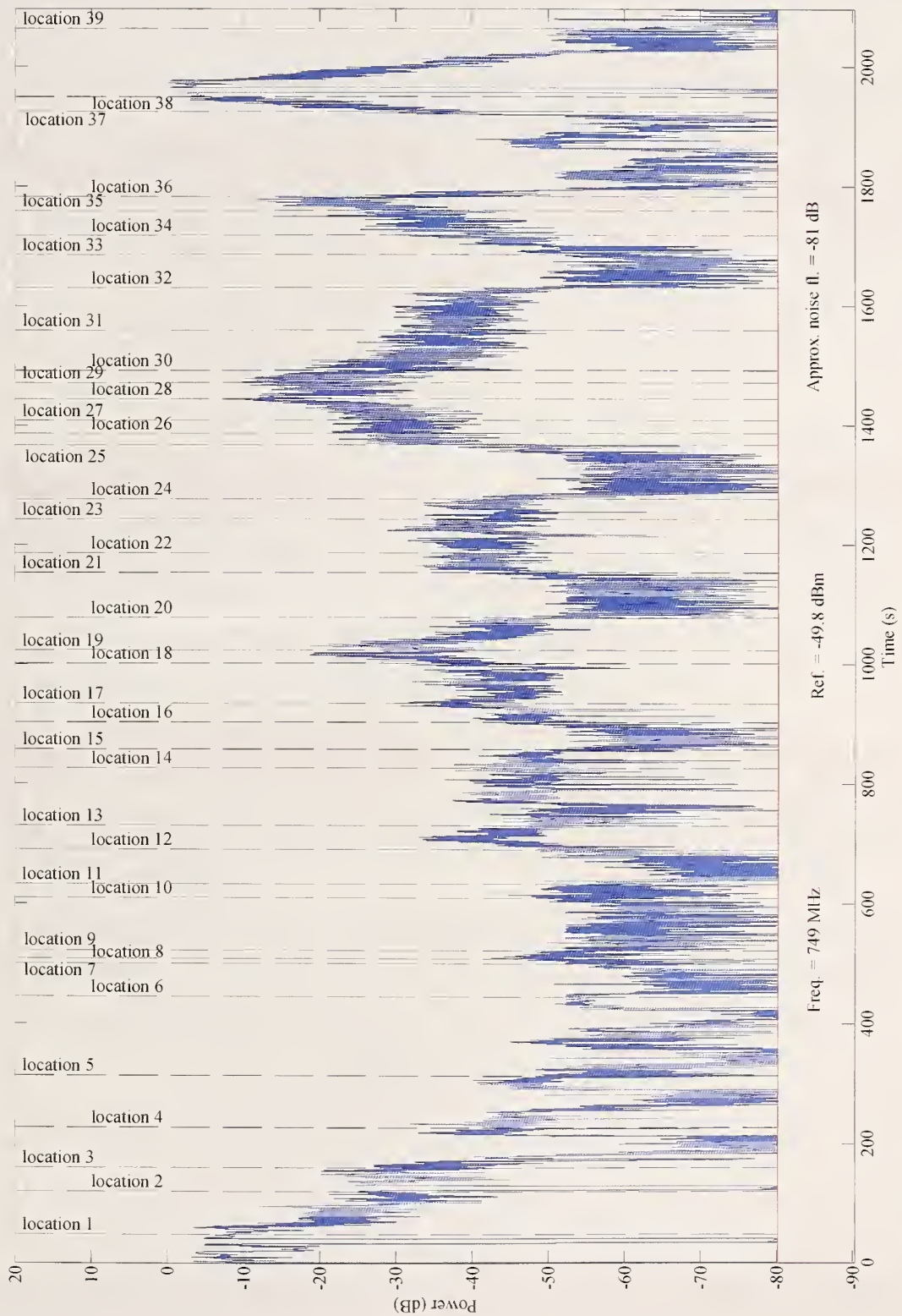

Figure 41. Republic Plaza, receive site 3. Normalized narrowband receiver signal power as 749 MHz transmitter is carried through the building.

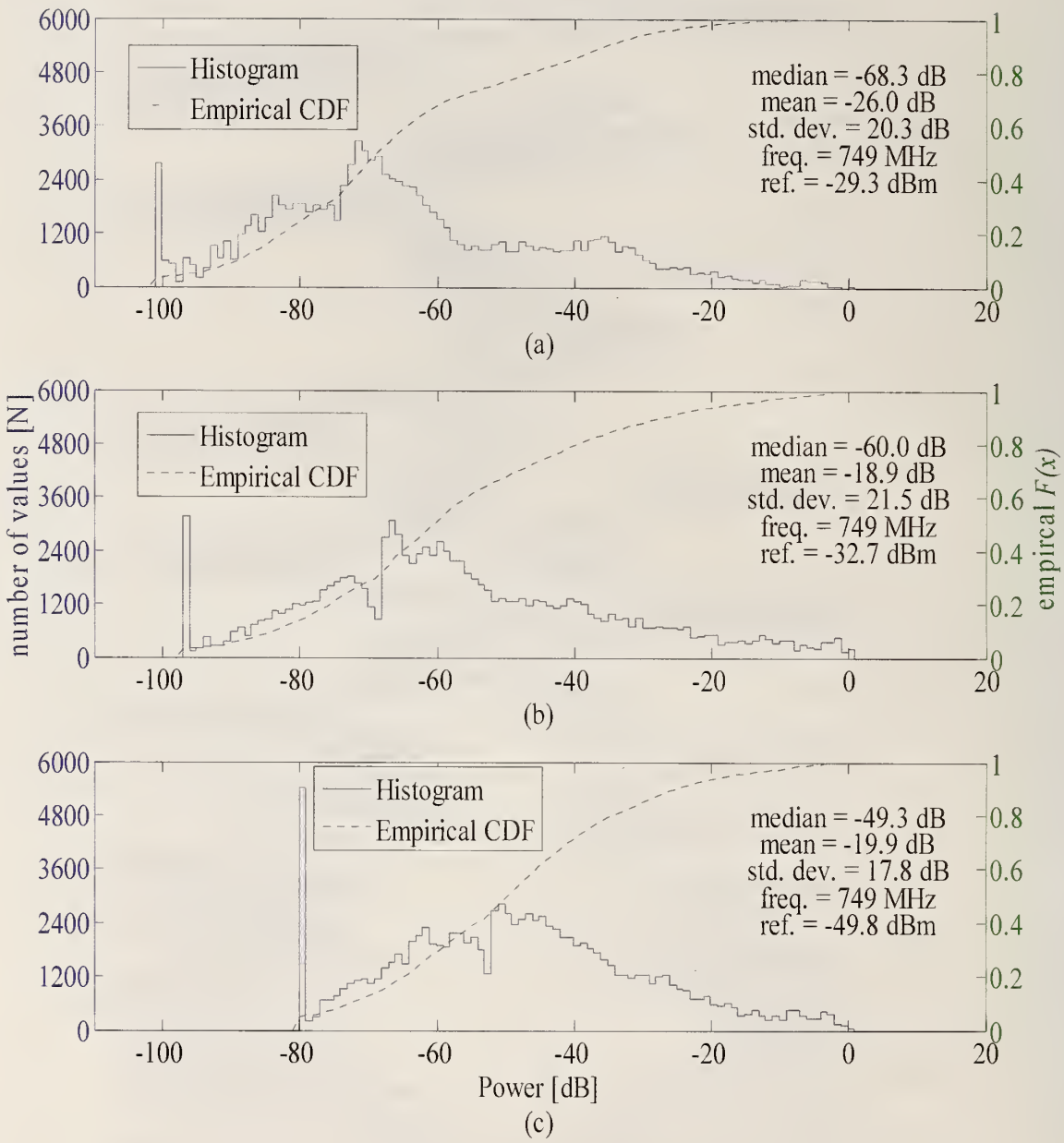

Figure 42. Histogram and empirical CDF of the narrowband receiver signal power at Republic Plaza for (a) receive site one, (b) receive site two, and (c) receive site three. Note that the discontinuities near the centers of the histograms are not due to the environment, but rather an artifact of the testing equipment.

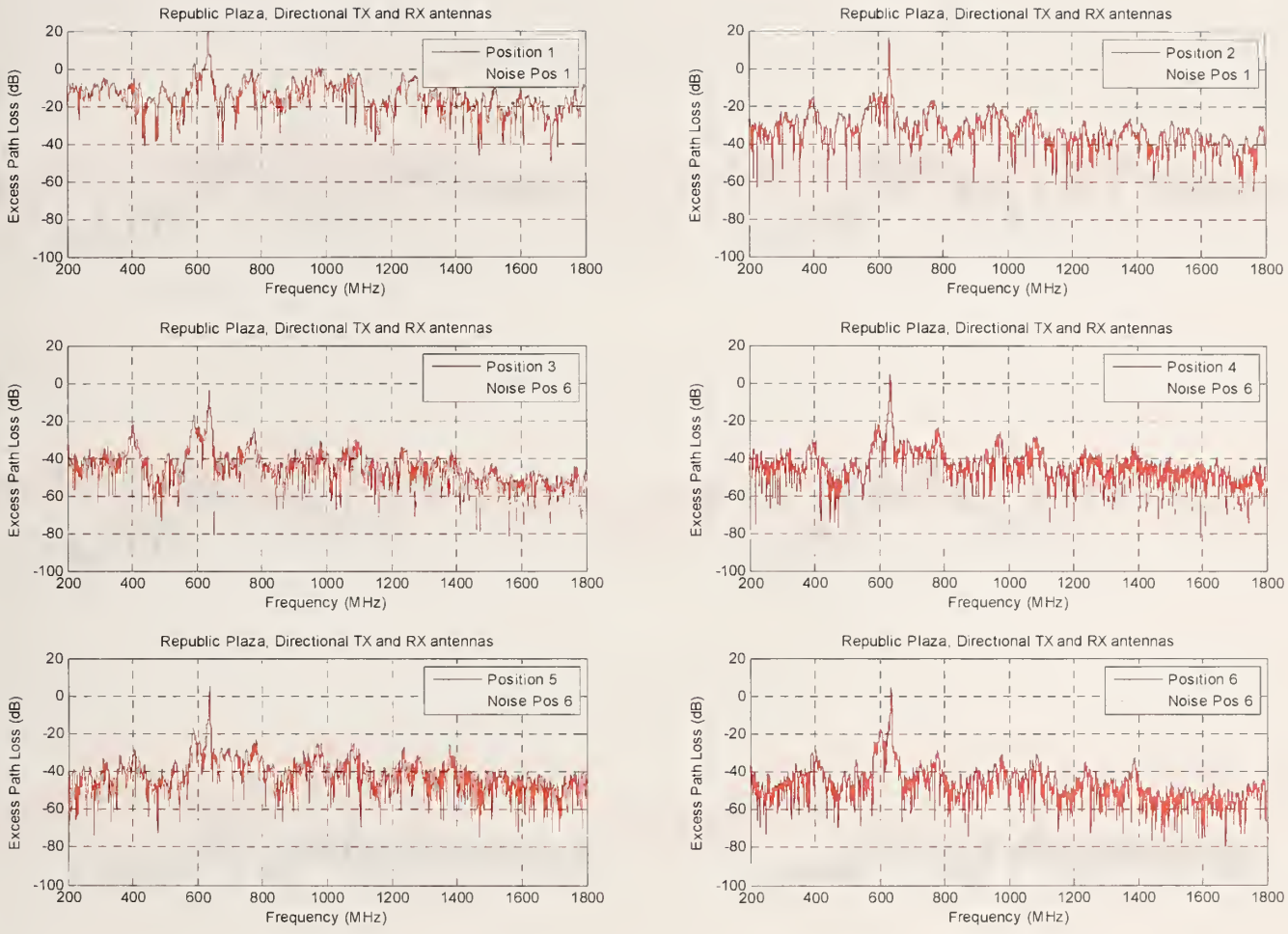

Figure 43. Republic Plaza 200 MHz to 1800 MHz VNA excess path loss measurements for positions 1 through 6.

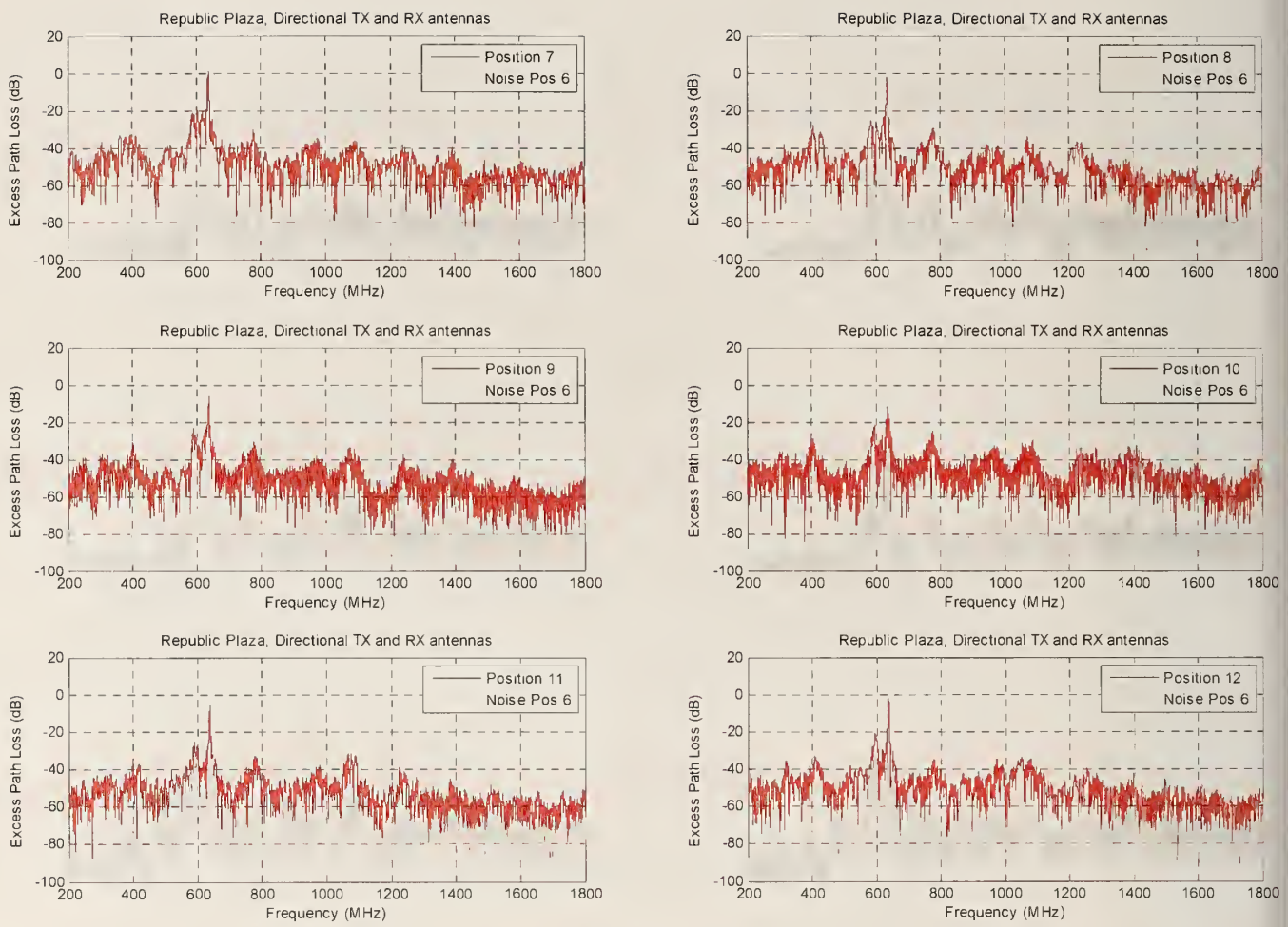

Figure 44. Republic Plaza 200 MHz to 1800 MHz VNA excess path loss measurements for positions 7 through 12.

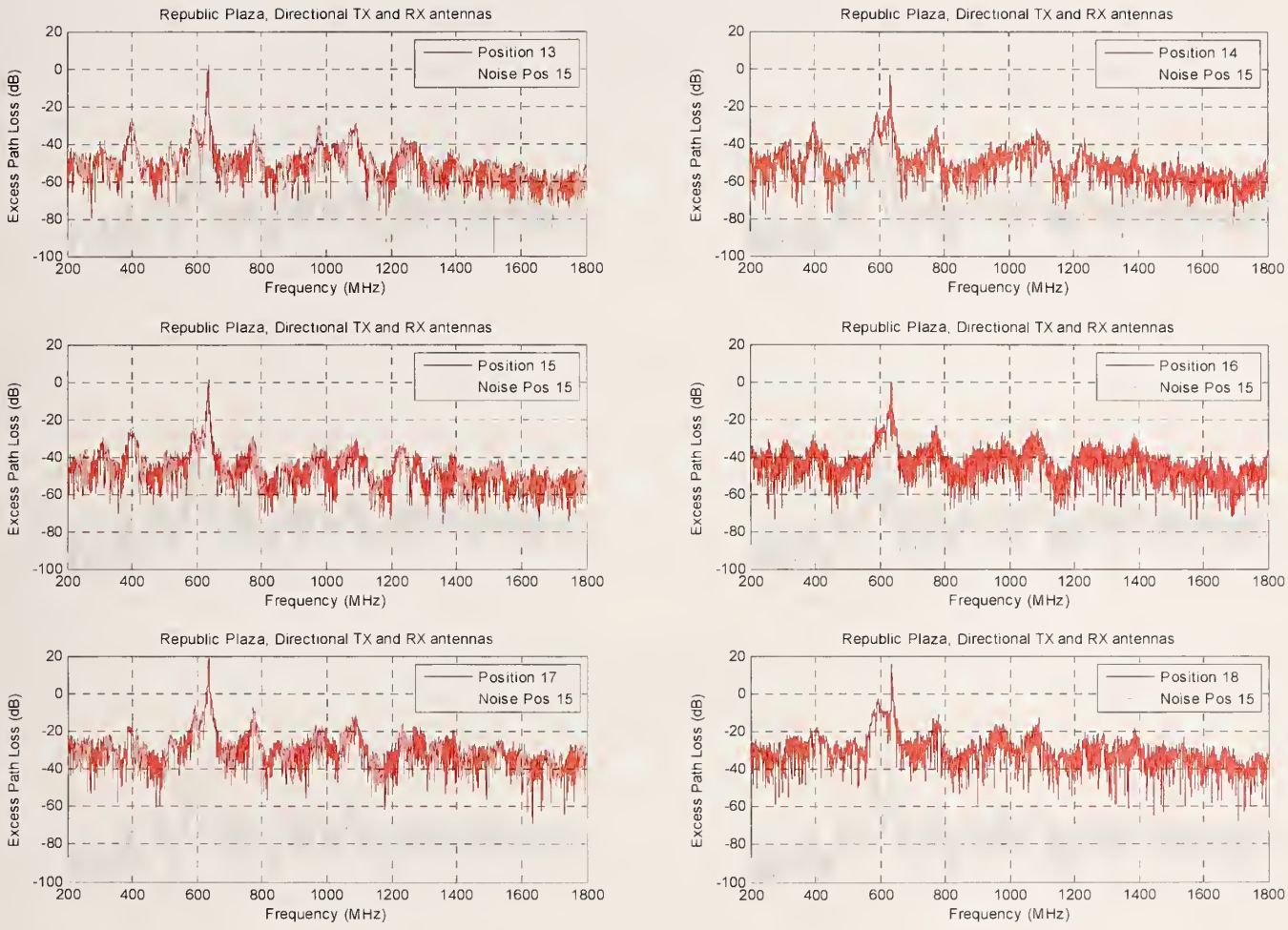

Figure 45. Republic Plaza 200 MHz to 1800 MHz VNA excess path loss measurements for positions 13 through 18.

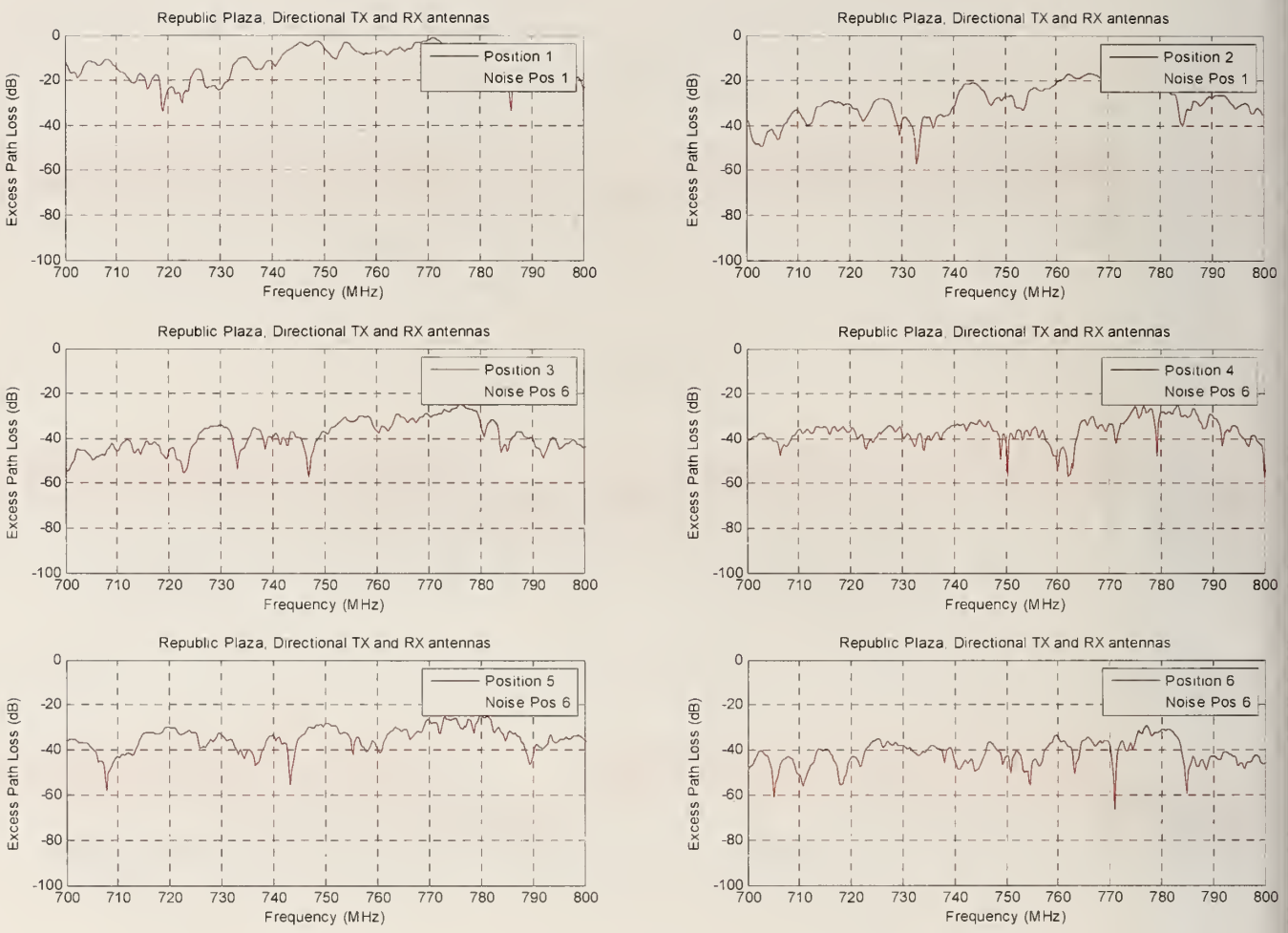

Figure 46. Republic Plaza 700 to 800 MHz VNA excess path loss measurements for positions 1 through 6.

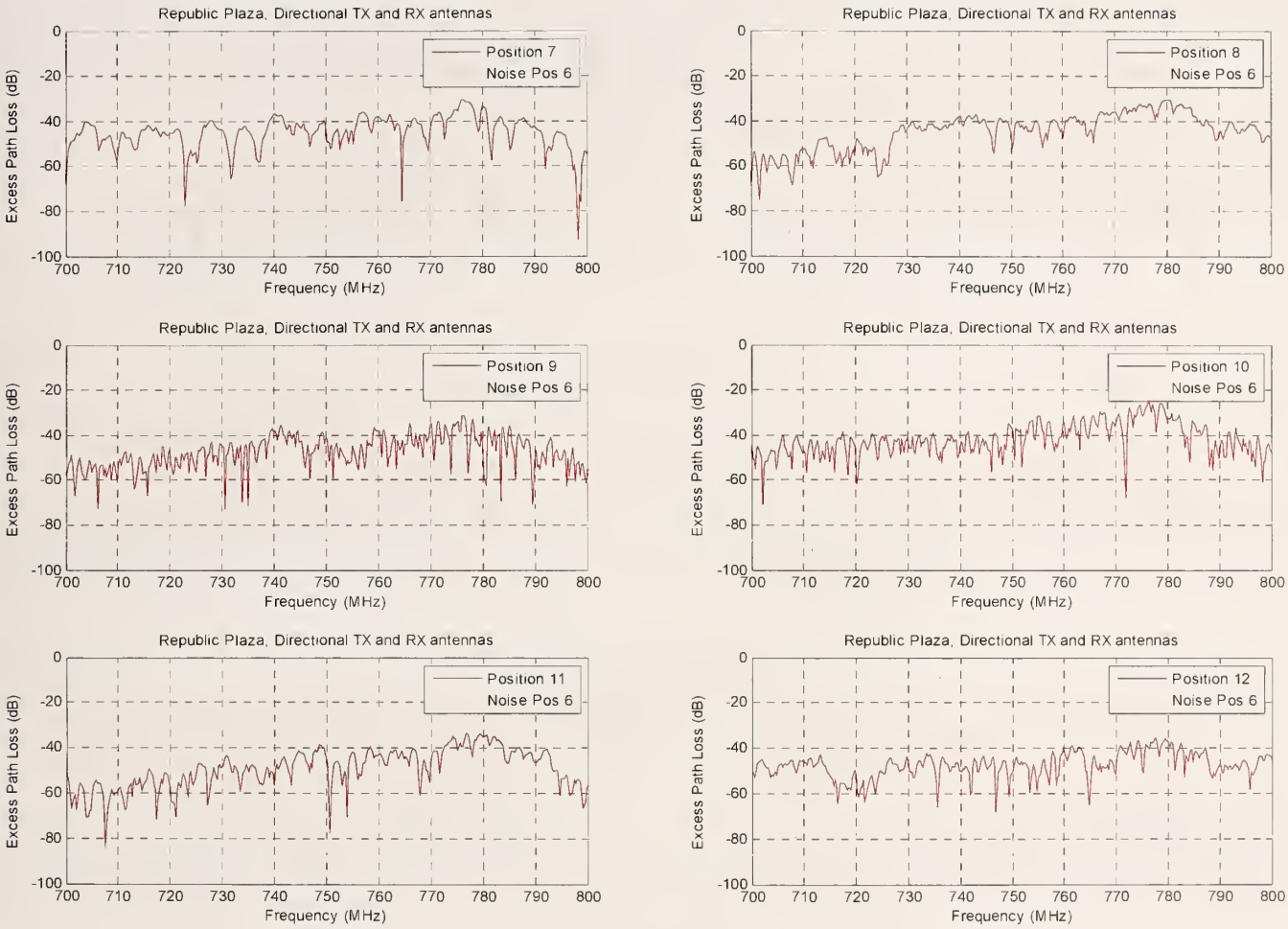

Figure 47. Republic Plaza 700 to 800 MHz VNA excess path loss measurements for positions 7 through 12.

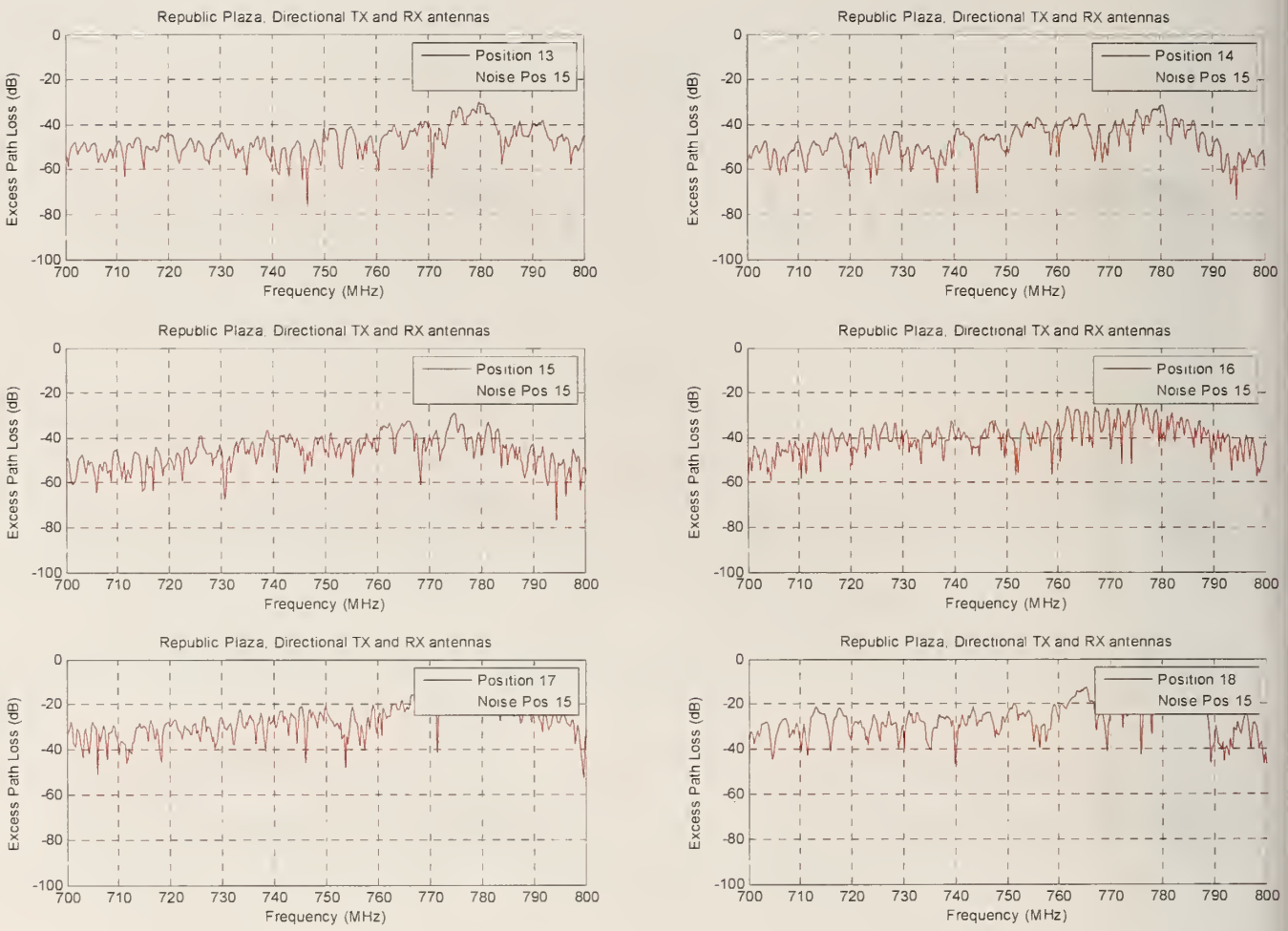

Figure 48. Republic Plaza 700 to 800 MHz VNA excess path loss measurements for positions 13 through 18.

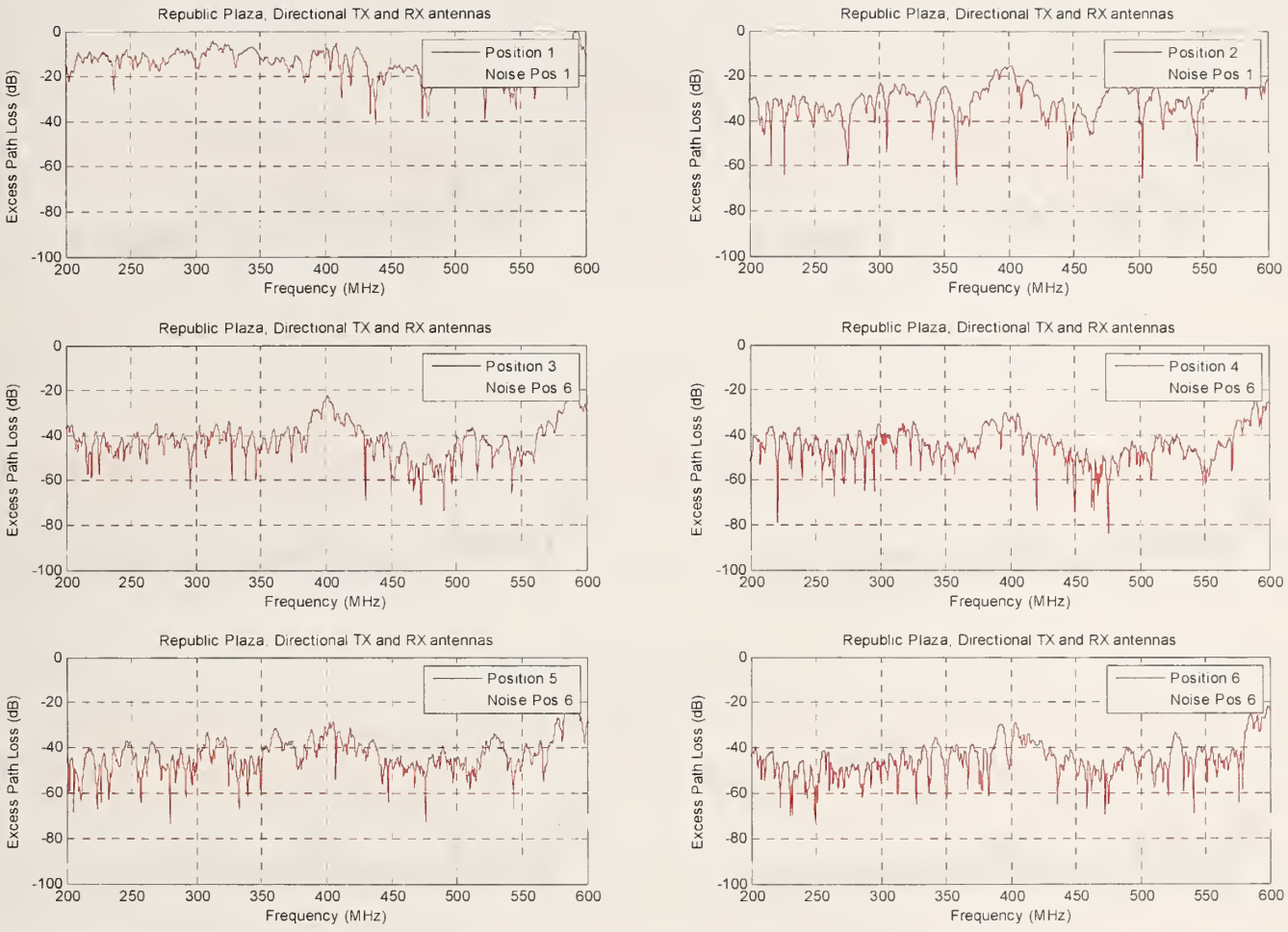

Figure 49. Republic Plaza 200 to 600 MHz VNA excess path loss measurements for positions 1 through 6.

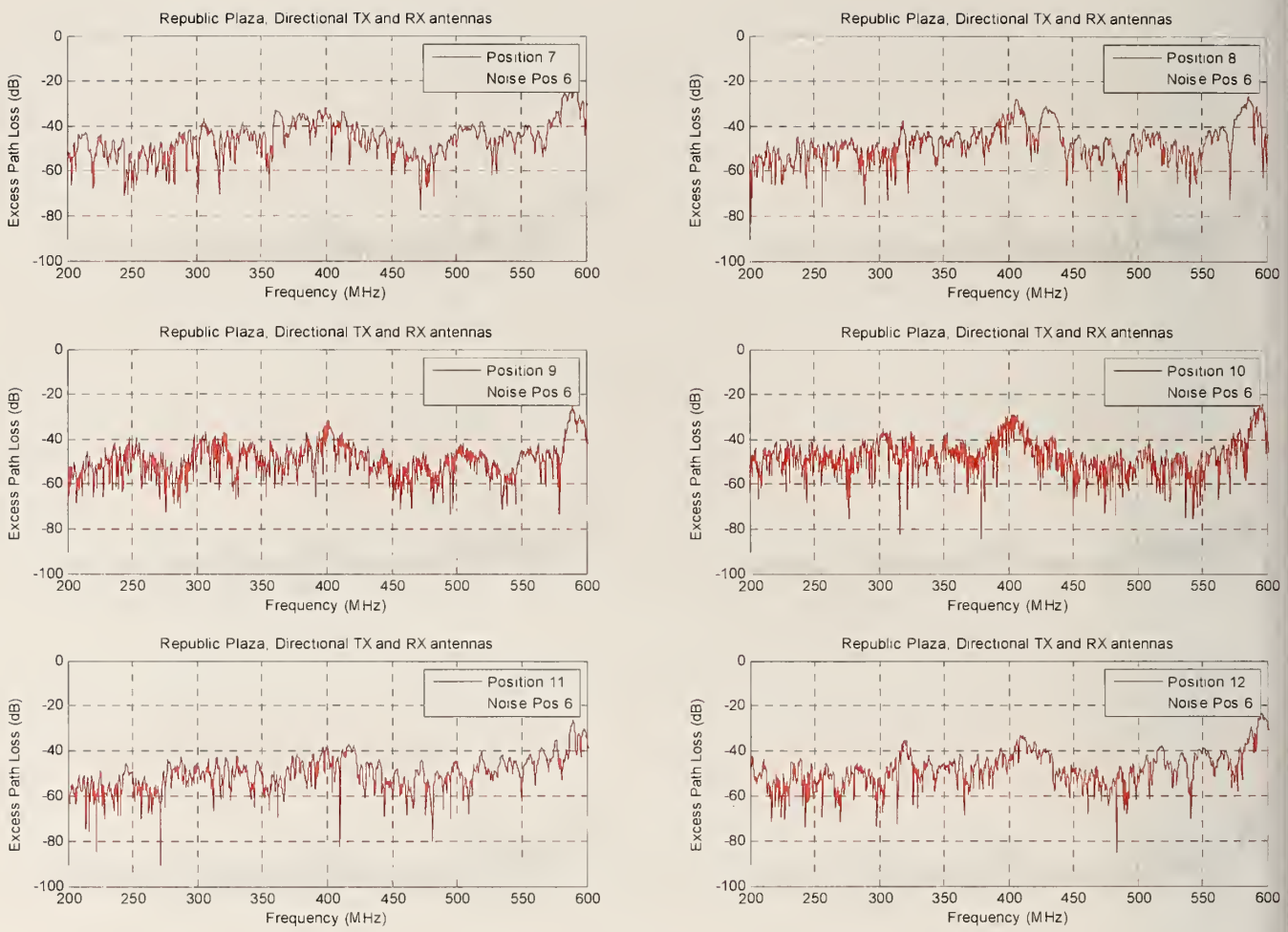

Figure 50. Republic Plaza 200 to 600 MHz VNA excess path loss measurements for positions 7 through 12.

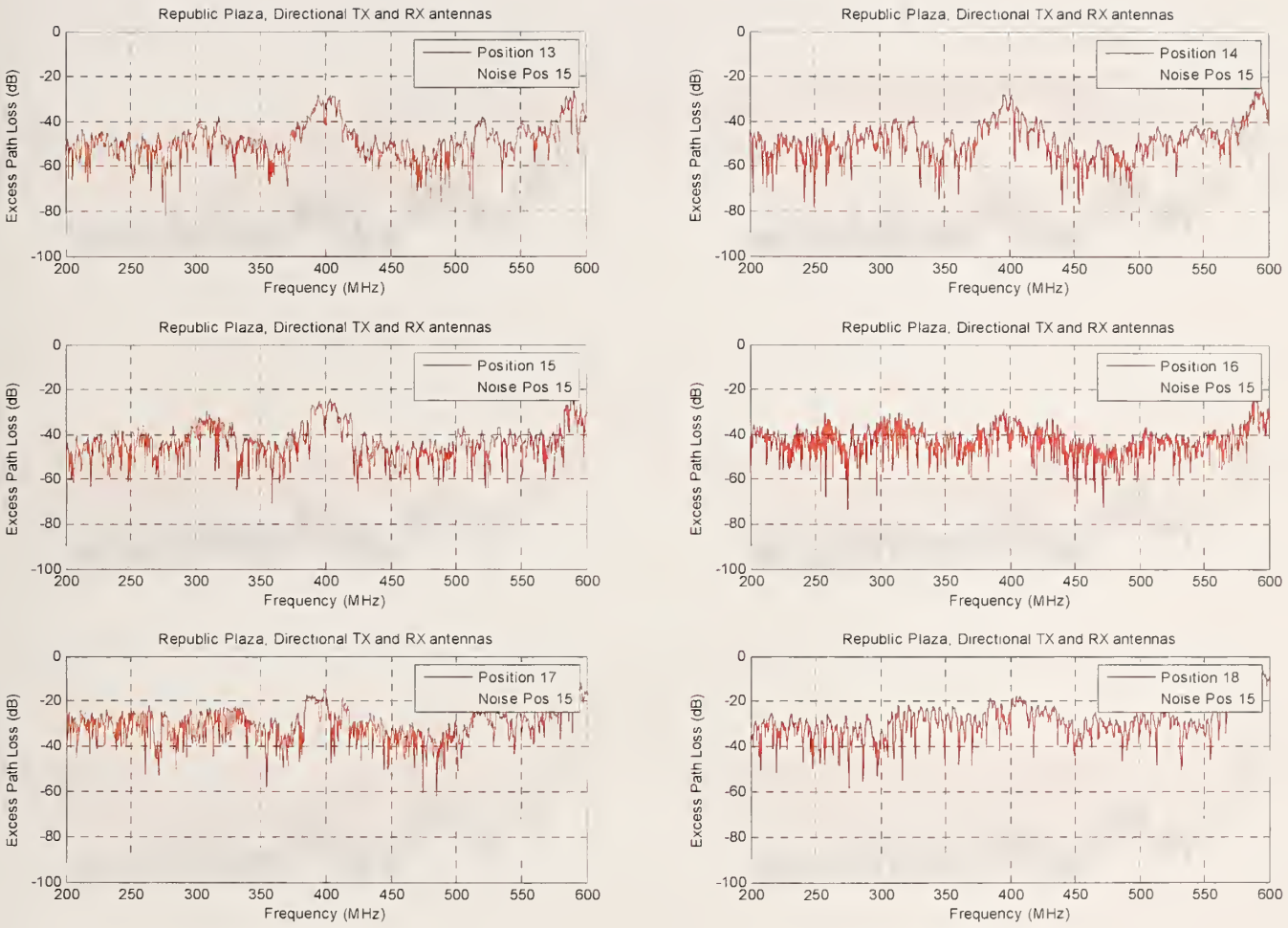

Figure 51. Republic Plaza 200 to 600 MHz VNA excess path loss measurements for positions 13 through 18.

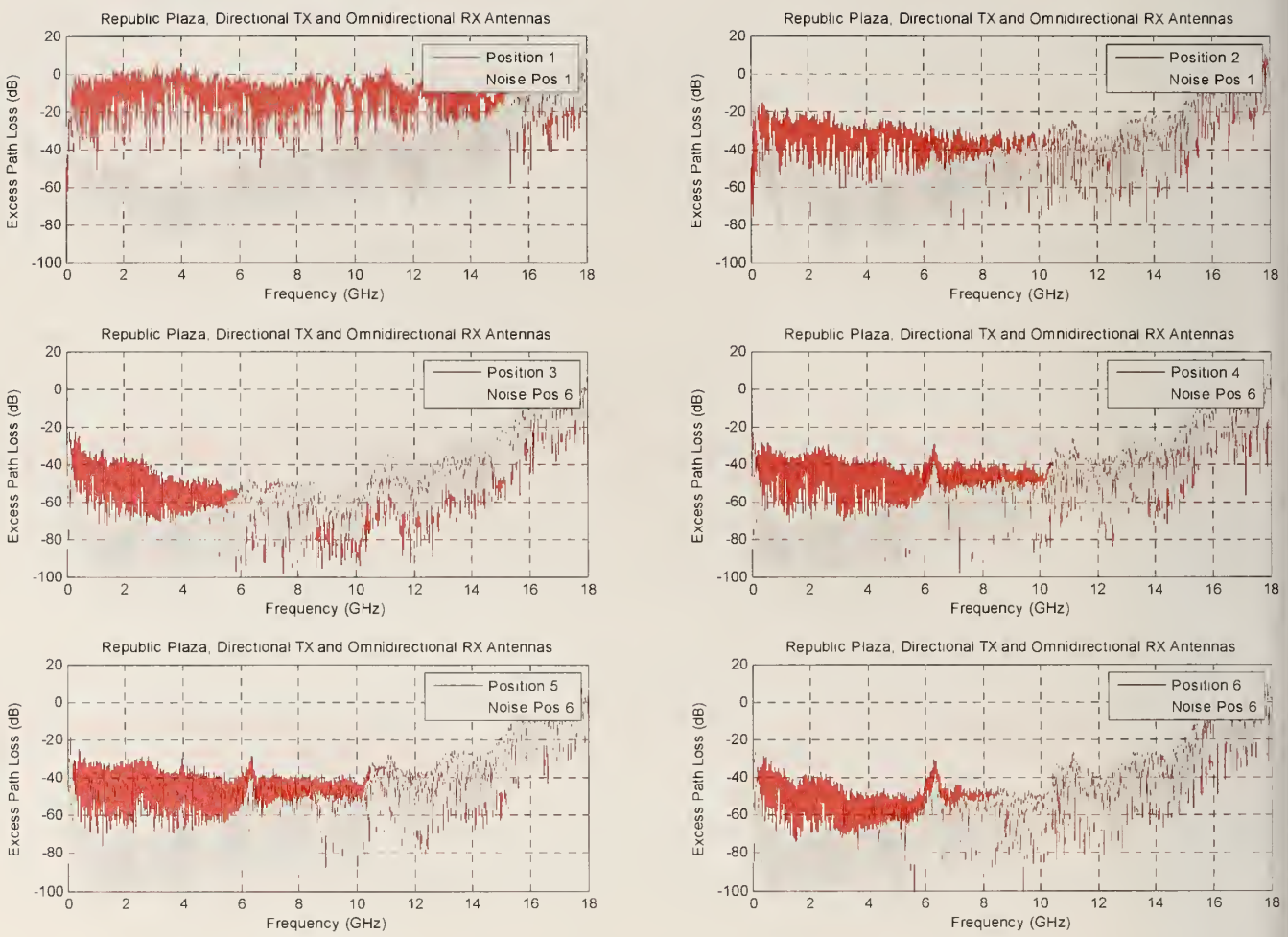

Figure 52. Republic Plaza 700 MHz to 18 GHz VNA excess path loss measurements for positions 1 through 6.

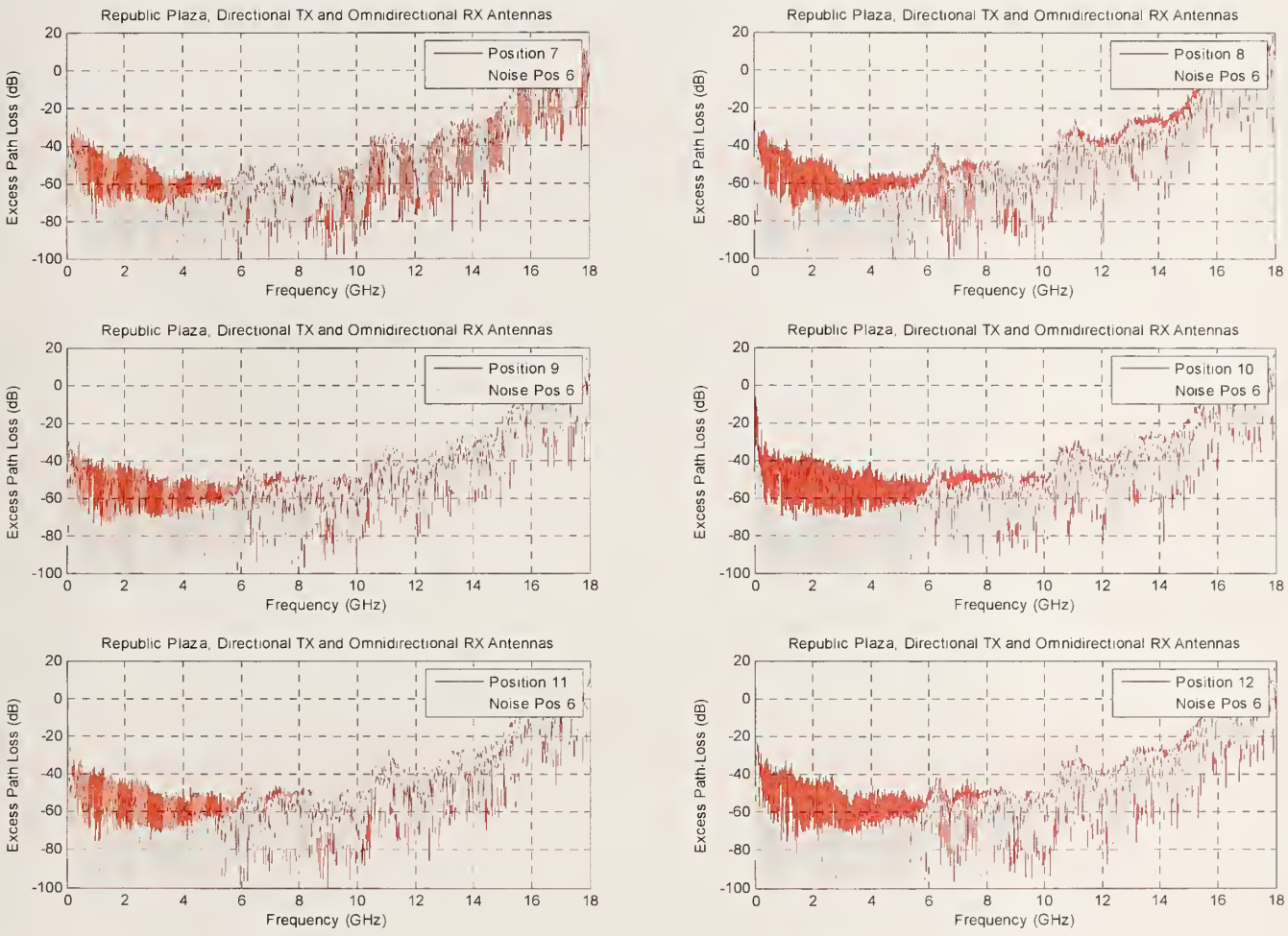

Figure 53. Republic Plaza 700 MHz to 18 GHz VNA excess path loss measurements for positions 7 through 12.

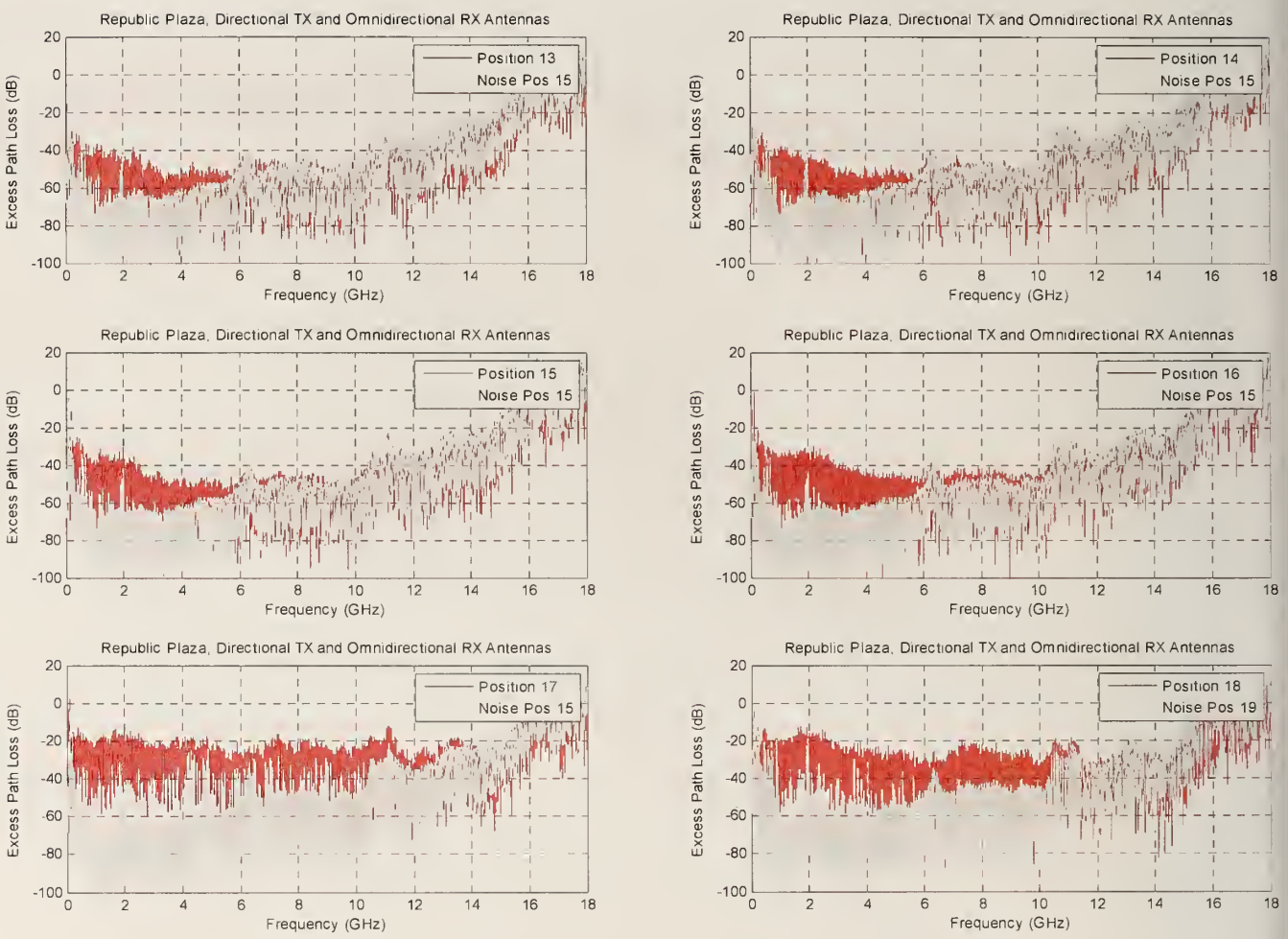

Figure 54. Republic Plaza 700 MHz to 18 GHz VNA excess path loss measurements for positions 13 through 18.

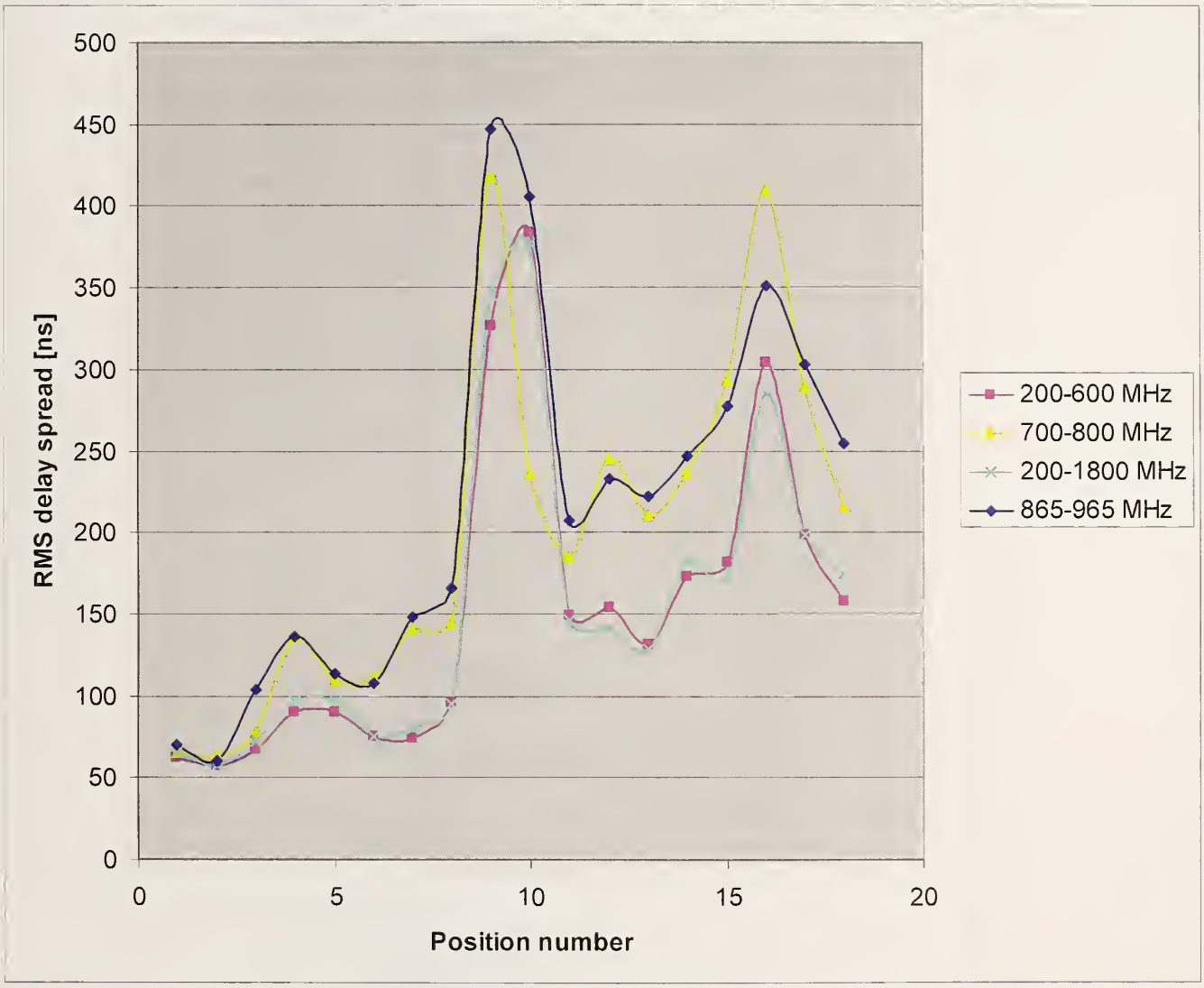

Figure 55. Republic Plaza RMS delay spread versus position based on four different frequency bands.

Table 4. Legend for locations in the Horizon West walk-through plots shown in Figures 56, 57, 59 and 60 below.

Index	Description	Index	Description
1	Building entrance	33	7th floor location 12
2	1st floor south	34	7th floor location 11
3	2nd floor south	35	7th floor location 10
4	2nd floor location 3	36	7th floor location 9
5	2nd floor location 2	37	7th floor location 8
6	2nd floor location 1	38	7th floor room 707
7	2nd floor location 0	39	7th floor location 7
8	2nd floor location 4	40	7th floor location 6
9	2nd floor location 5	41	7th floor location 5
10	2nd floor location 6	42	7th floor location 0
11	2nd floor location 7	43	7th floor location 4
12	2nd floor location 8	44	7th floor location 0
13	2nd floor location 9	45	7th floor location 1
14	2nd floor location 10	46	7th floor location 2
15	2nd floor location 11	47	7th floor location 3
16	2nd floor location 12	48	7th floor south
17	2nd floor location 13	49	8th floor south
18	2nd floor north	50	8th floor elevator
19	3rd floor north	51	8th floor north
20	3rd elevator	52	9th floor north
21	3rd floor south	53	9th floor elevator
22	4th floor south	54	10th floor south
23	4th floor elevator	55	10th floor elevator
24	4th floor north	56	10th floor north
25	5th floor north	57	11th floor north
26	5th floor elevator	58	11th floor elevator
27	5th floor south	59	11th floor south
28	6th floor south	60	11th floor wait for elevator
29	6th floor elevator	61	11th floor elevator in
30	6th floor north	62	1st floor elevator out
31	7th floor north	63	outside building south
32	7th floor location 13	64	Reference

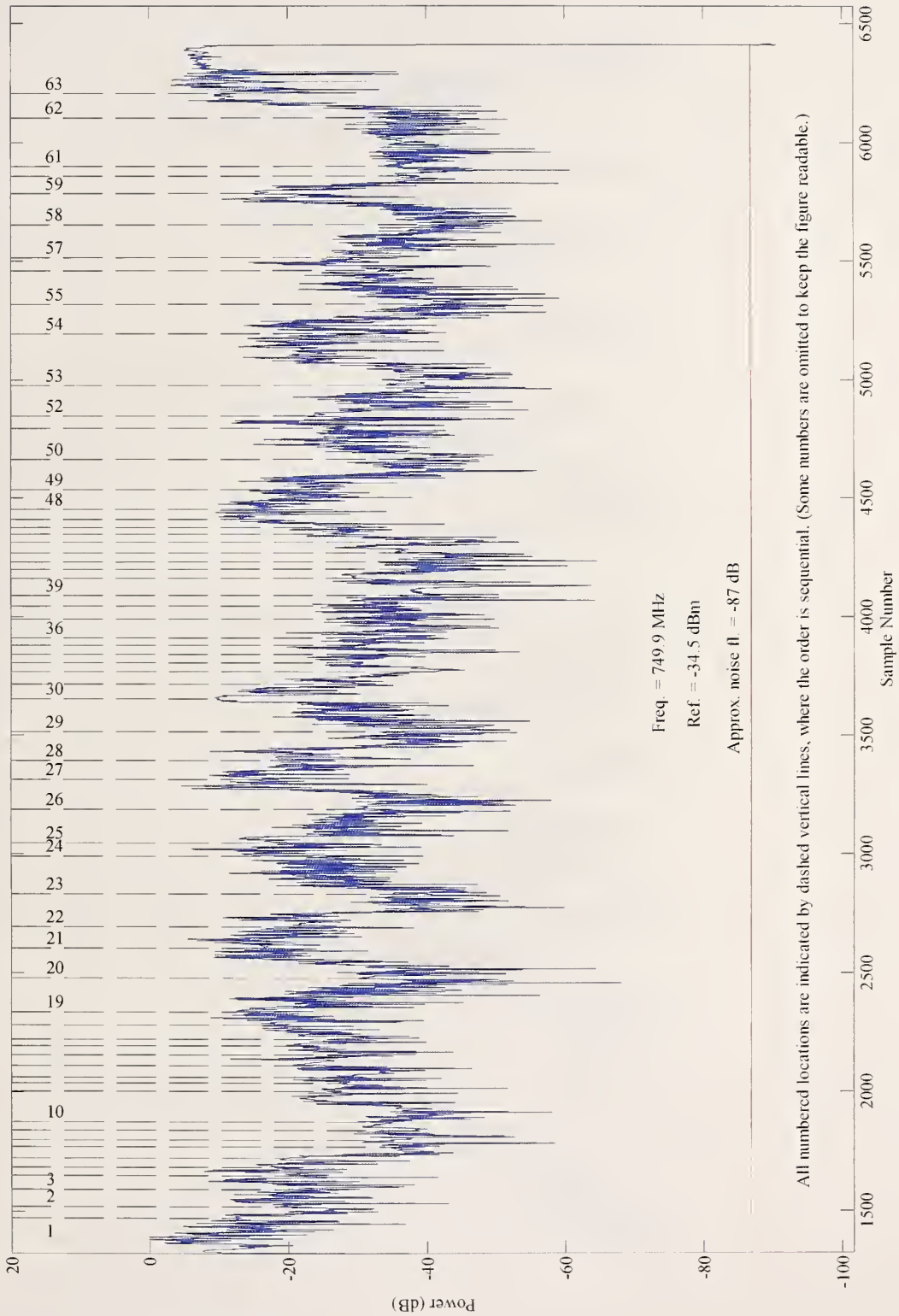

Figure 56. Horizon West. receive site 1. Normalized received signal power from the spectrum analyzer as the 750 MHz transmitter is carried through the building.

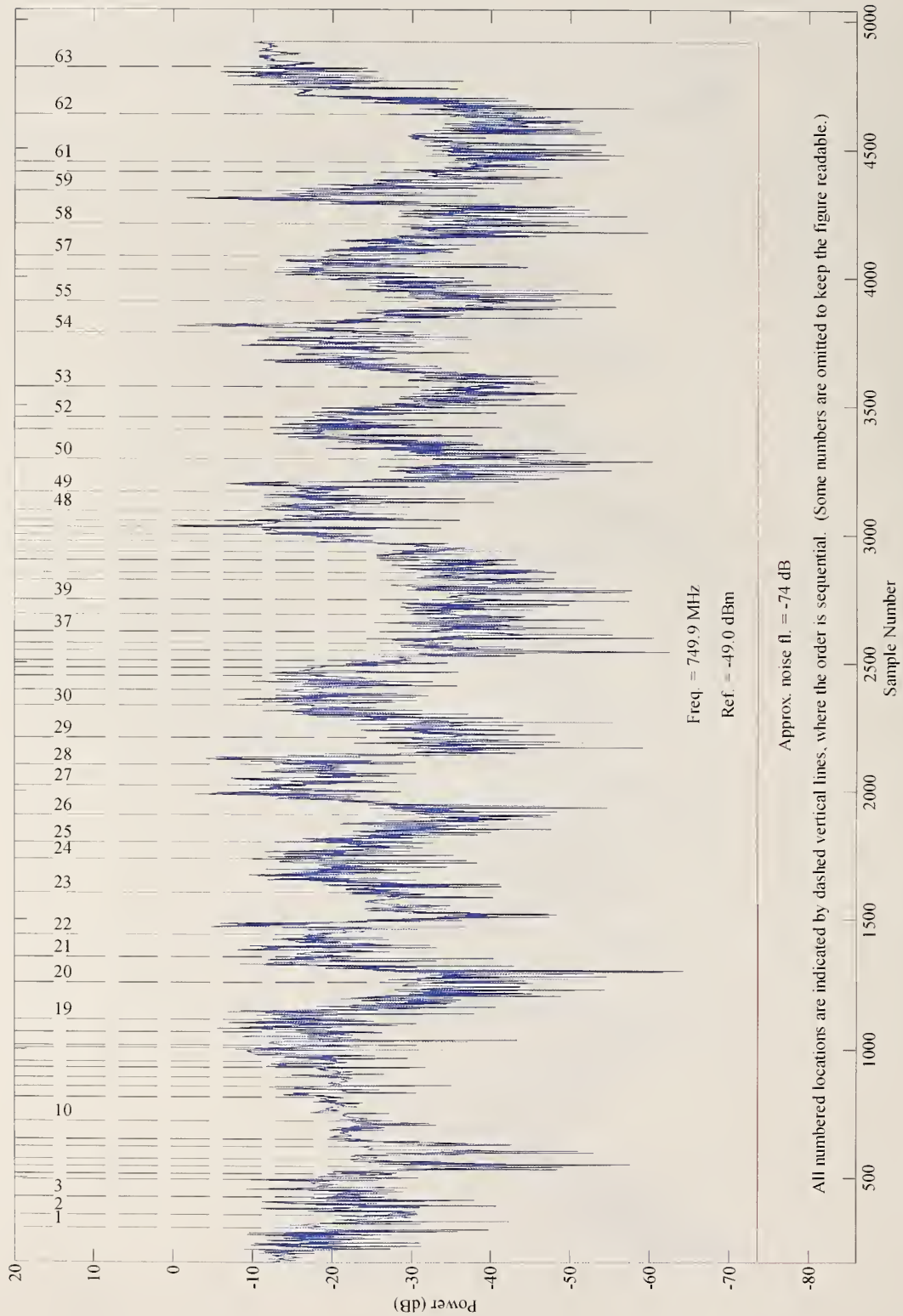

Figure 57. Horizon West, receive site 2. Normalized received signal power from the spectrum analyzer as the 750 MHz transmitter is carried through the building.

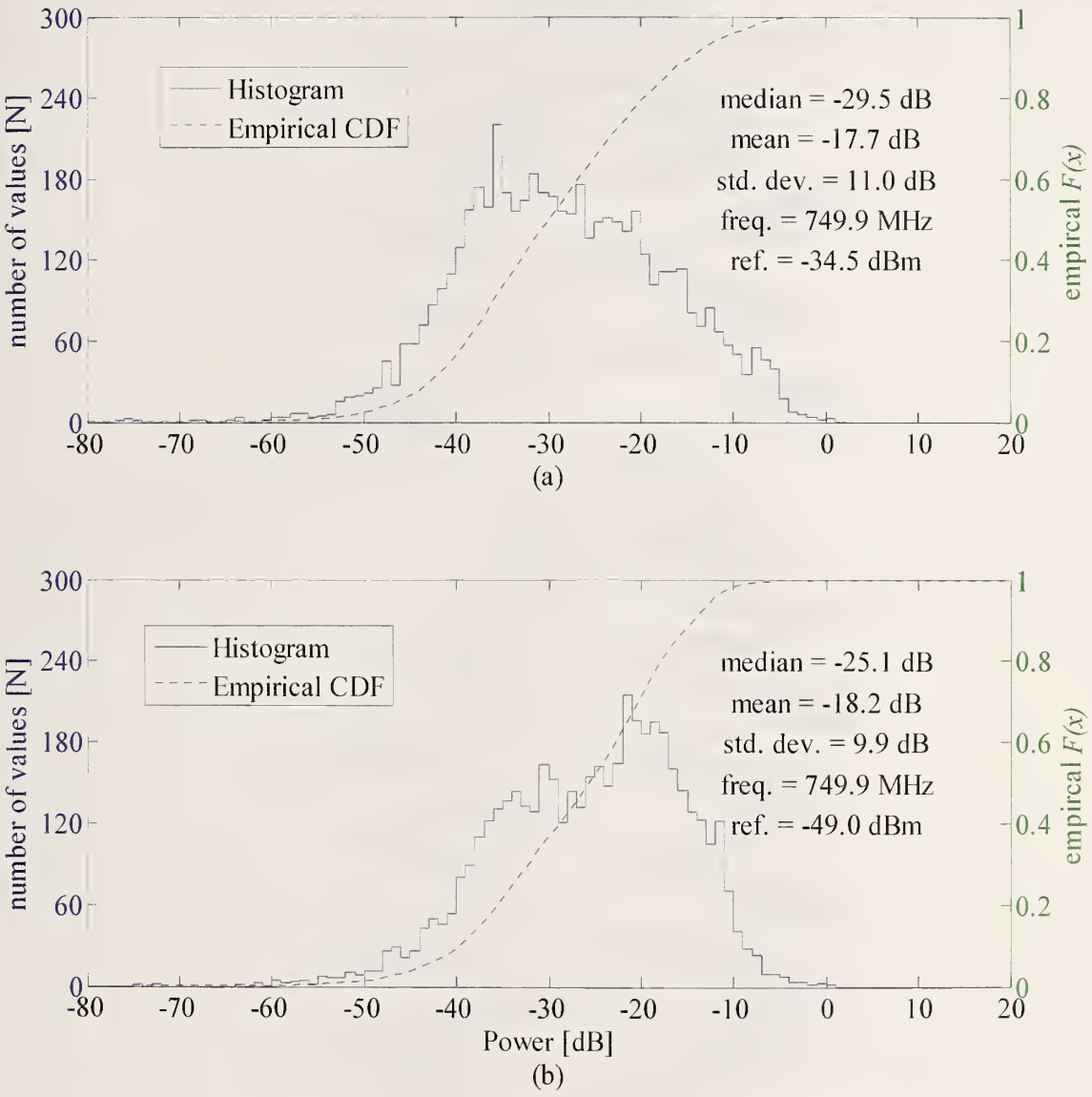

Figure 58. Histogram and empirical CDF of the received spectrum analyzer signal power at Horizon West for (a) receive site one and (b) receive site two.

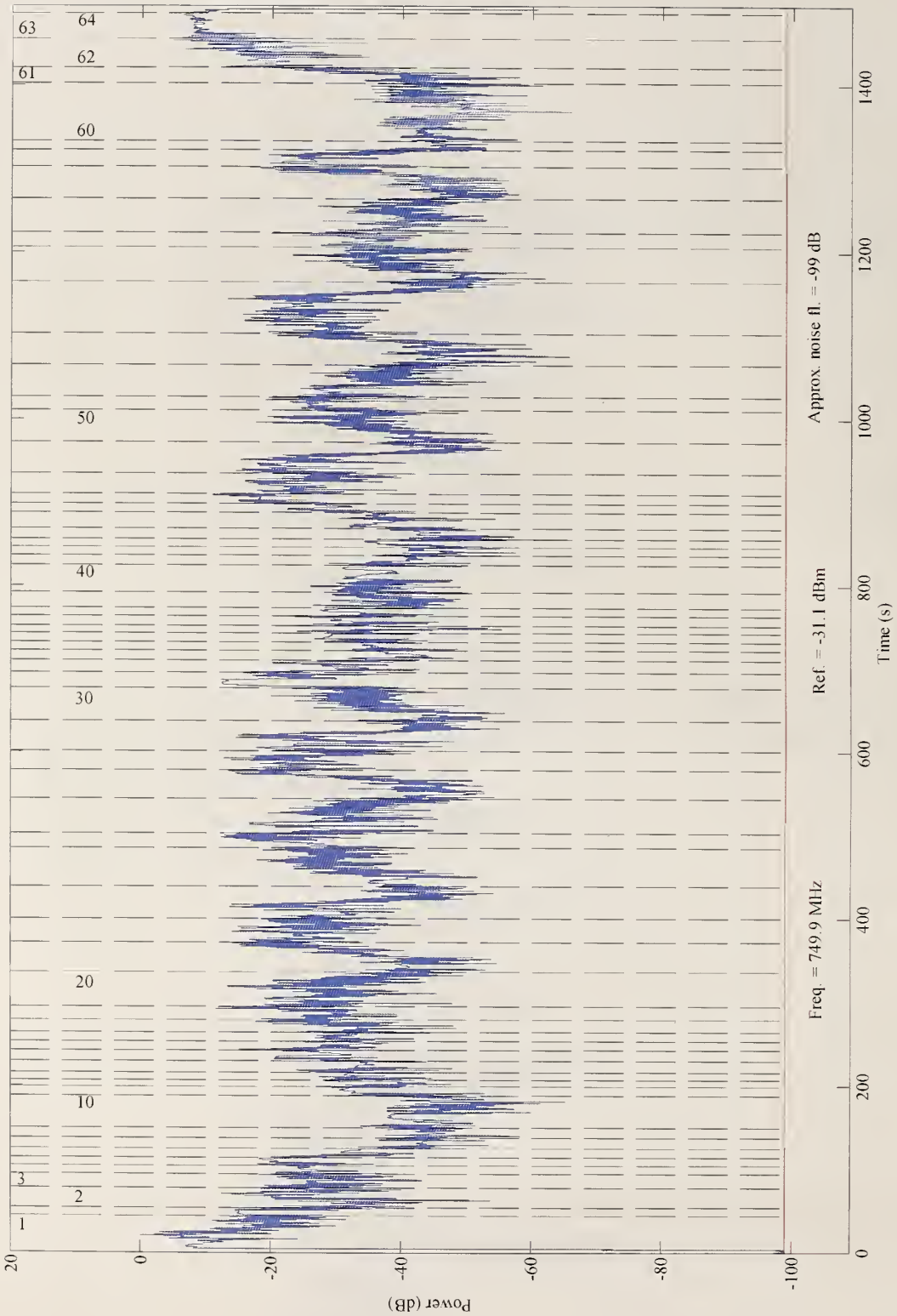

Figure 59. Horizon West, receive site 1. Normalized narrowband receiver signal power as the 750 MHz transmitter is carried through the building.

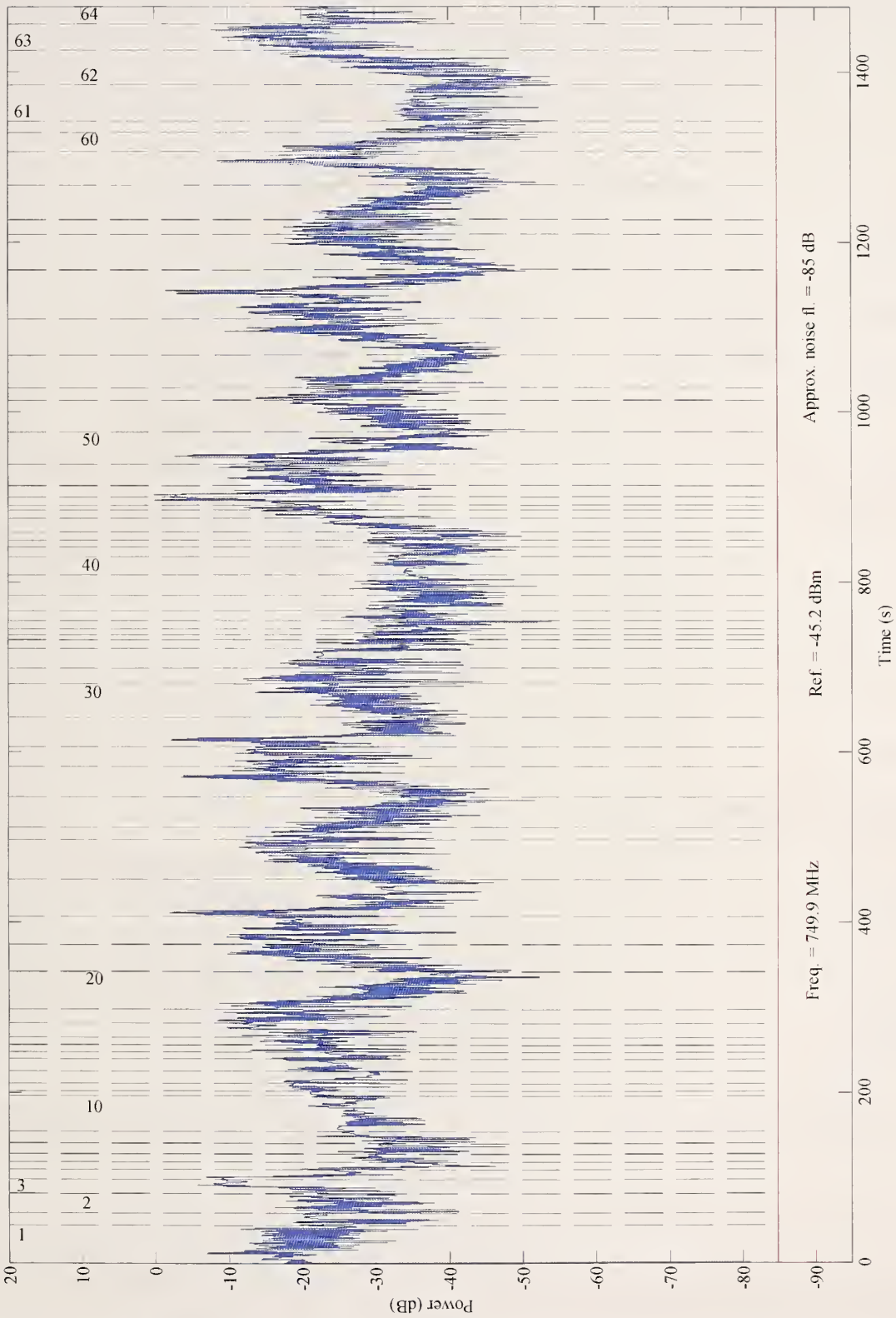

Figure 60. Horizon West, receive site 2. Normalized narrowband receiver signal power as the 750 MHz transmitter is carried through the building.

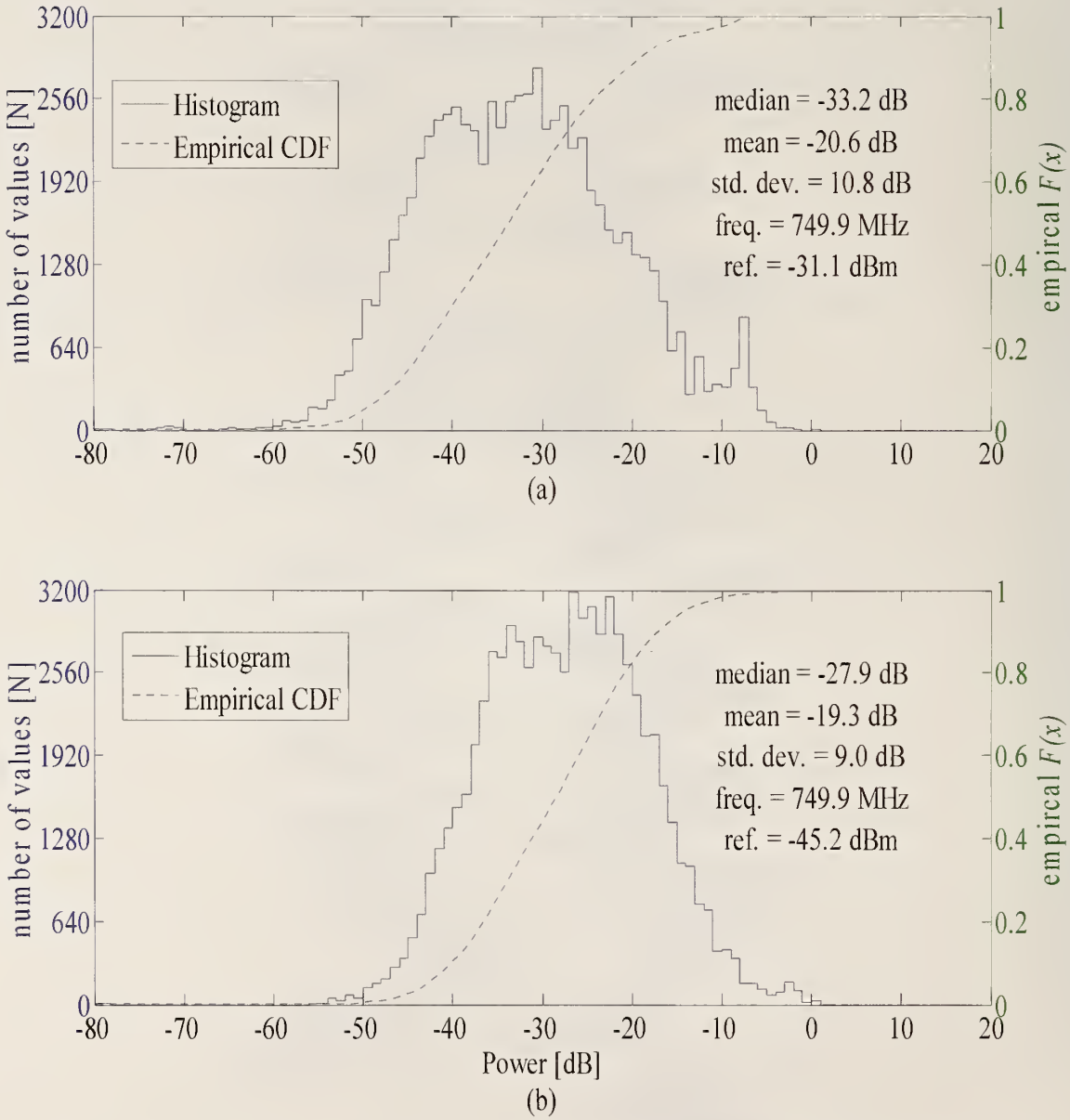

Figure 61. Histogram and empirical CDF of the narrowband receiver signal power at Horizon West for (a) receive site one and (b) receive site two.

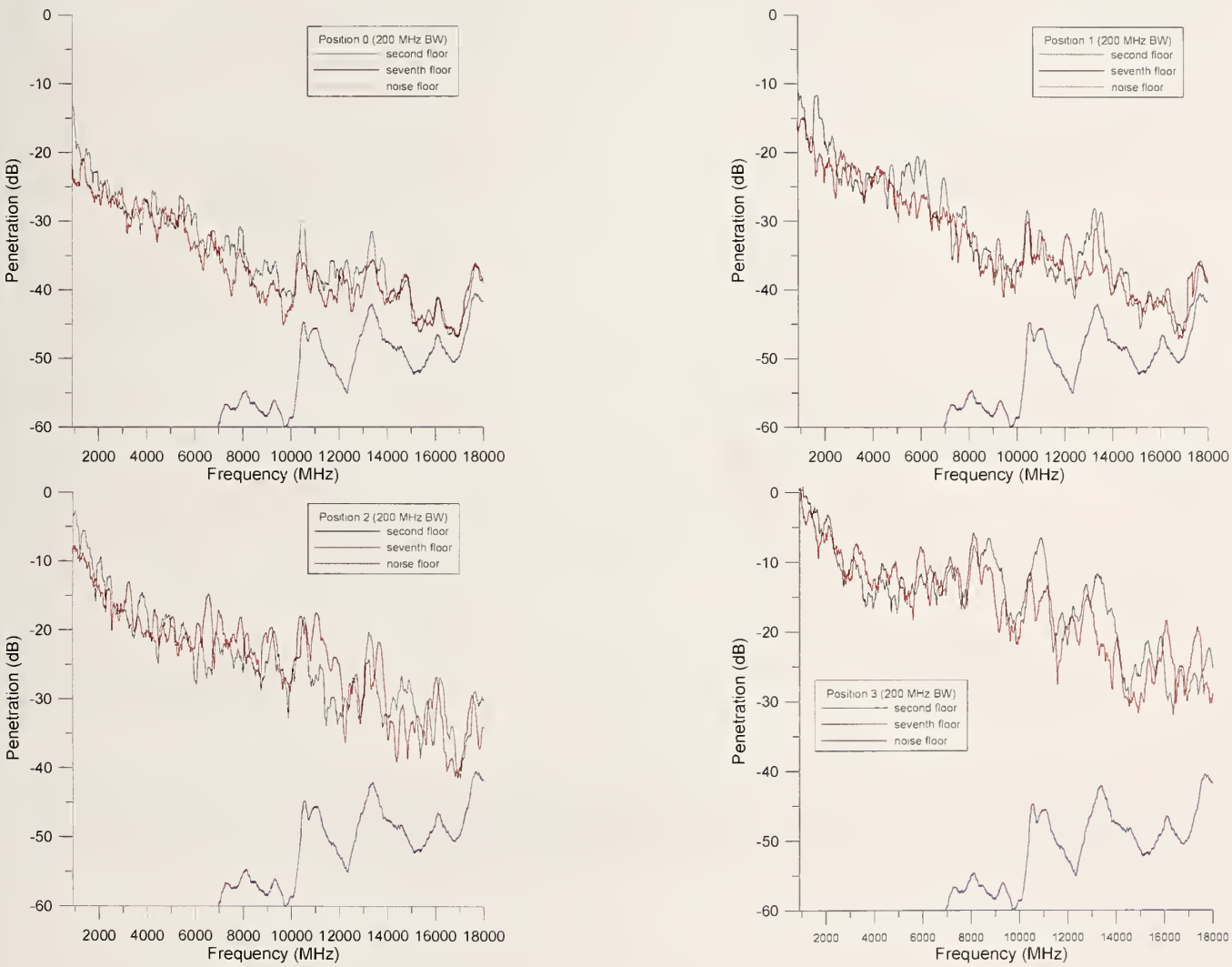

Figure 62. Excess path loss data for positions 0 through 3 at the Horizon West apartment building. Black: floor two. Red: floor seven. Blue: Noise floor.

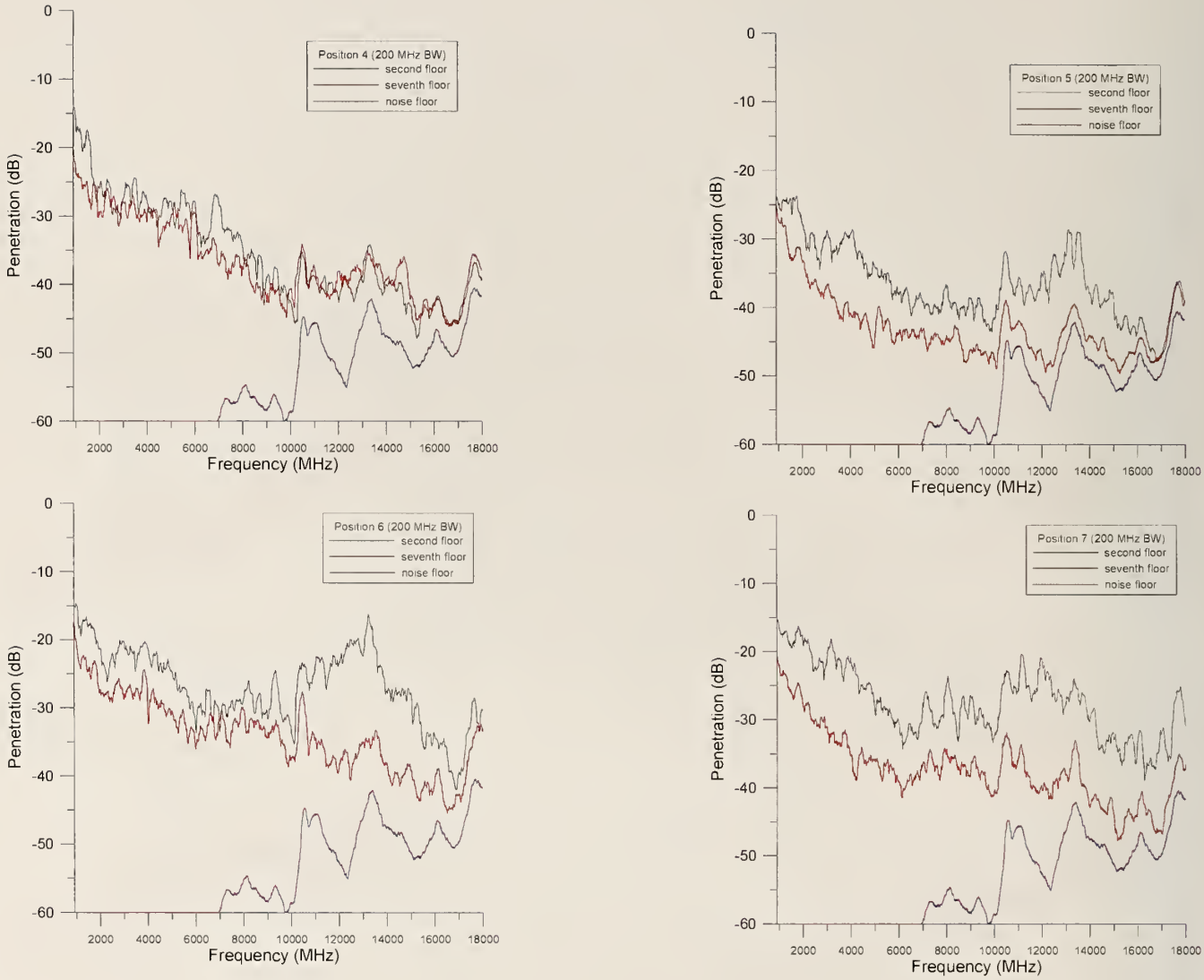

Figure 63.Excess path loss data for positions 4 through 7 at the Horizon West apartment building. Black: floor two. Red: floor seven. Blue: Noise floor.

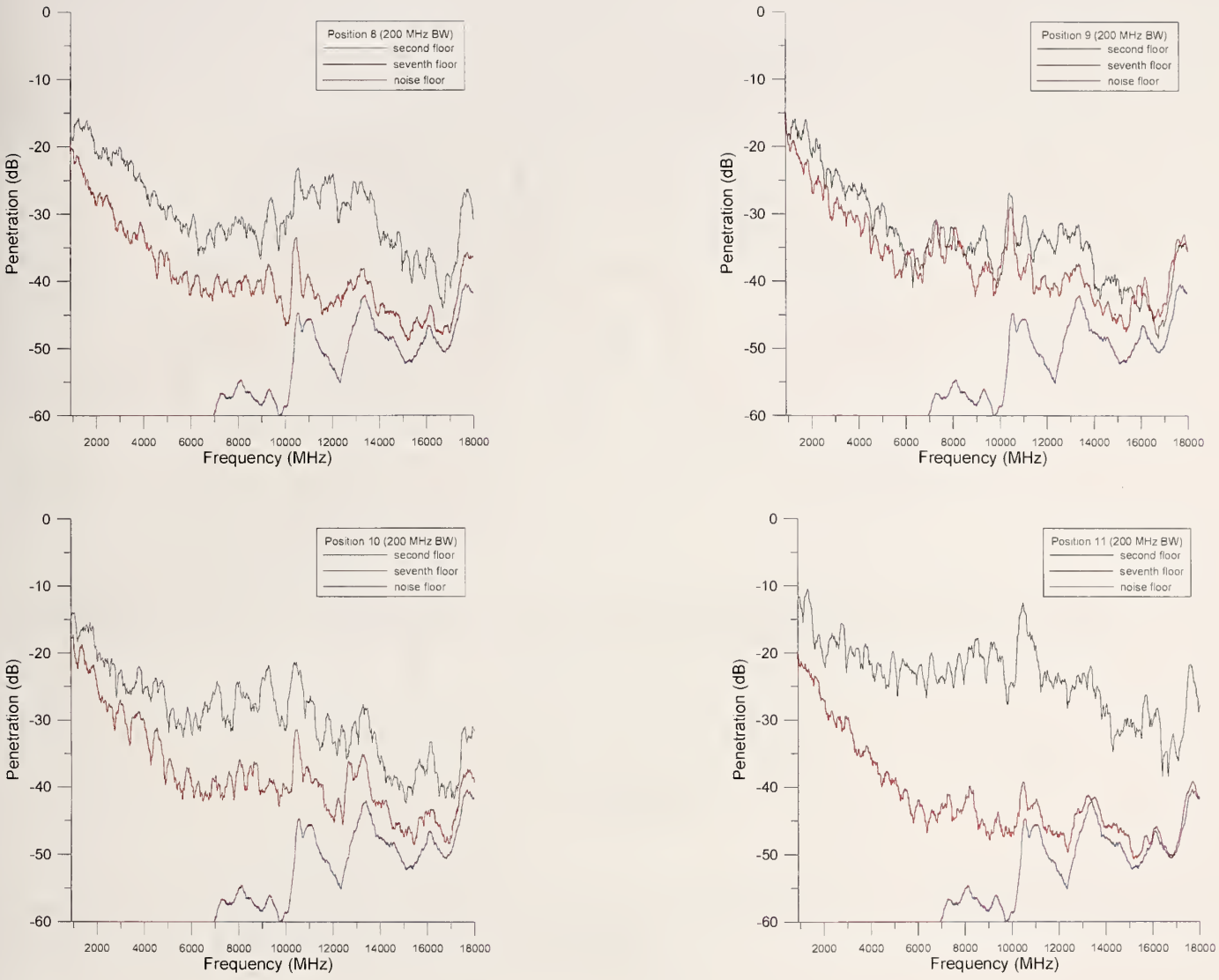

Figure 64. Excess path loss data for positions 8 through 11 at the Horizon West apartment building. Black: floor two. Red: floor seven. Blue: Noise floor.

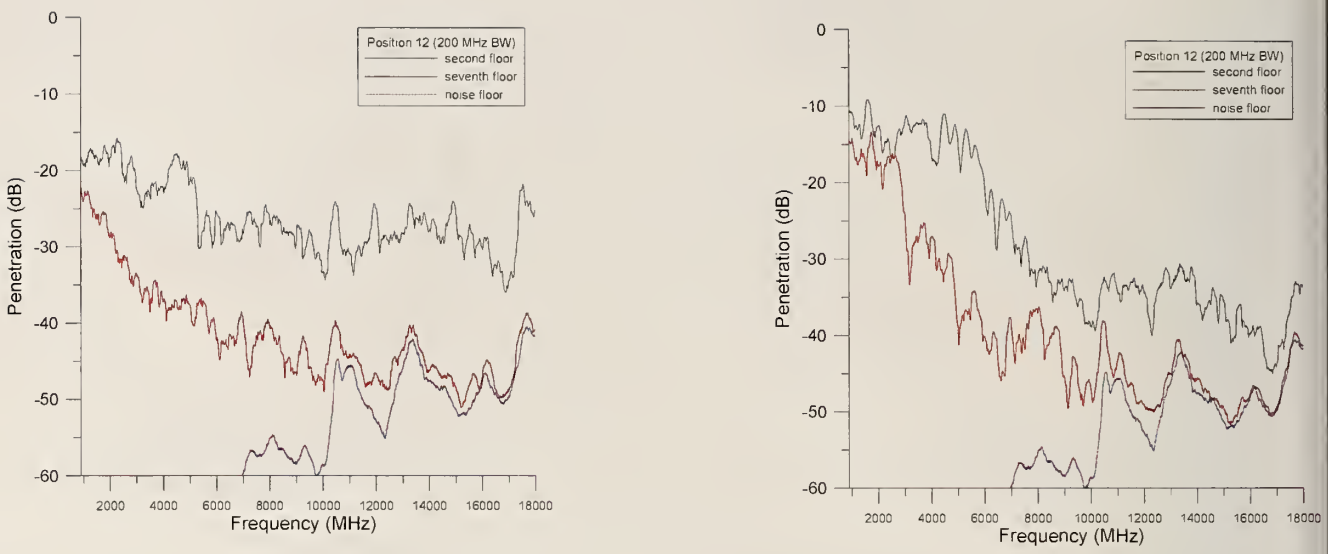

Figure 65. Excess path loss data for positions 12 and 13 at the Horizon West apartment building. Black: floor two. Red: floor seven. Blue: Noise floor.

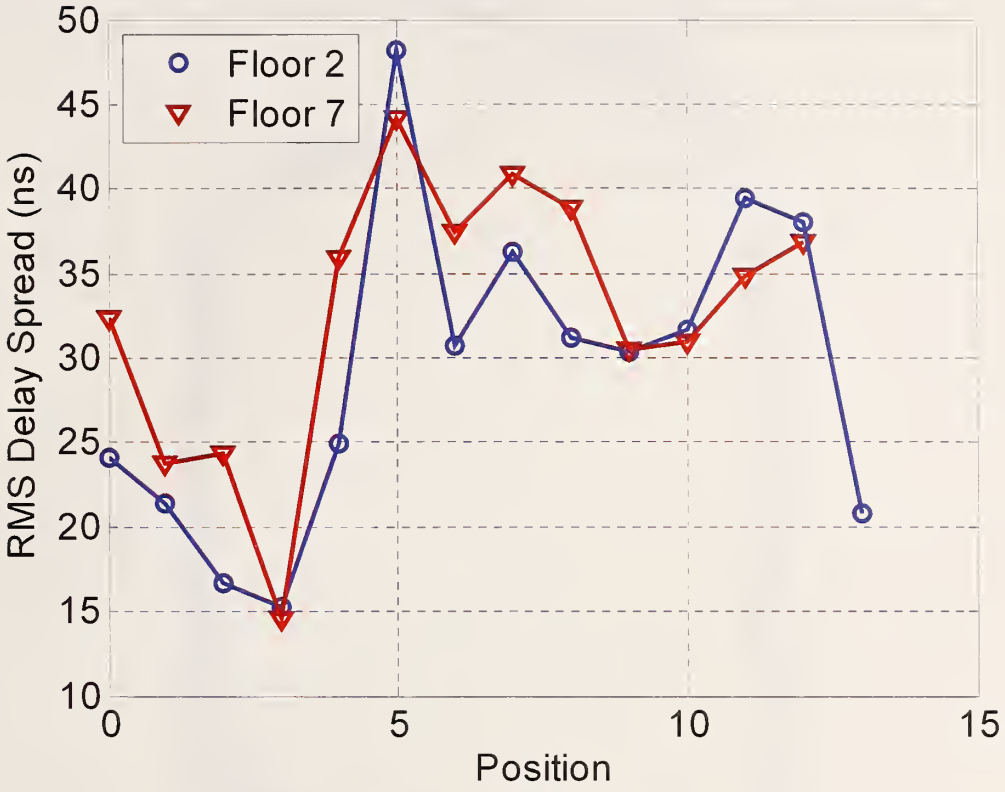

Figure 66. Summary of RMS delay spread values calculated at the Horizon West apartment building. Data were calculated using the frequency band from 1 GHz to 18 GHz.

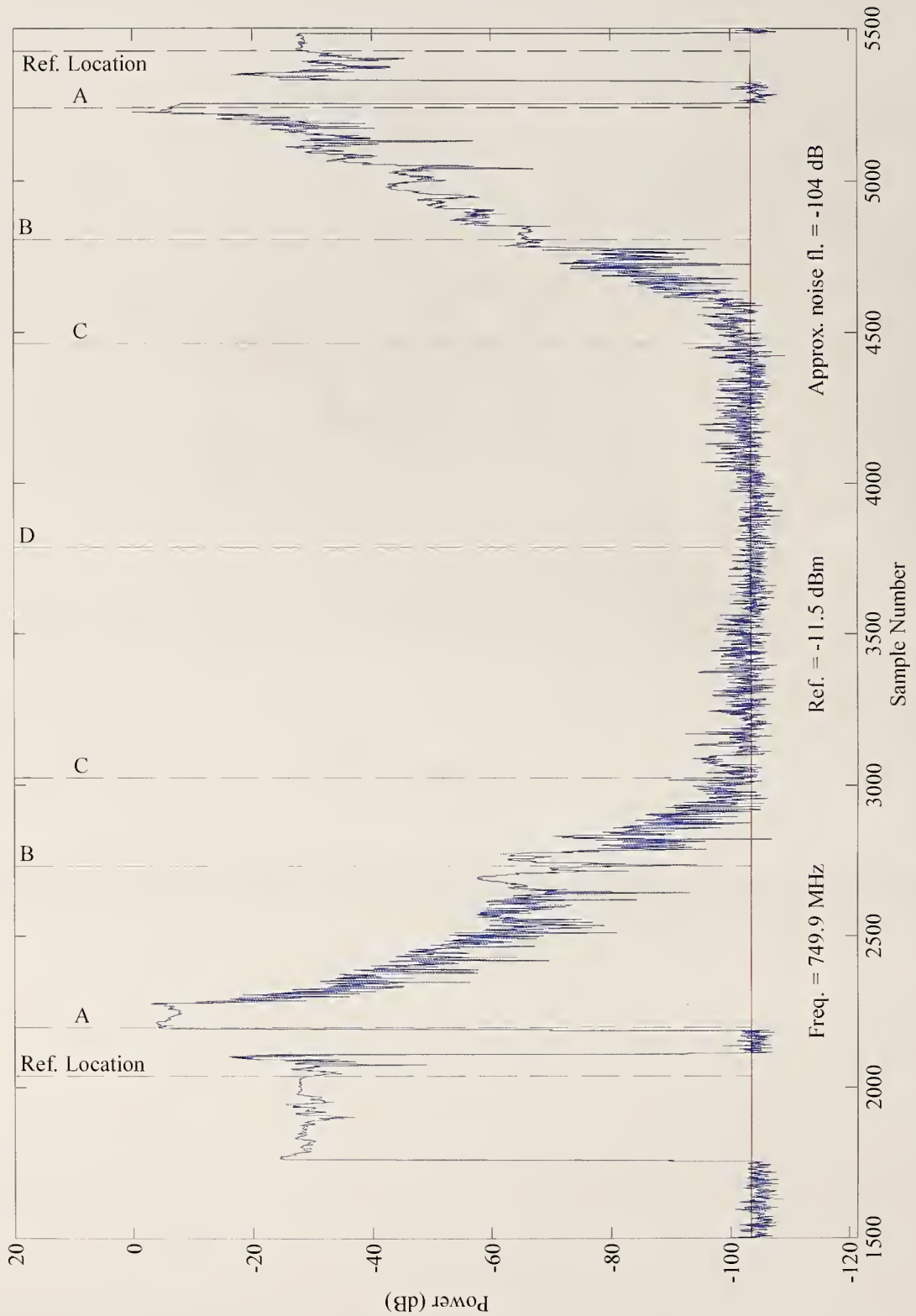

Figure 67. NIST Boulder laboratory, receive site 1. Normalized received signal power from the spectrum analyzer as the 750 MHz transmitter is carried through the building. Path I, walk 1.

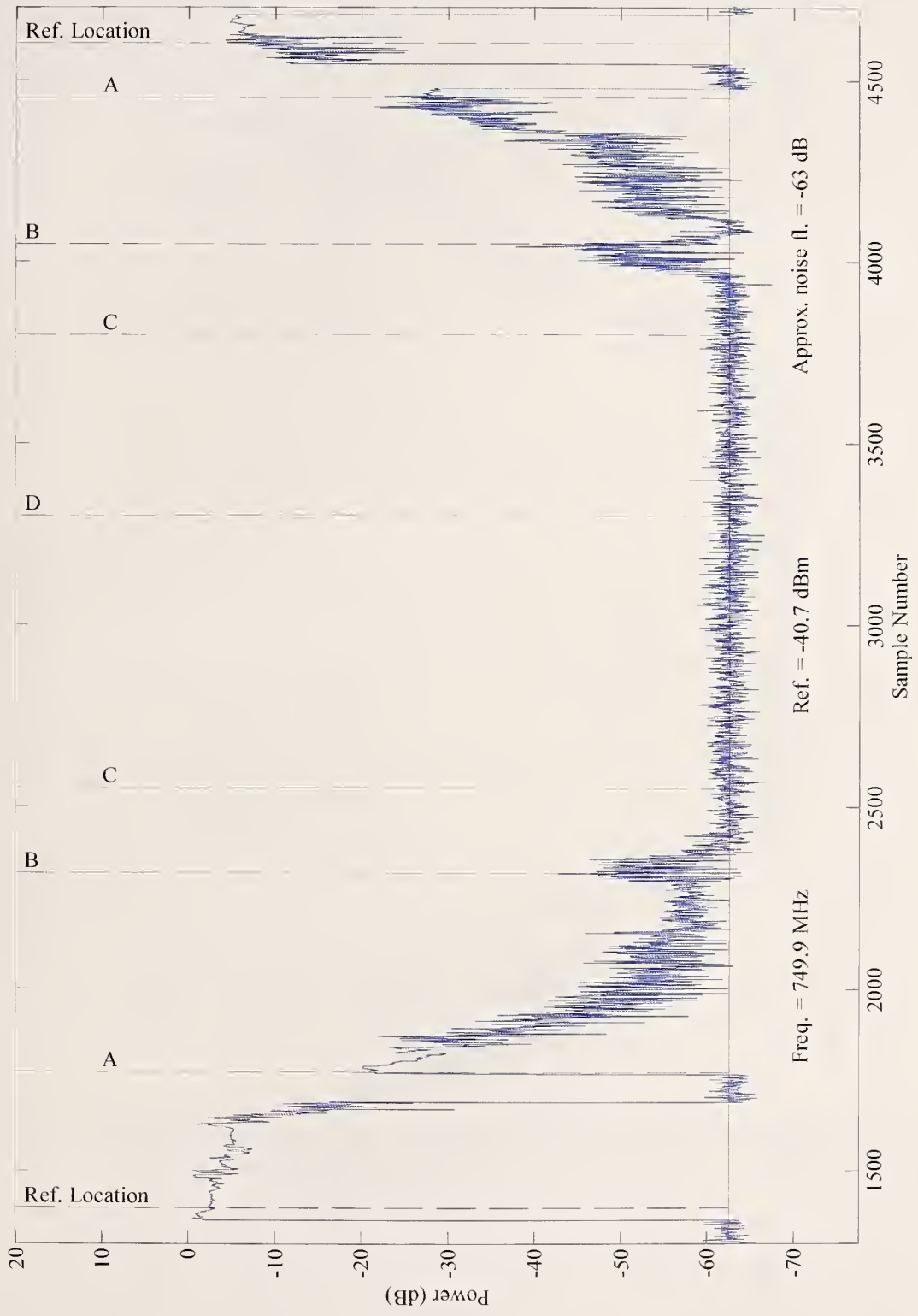

Figure 68. NIST Boulder laboratory, receive site 2. Normalized received signal power from the spectrum analyzer as the 750 MHz transmitter is carried through the building. Path I, walk 1.

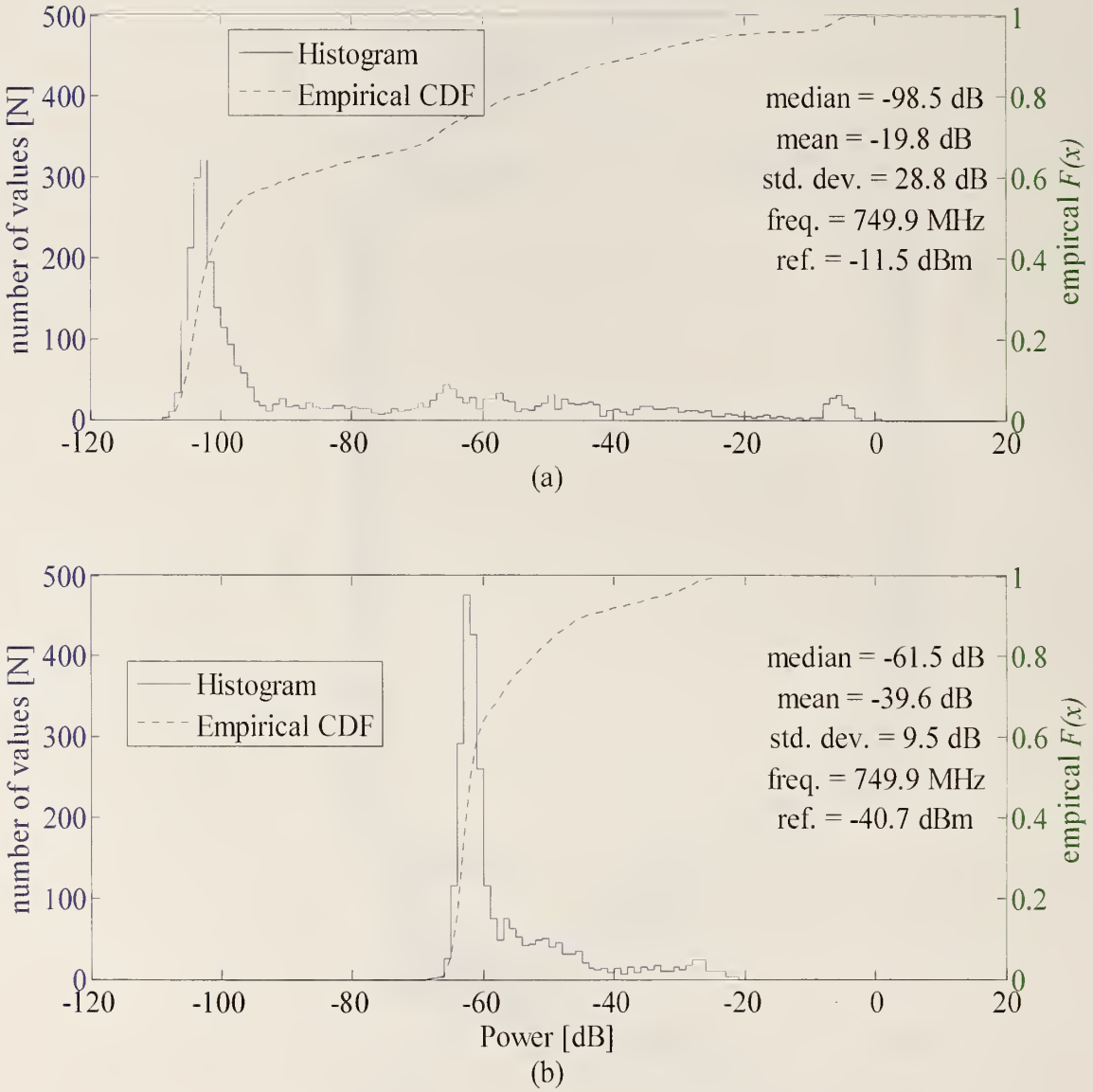

Figure 69. Histogram and empirical CDF of the spectrum analyzer signal power at NIST Boulder laboratory for (a) receive site one and (b) receive site two. Path I, walk 1.

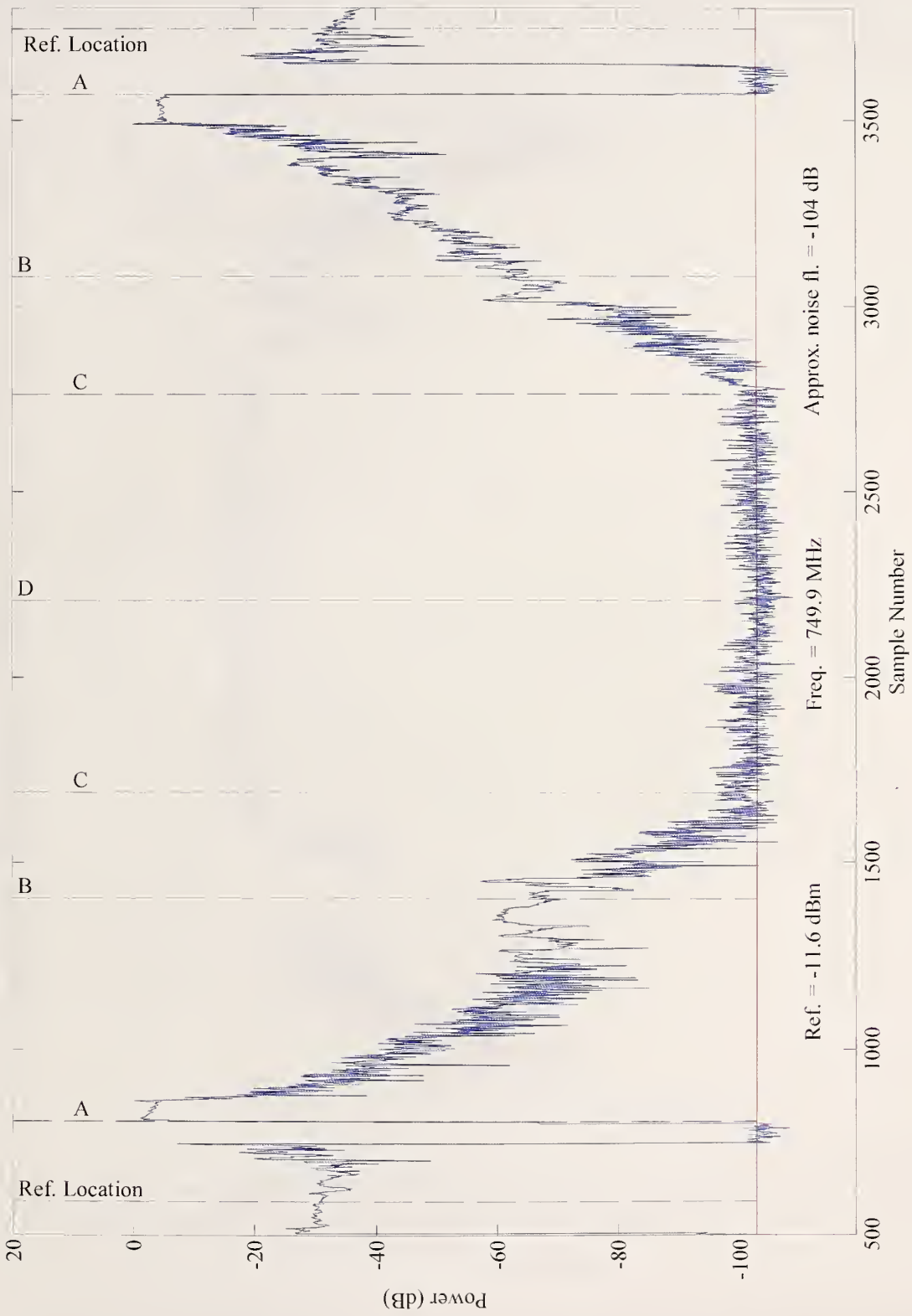

Figure 70. NIST Boulder laboratory, receive site 1. Normalized received signal power from the spectrum analyzer as the 750 MHz transmitter is carried through the building. Path I, walk 2.

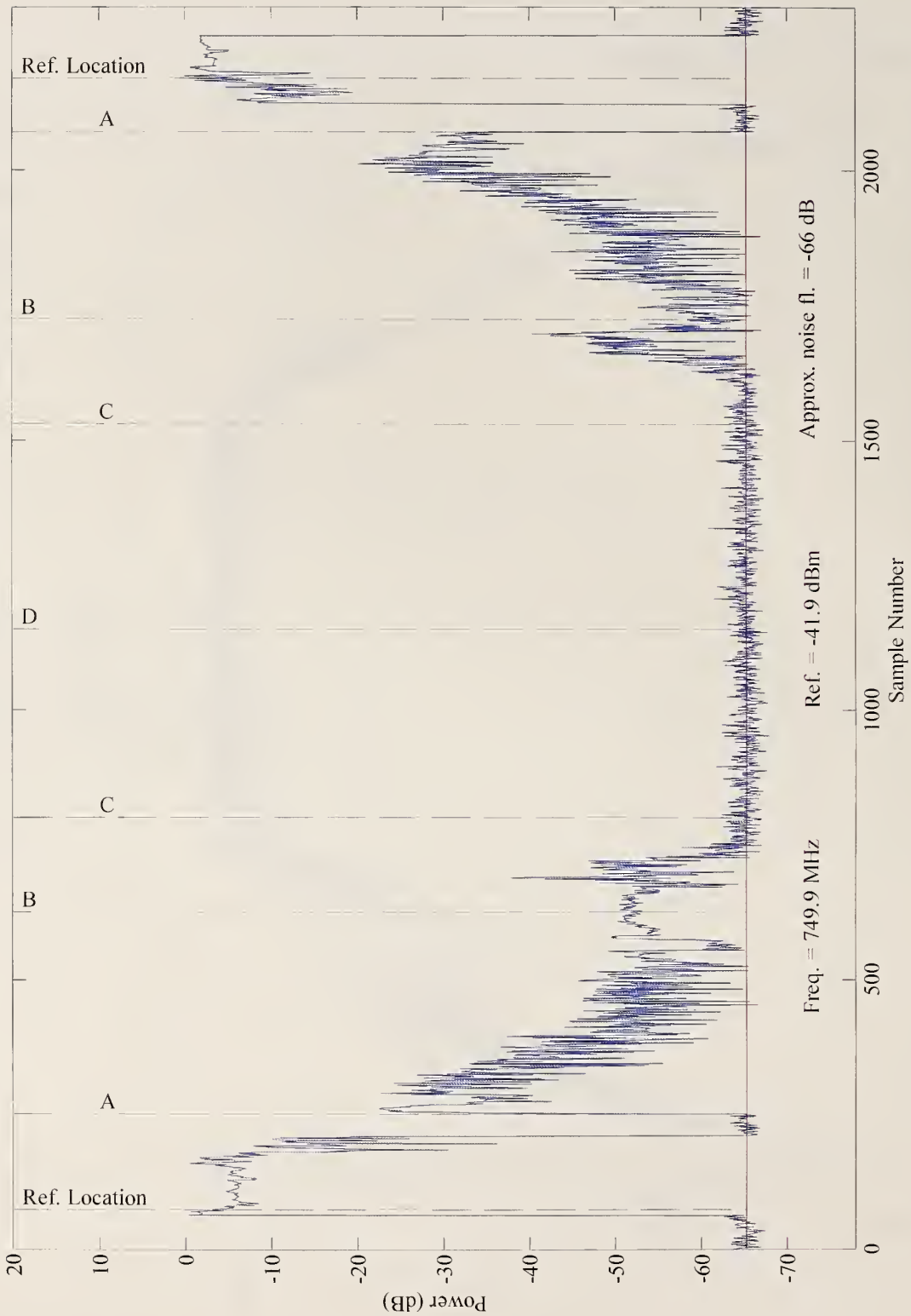

Figure 71. NIST Boulder laboratory, receive site 2. Normalized received signal power from the spectrum analyzer as the 750 MHz transmitter is carried through the building. Path I, walk 2.

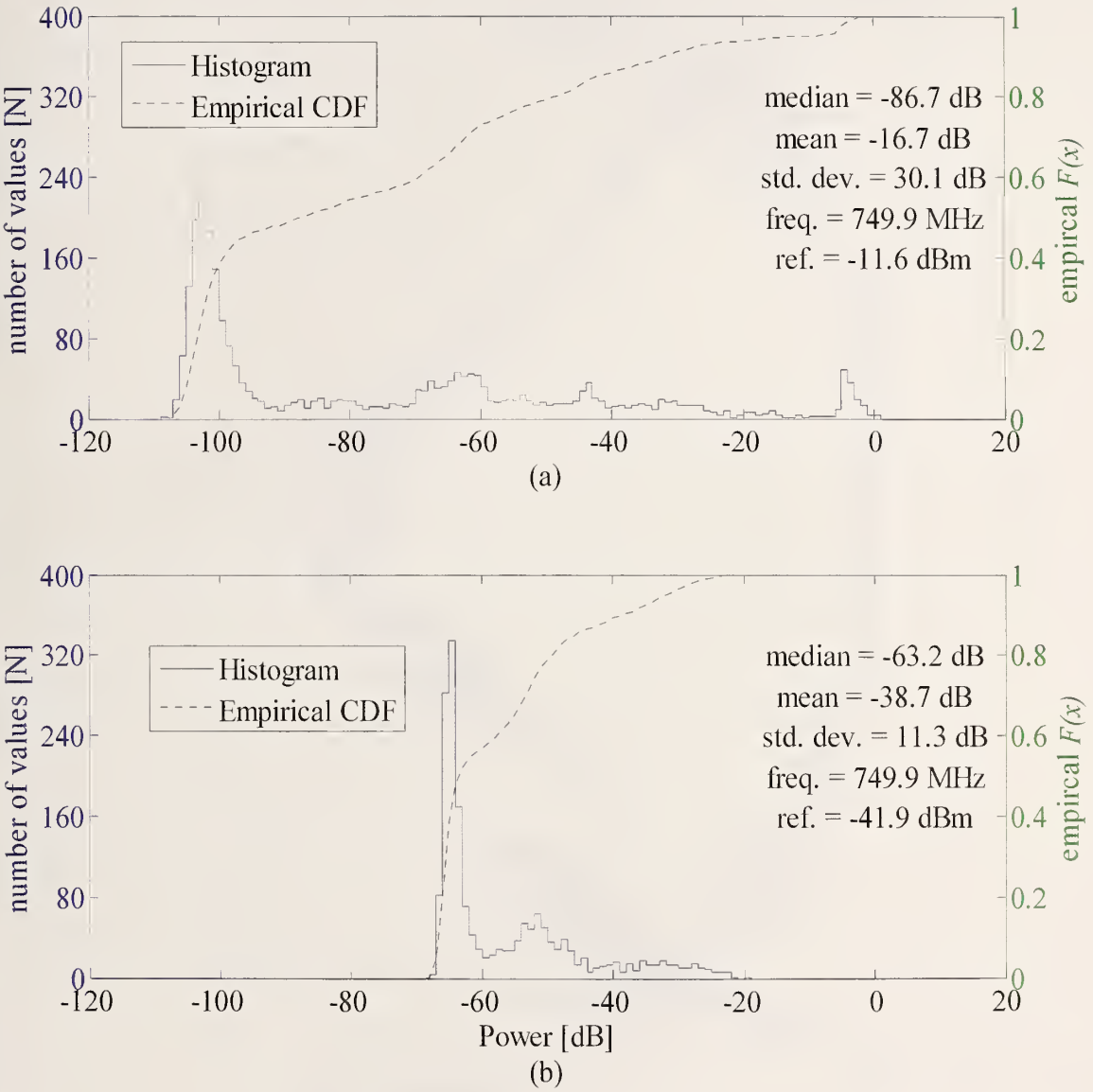

Figure 72. Histogram and empirical CDF of the spectrum analyzer signal power at NIST Boulder laboratory for (a) receive site one and (b) receive site two. Path I, walk 2.

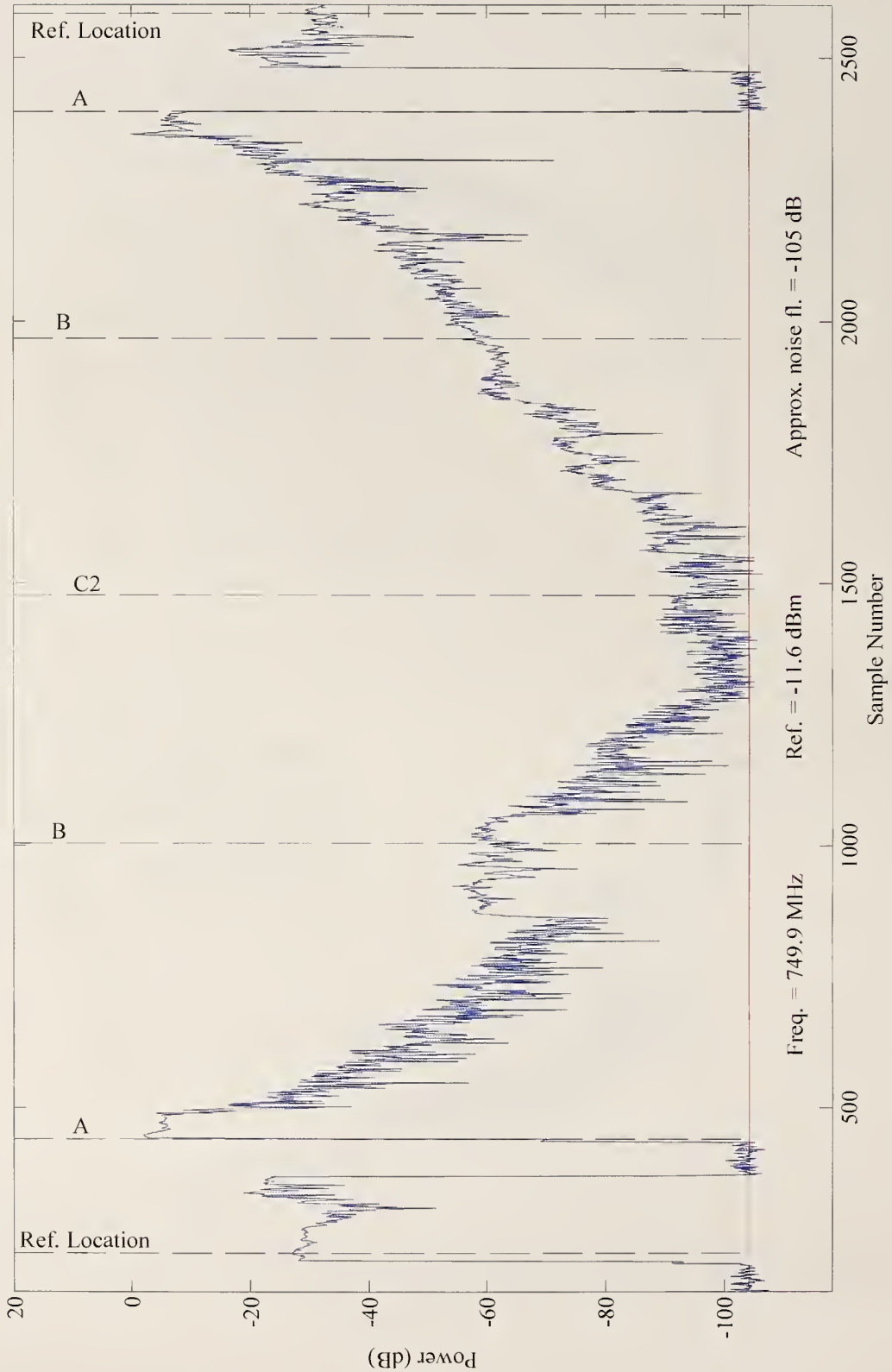

Figure 73. NIST Boulder laboratory, receive site 1. Normalized received signal power from the spectrum analyzer as the 750 MHz transmitter is carried through the building. Path II, walk 1.

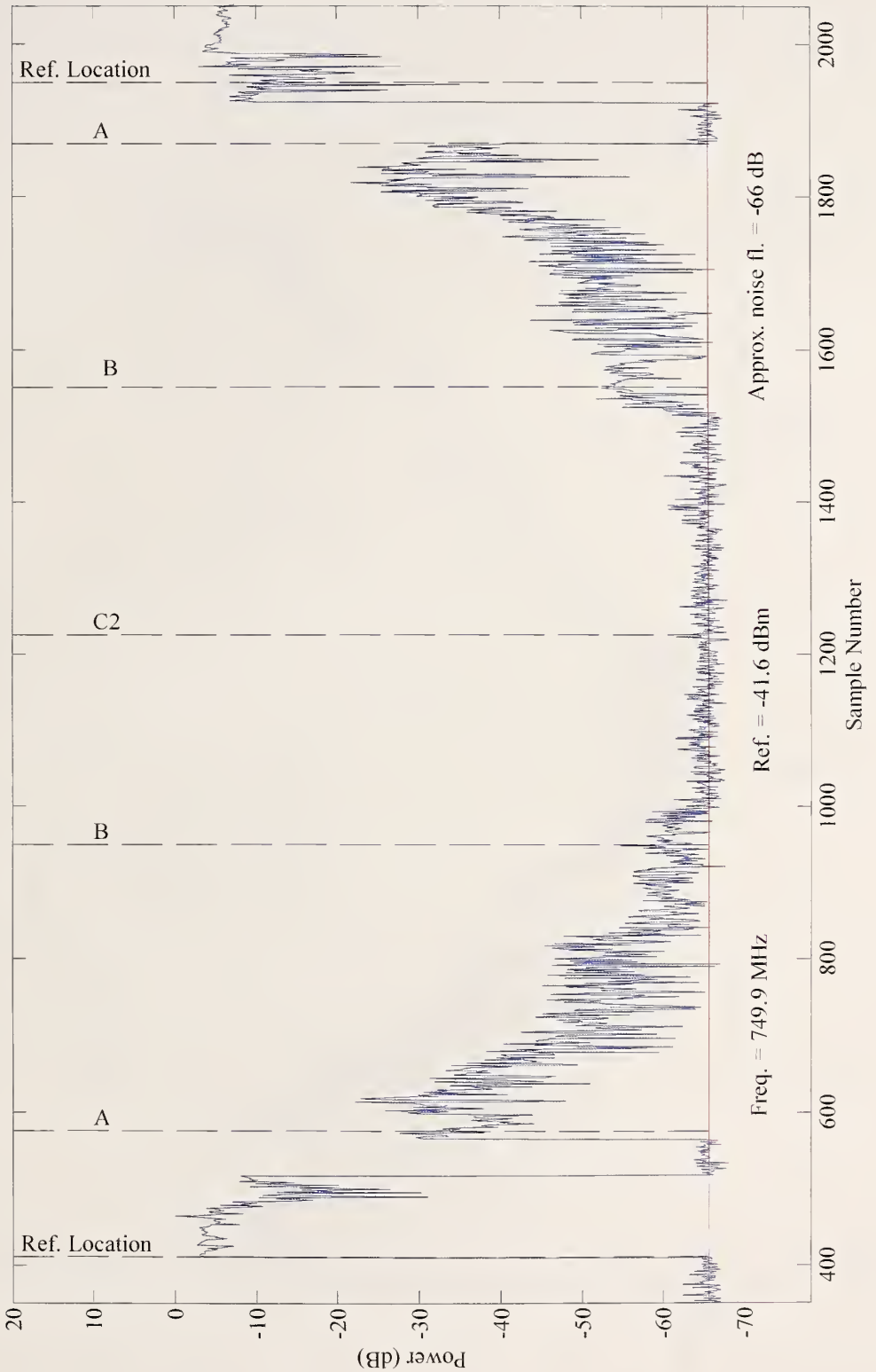

Figure 74. NIST Boulder laboratory, receive site 2. Normalized received signal power from the spectrum analyzer as the 750 MHz transmitter is carried through the building. Path II, walk 1.

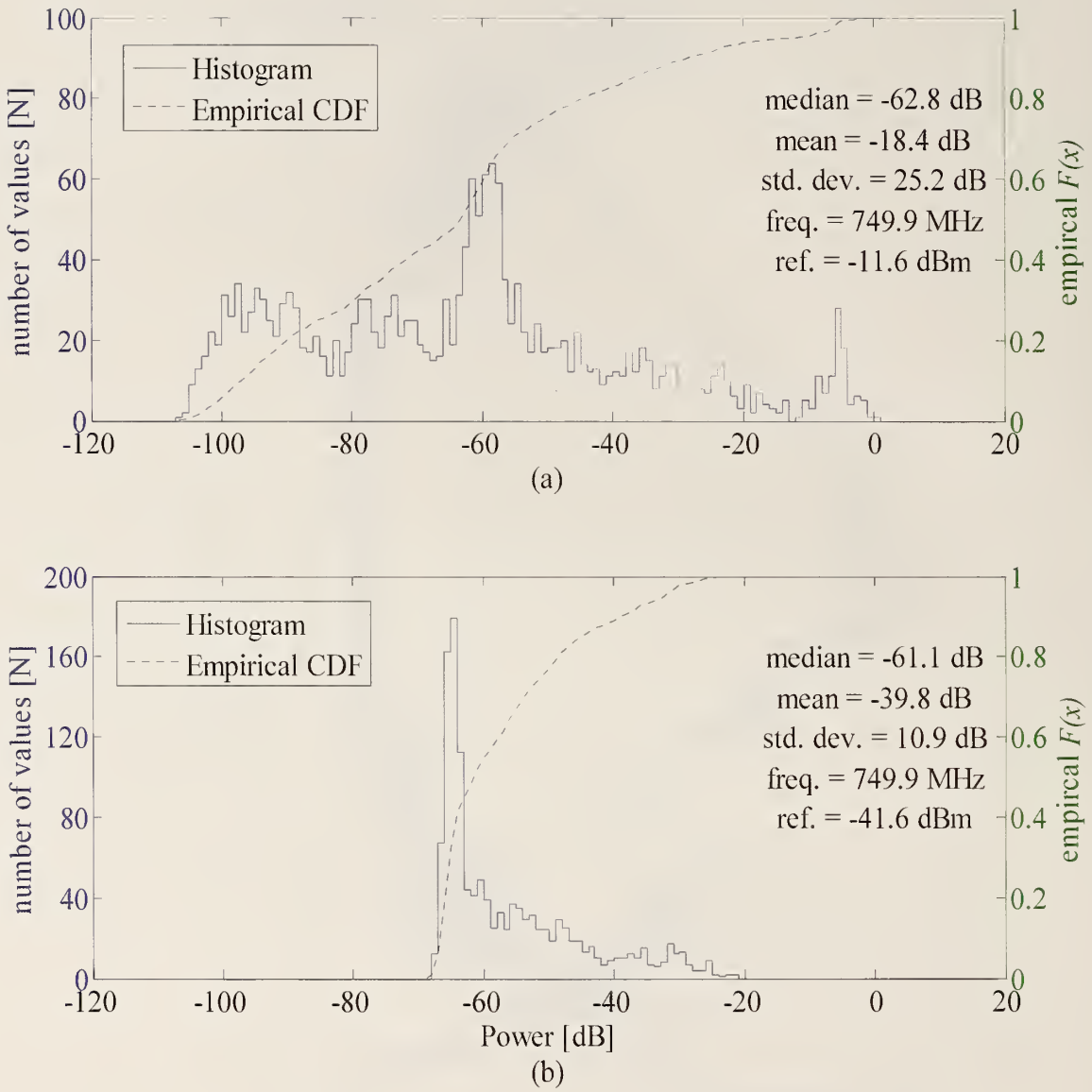

Figure 75. Histogram and empirical CDF of the spectrum analyzer signal power at NIST Boulder laboratory for (a) receive site one and (b) receive site two. Path II. walk 1.

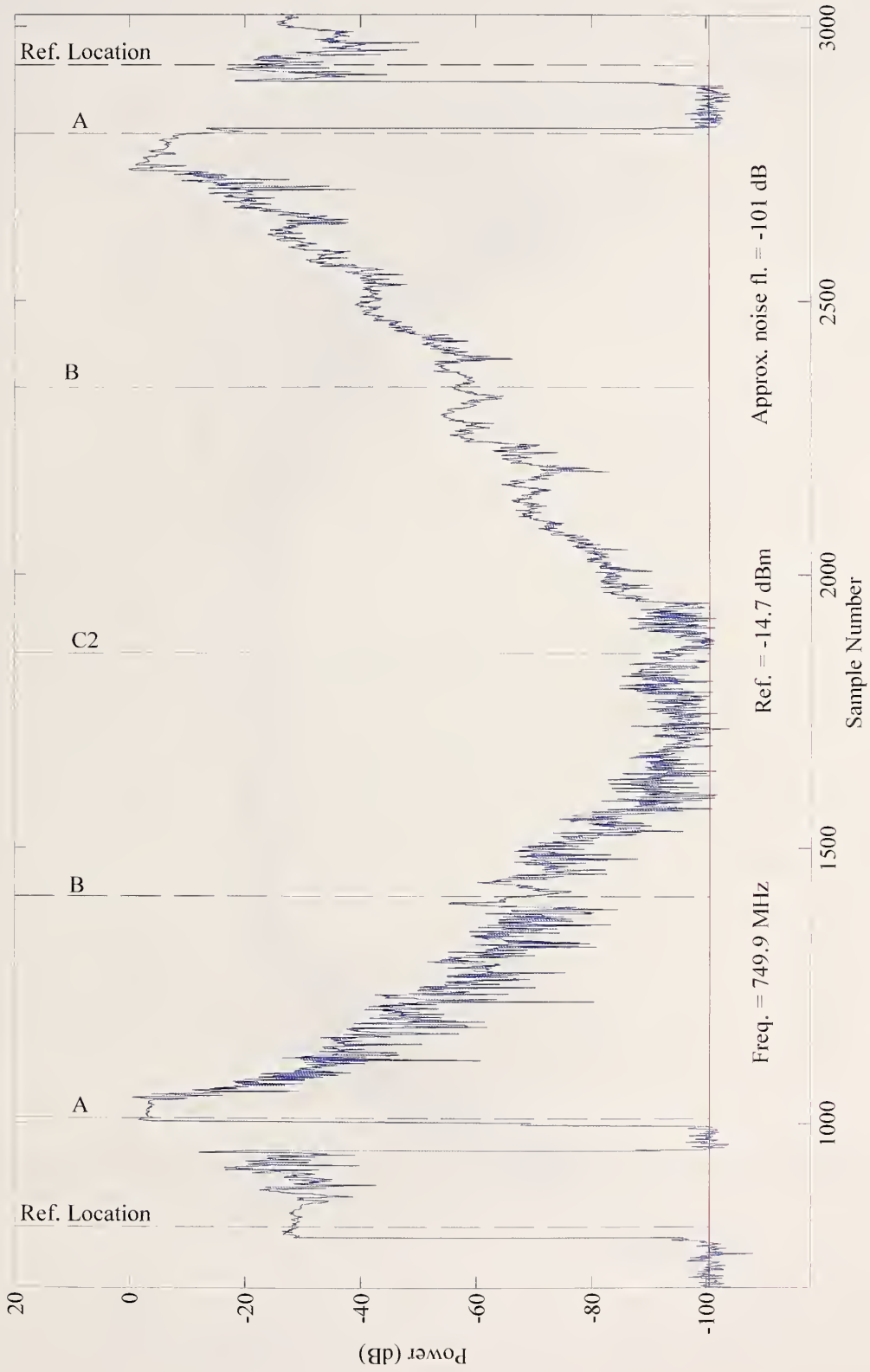

Figure 76. NIST Boulder laboratory, receive site 1. Normalized received signal power from the spectrum analyzer as the 750 MHz transmitter is carried through the building. Path II, walk 2.

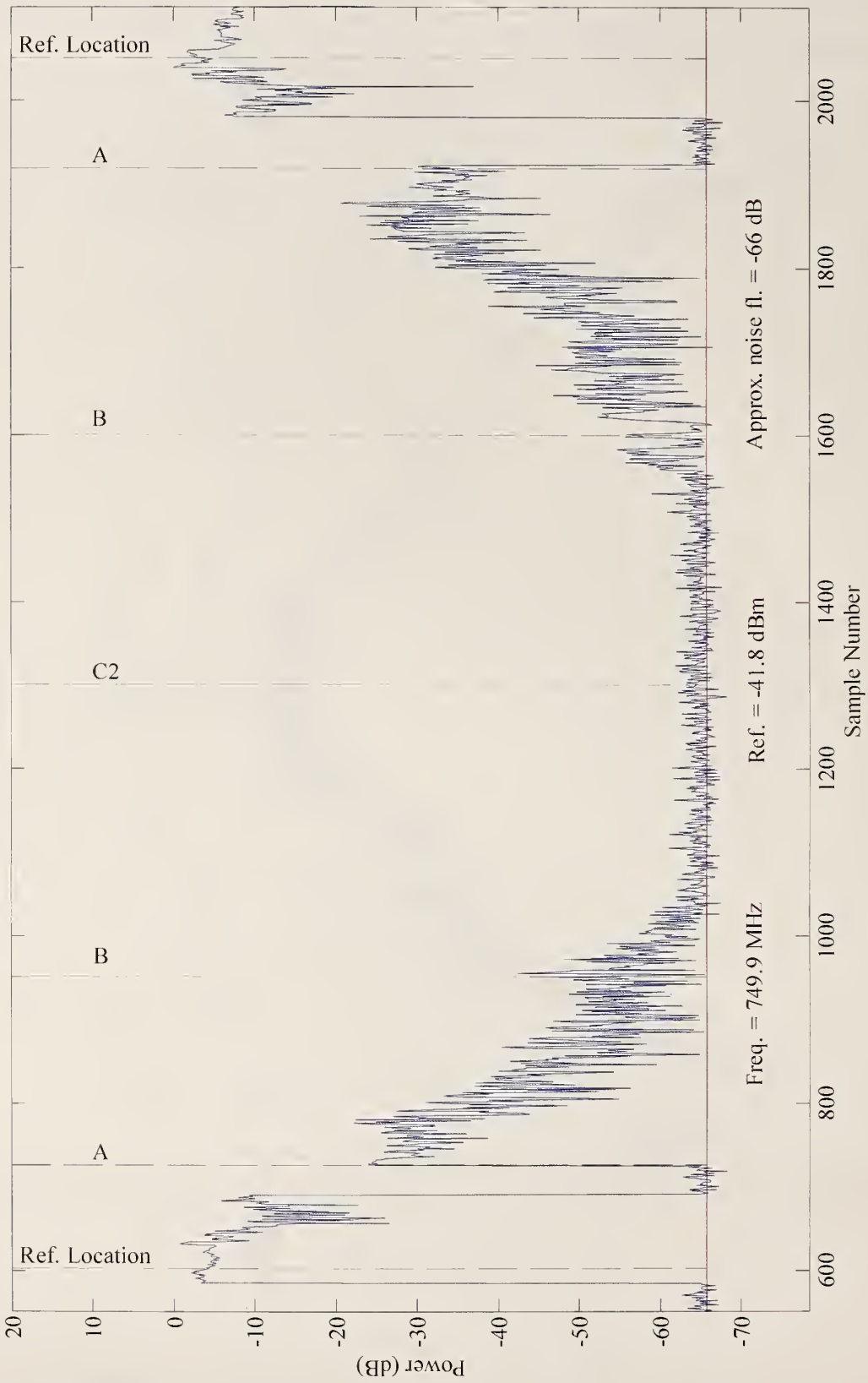

Figure 77. NIST Boulder laboratory, receive site 2. Normalized received signal power from the spectrum analyzer as the 750 MHz transmitter is carried through the building. Path II, walk 2.

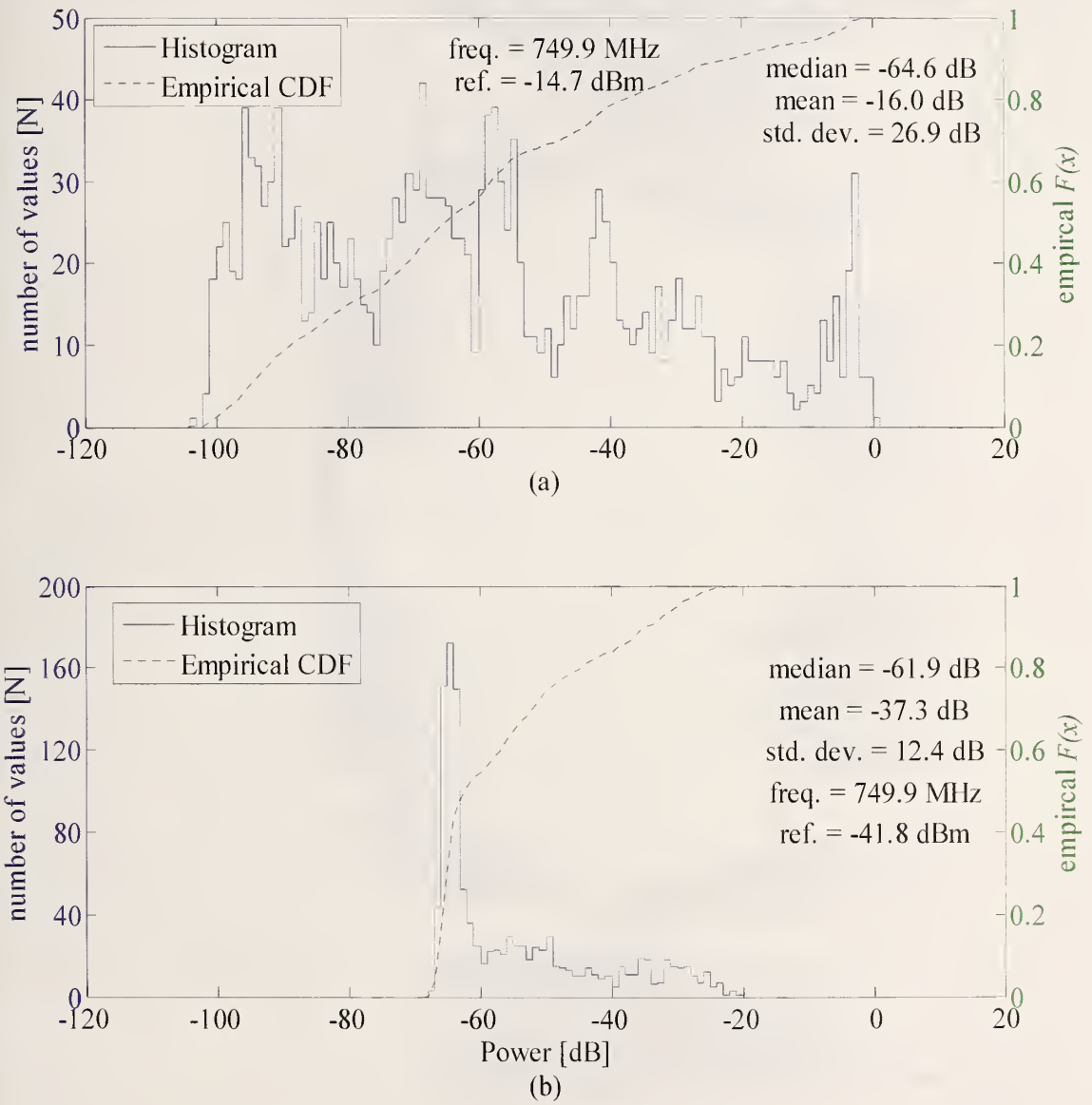

Figure 78. Histogram and empirical CDF of the spectrum analyzer signal power at NIST Boulder laboratory for (a) receive site one and (b) receive site two. Path II, walk 2.

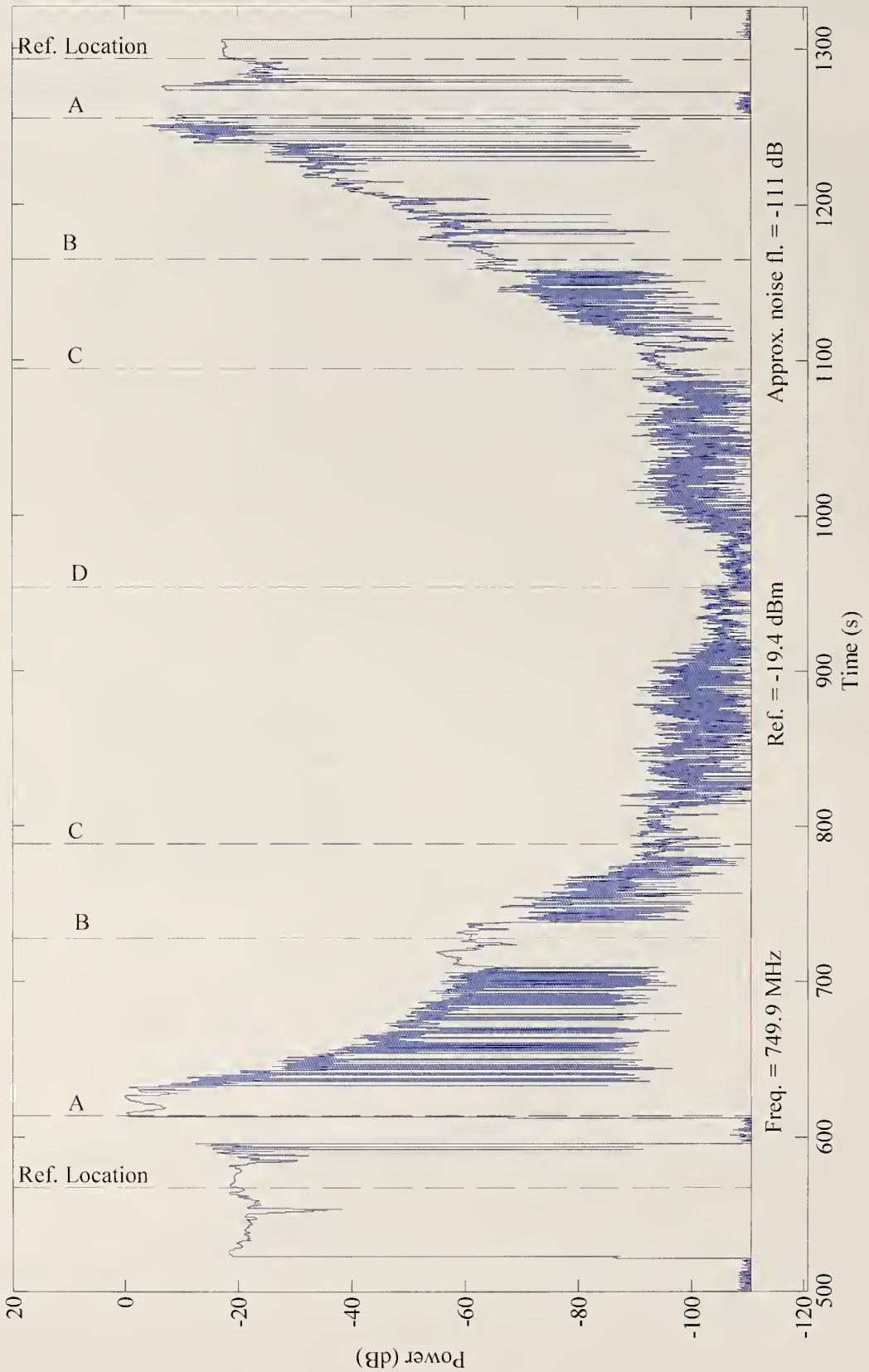

Figure 79. NIST Boulder laboratory, receive site 1. Normalized received signal power from the narrowband receiver as the 750 MHz transmitter is carried through the building. Path I, walk 1.

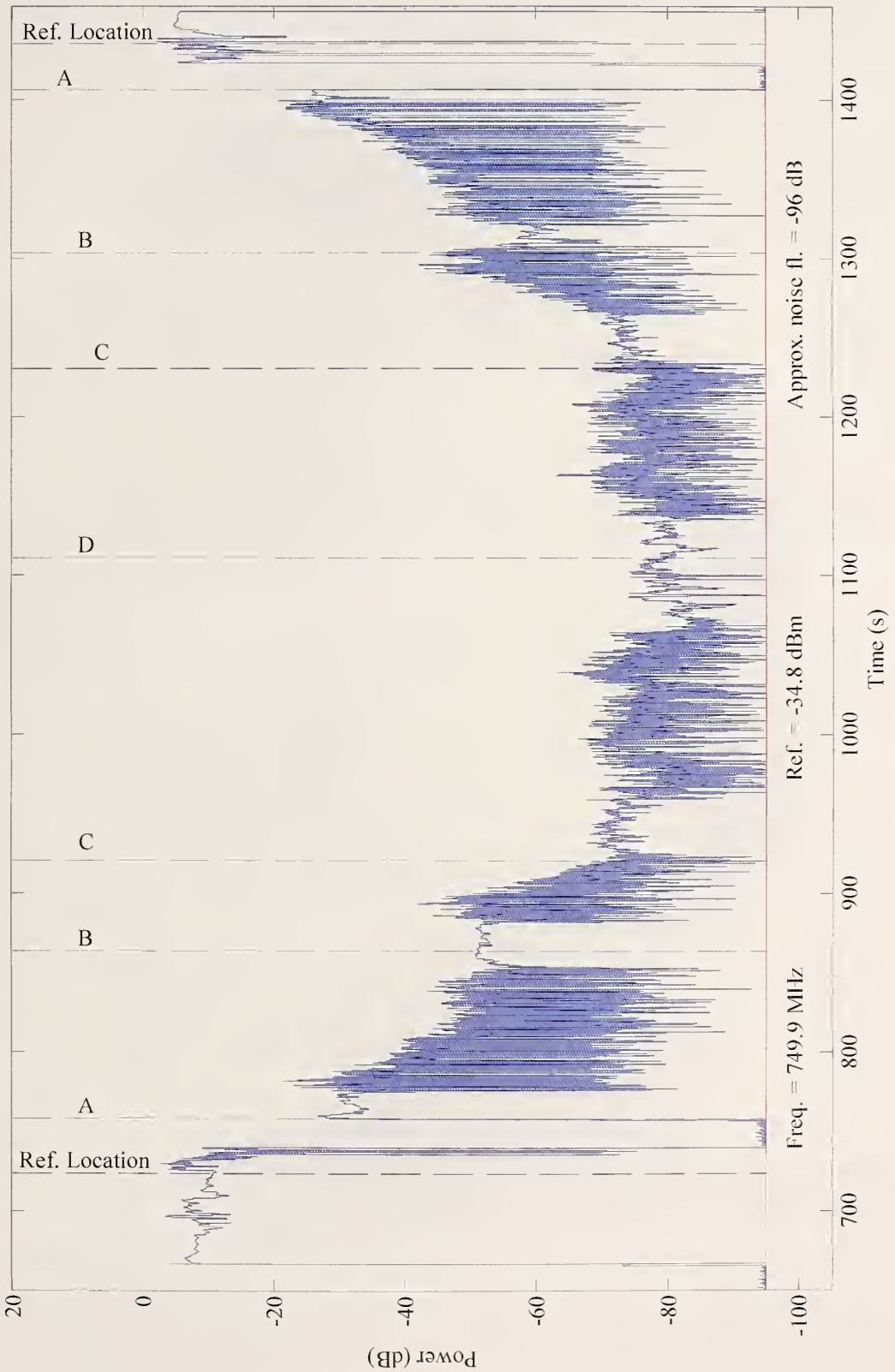

Figure 80. NIST Boulder laboratory, receive site 2. Normalized received signal power from the narrowband receiver as the 750 MHz transmitter is carried through the building. Path I, walk 1.

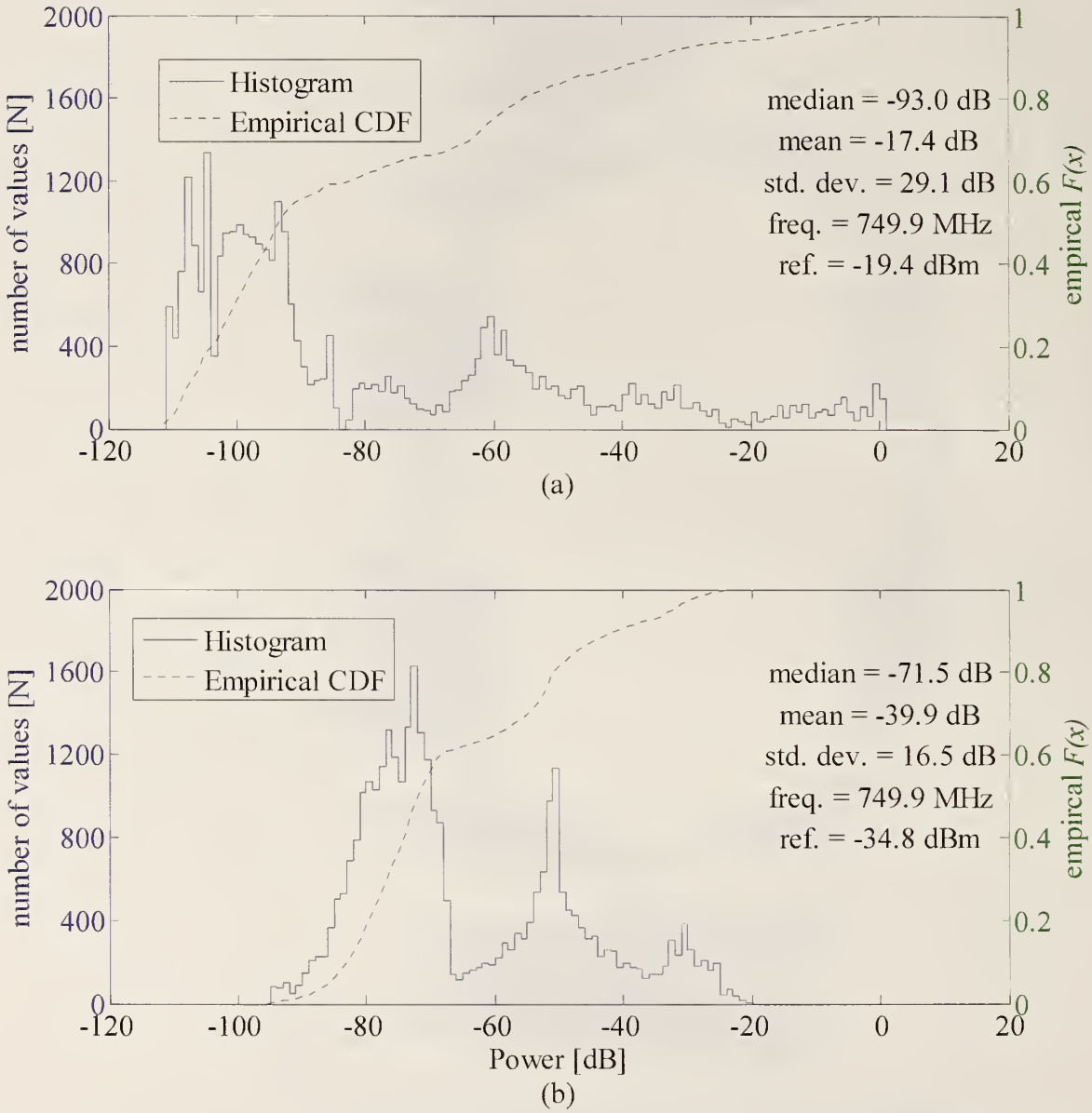

Figure 81. Histogram and empirical CDF of the narrowband receiver signal power at NIST Boulder laboratory for (a) receive site one and (b) receive site two. Path I, walk 1.

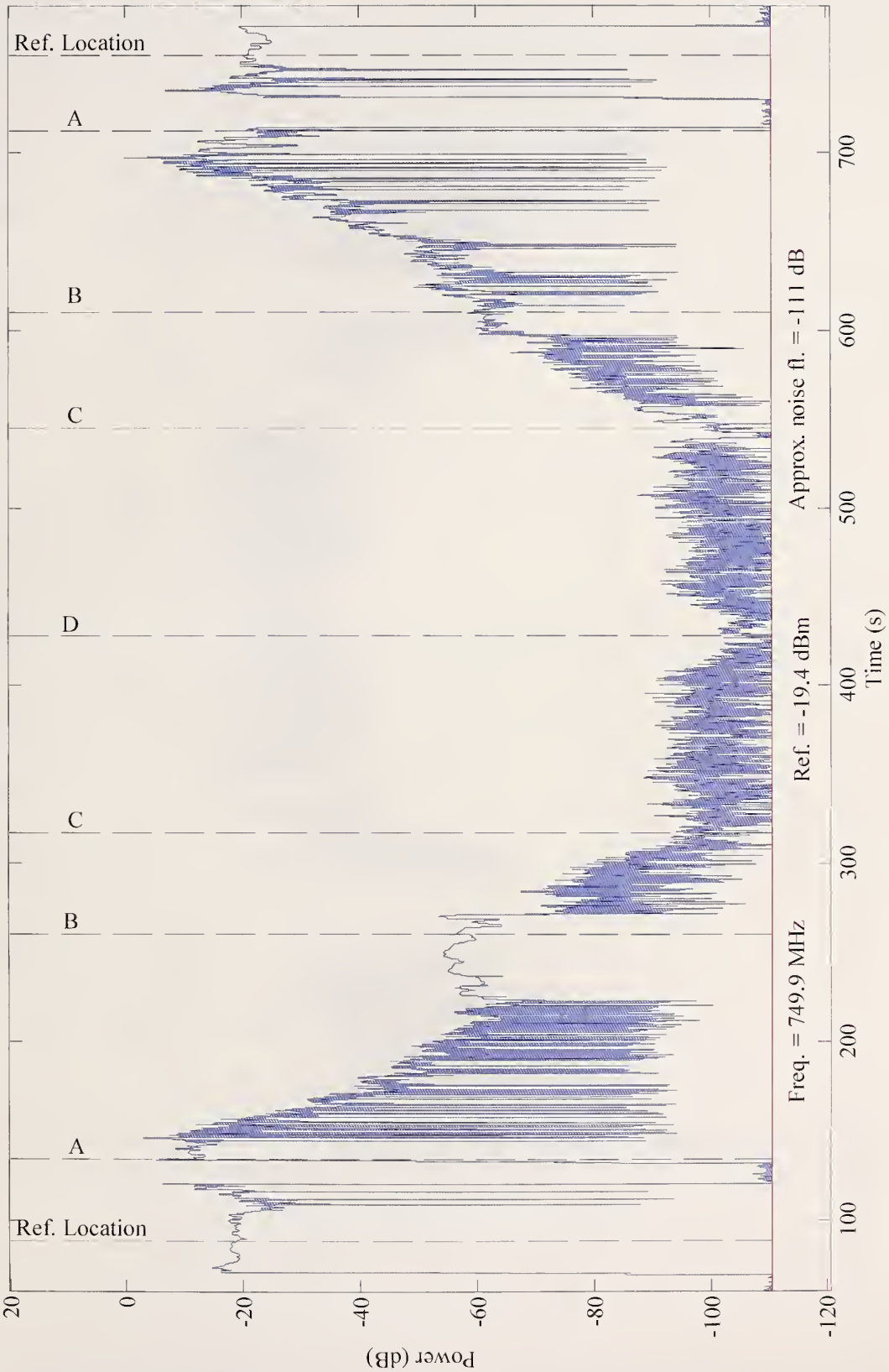

Figure 82. NIST Boulder laboratory, receive site 1. Normalized received signal power from the narrowband receiver as the 750 MHz transmitter is carried through the building. Path I, walk 2.

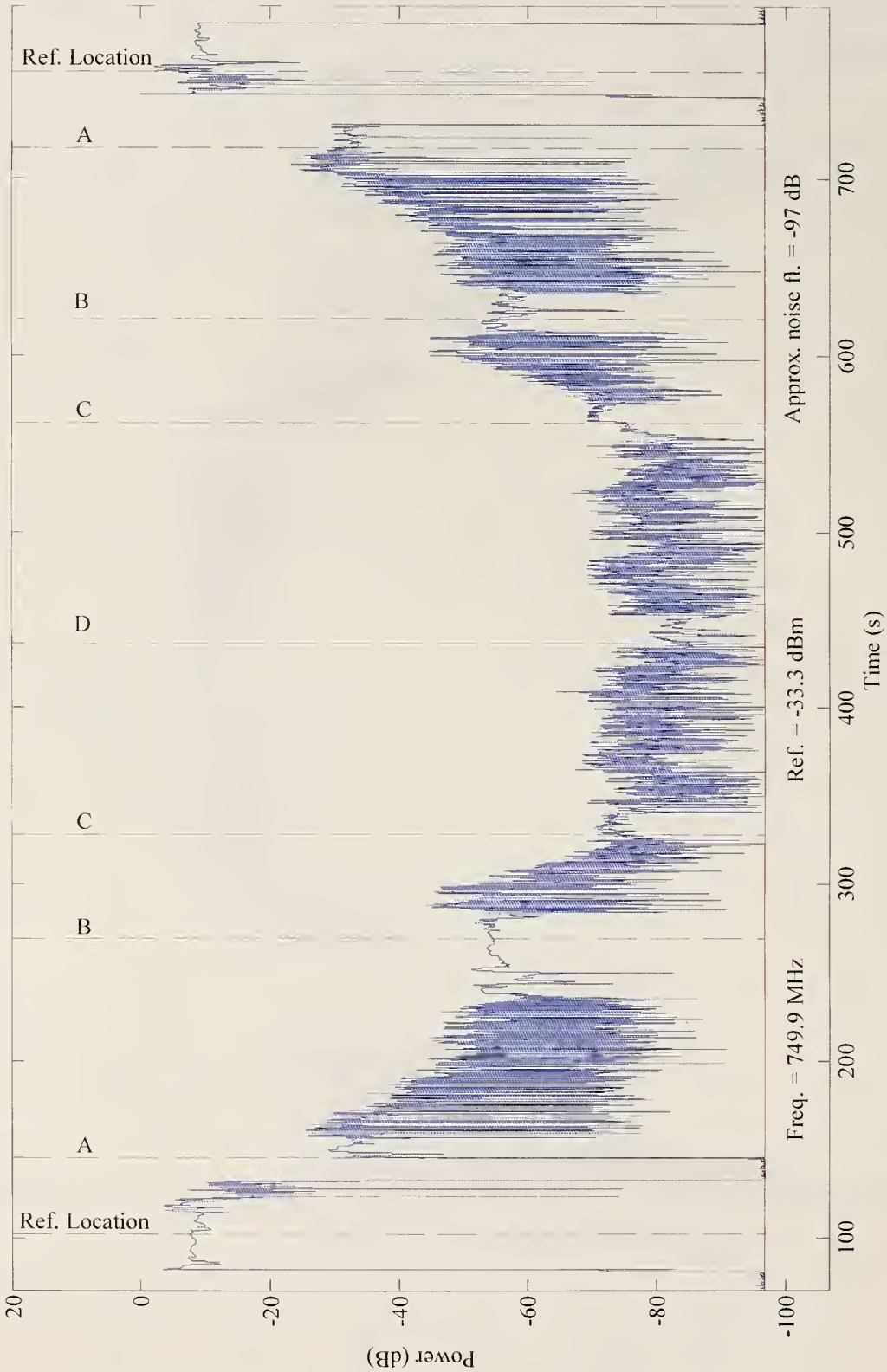

Figure 83. NIST Boulder laboratory, receive site 2. Normalized received signal power from the narrowband receiver as the 750 MHz transmitter is carried through the building. Path I, walk 2.

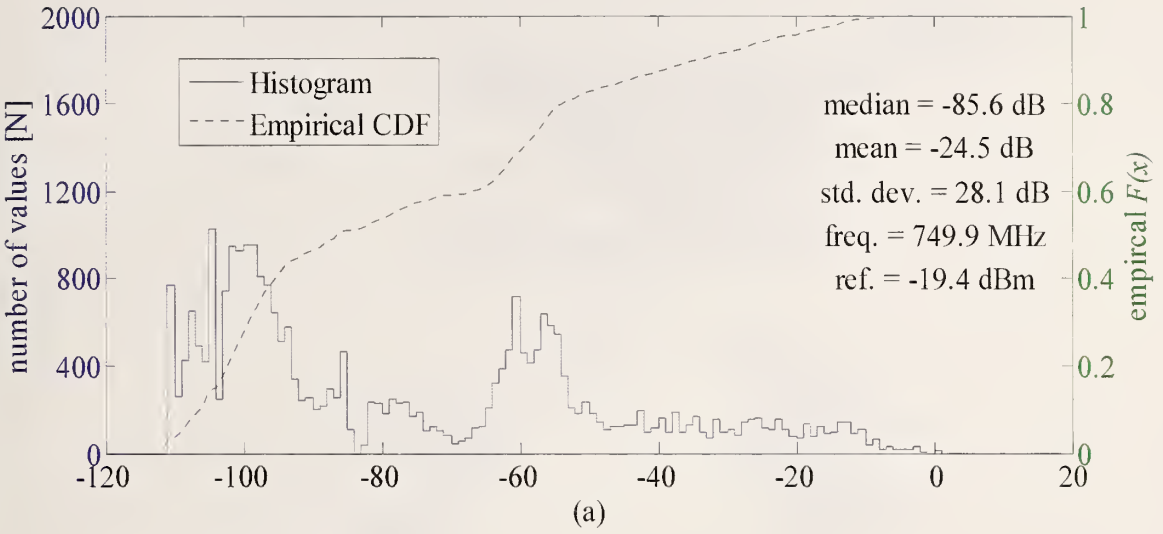

(a)

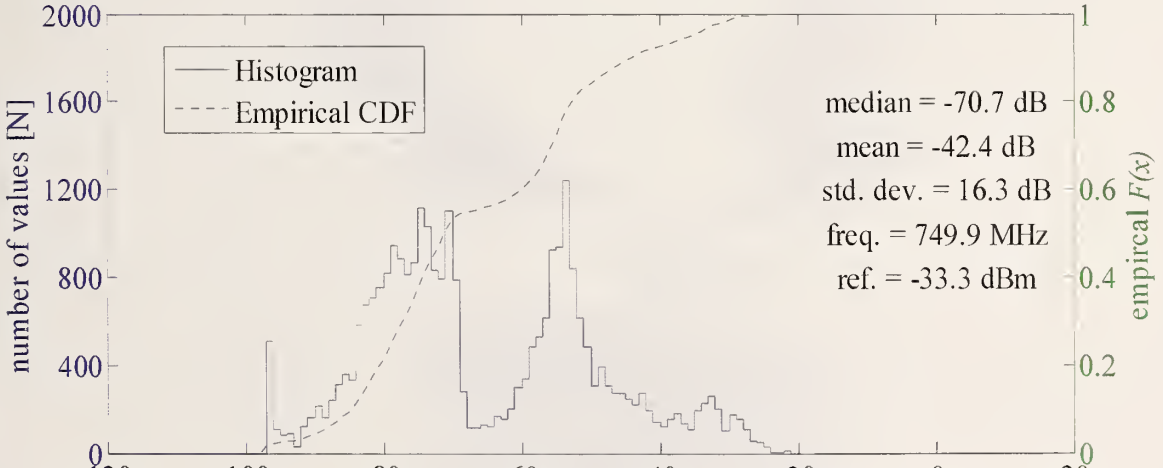

(b)

Figure 84. Histogram and empirical CDF of the narrowband receiver signal power at NIST Boulder laboratory for (a) receive site one and (b) receive site two. Path I, walk 2.

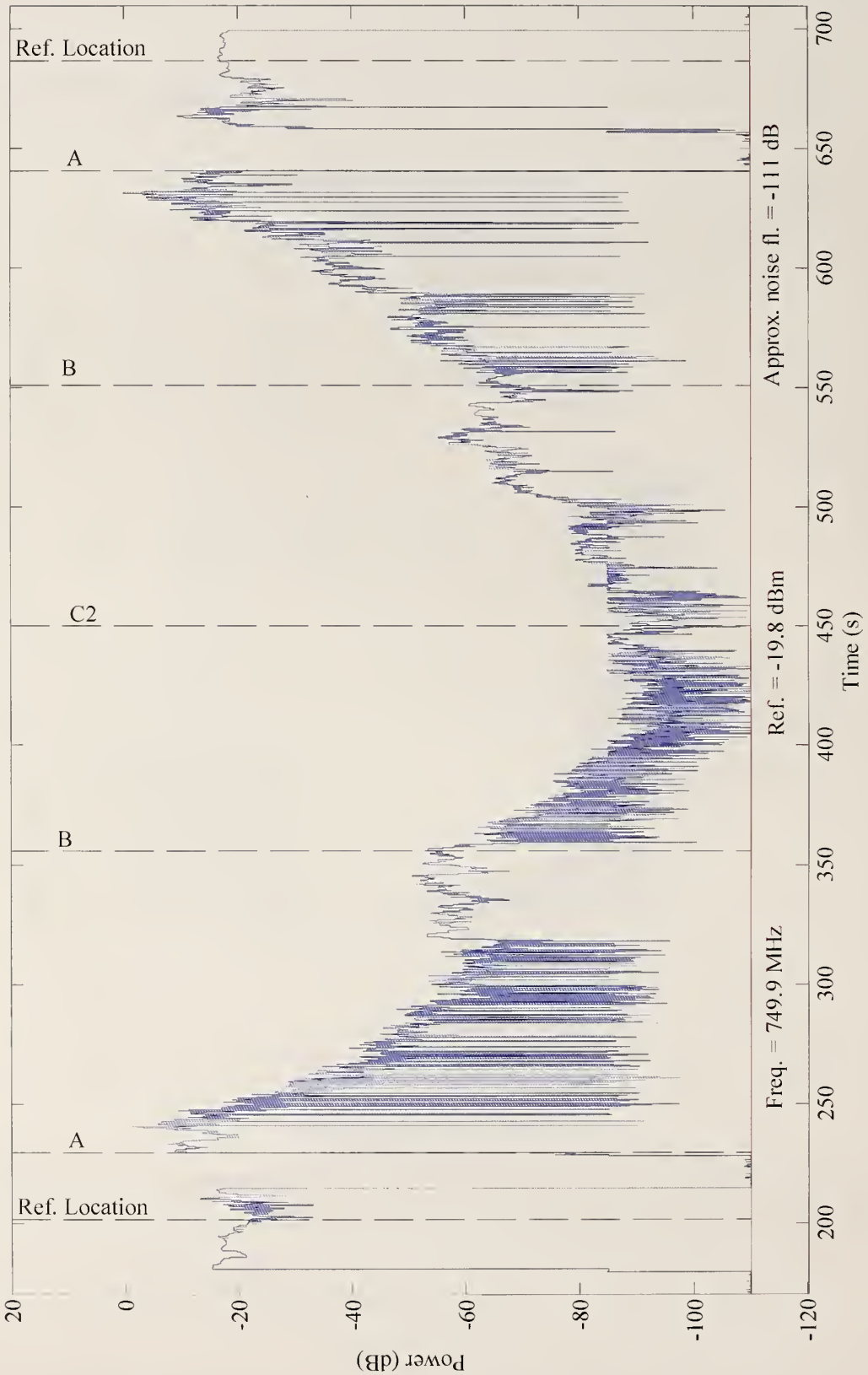

Figure 85. NIST Boulder laboratory, receive site 1. Normalized received signal power from the narrowband receiver as the 750 MHz transmitter is carried through the building. Path II, walk 1.

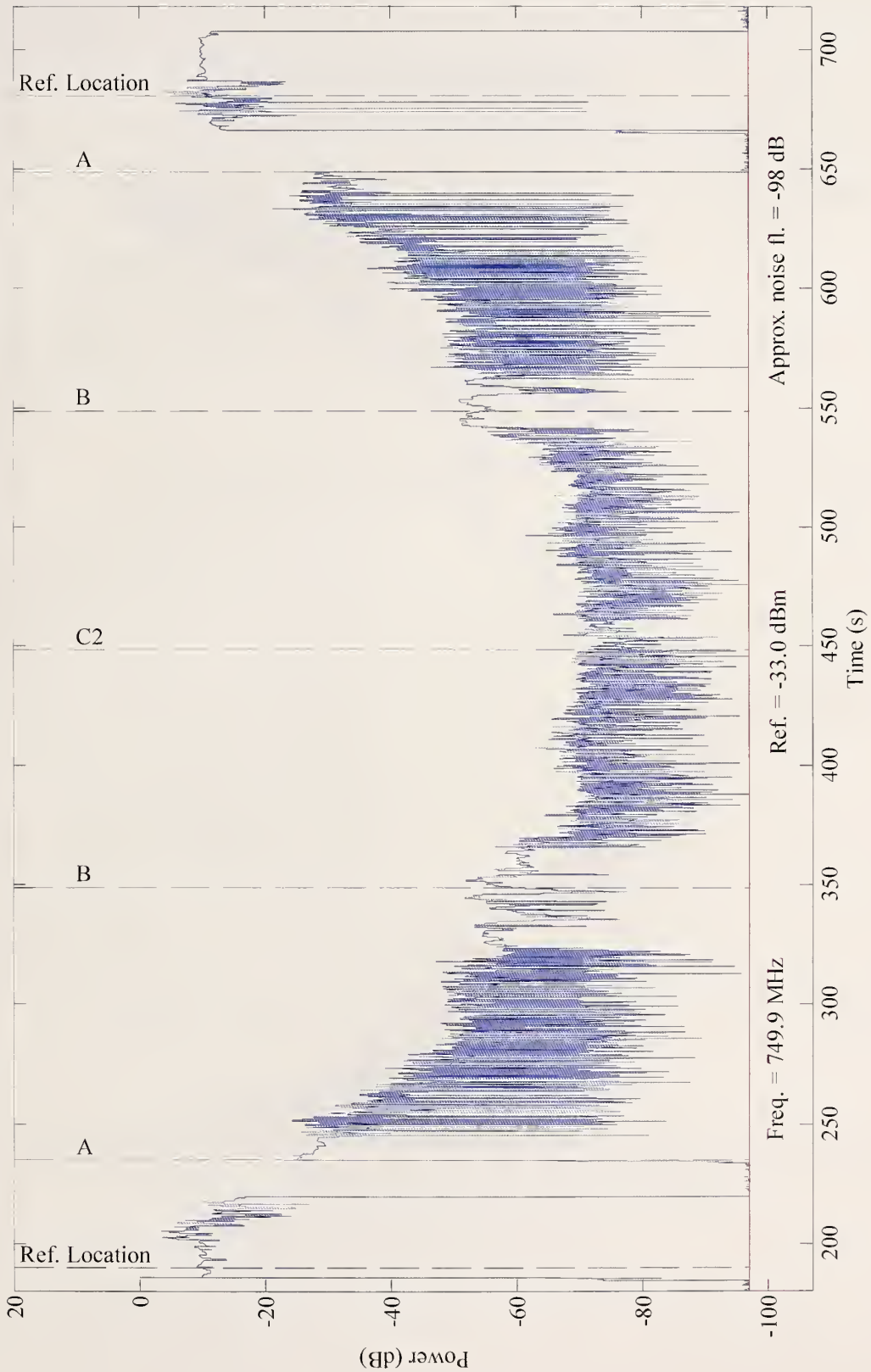

Figure 86. NIST Boulder laboratory, receive site 2. Normalized received signal power from the narrowband receiver as the 750 MHz transmitter is carried through the building. Path II, walk 1.

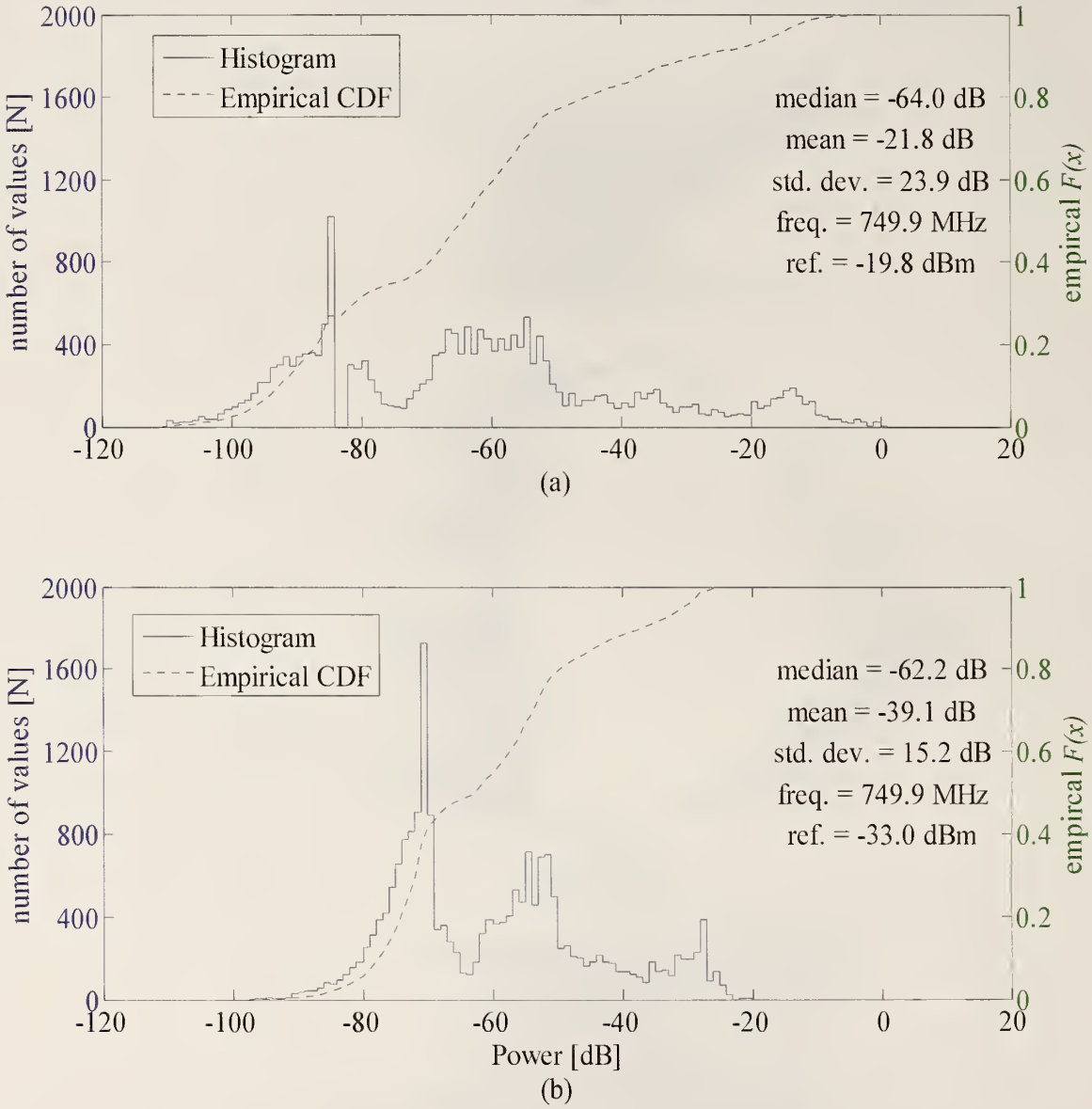

Figure 87. Histogram and empirical CDF of the narrowband receiver signal power at NIST Boulder laboratory for (a) receive site one and (b) receive site two. Path II, walk 1.

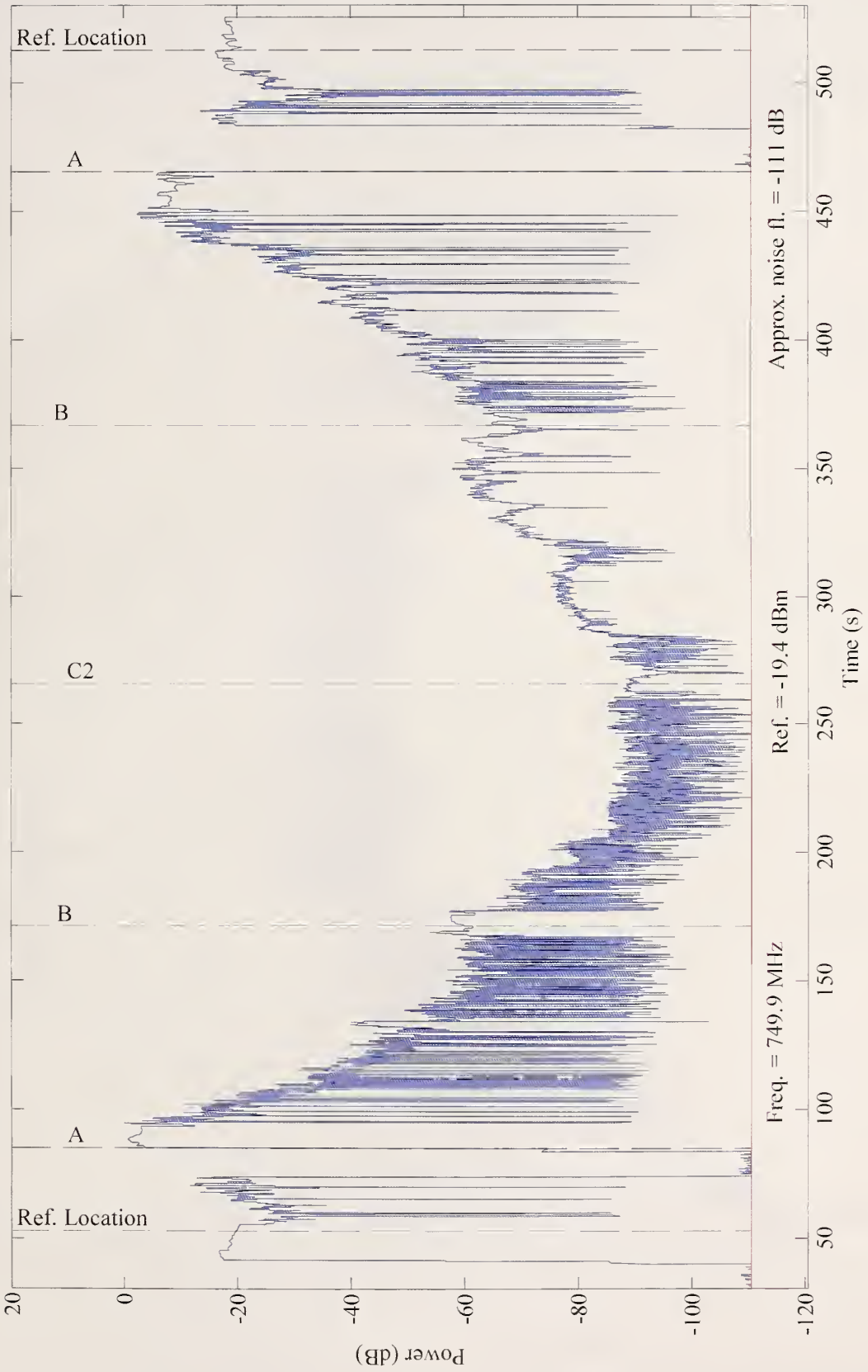

Figure 88. NIST Boulder laboratory, receive site 1. Normalized received signal power from the narrowband receiver as the 750 MHz transmitter is carried through the building. Path II, walk 2.

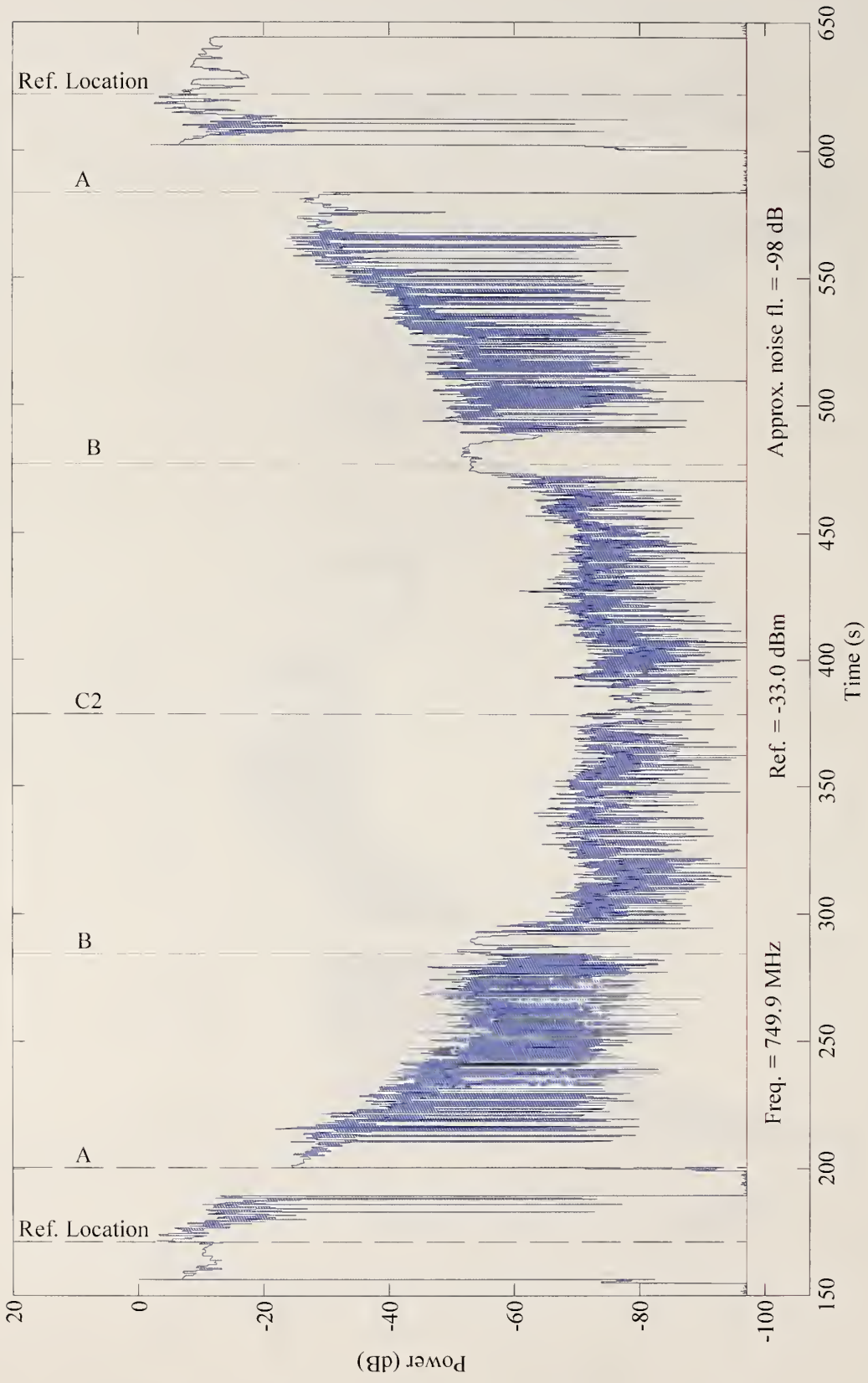

Figure 89. NIST Boulder laboratory, receive site 2. Normalized received signal power from the narrowband receiver as the 750 MHz transmitter is carried through the building. Path II, walk 2.

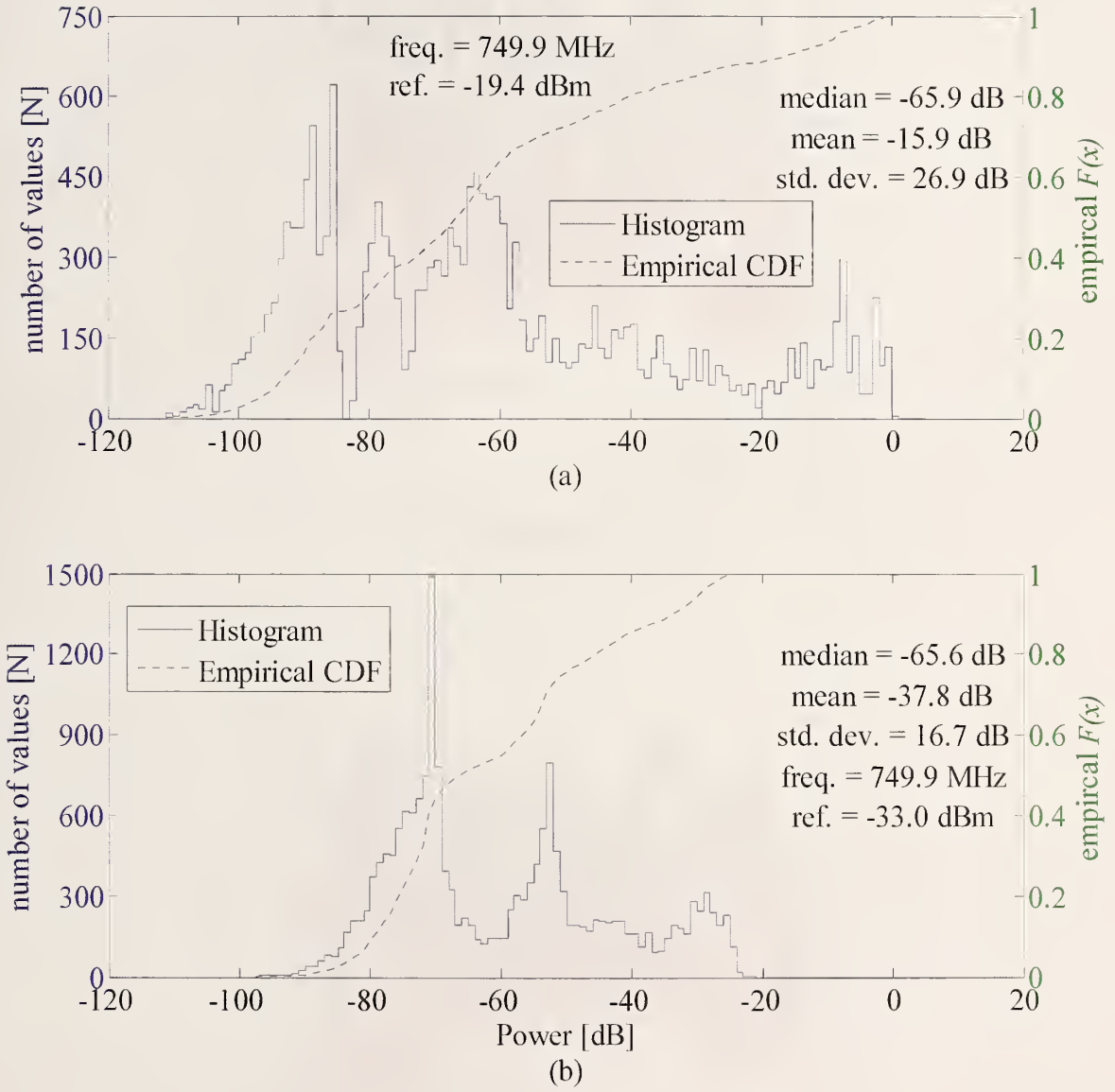

Figure 90. Histogram and empirical CDF of the narrowband receiver signal power at NIST Boulder laboratory for (a) receive site one and (b) receive site two. Path II, walk 2.

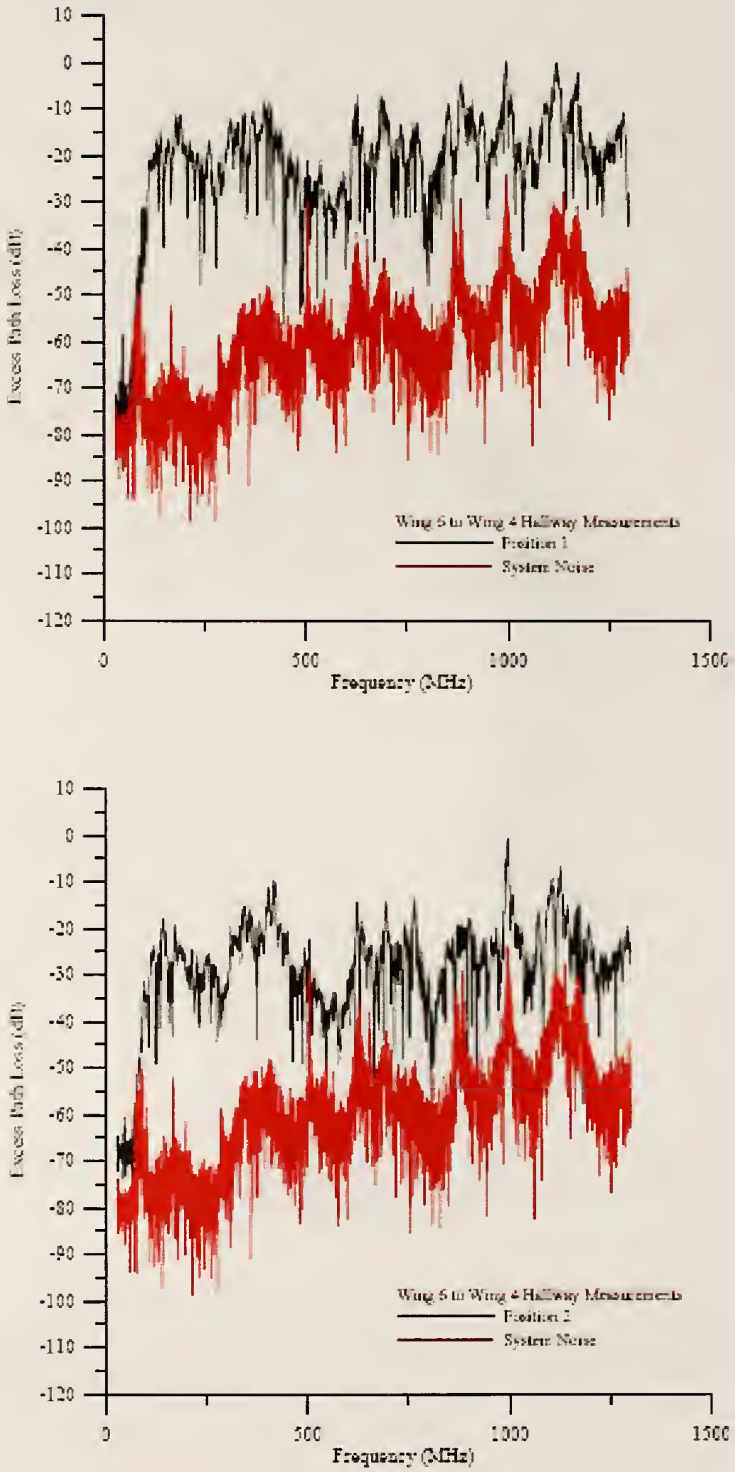

Figure 91. Excess path loss data from 25 MHz to 1.3 GHz for a path that includes building penetration obtained with data for the Wing 4 hallway. Omnidirectional antennas were used. Distance down the corridor is D = 2.40 m (top) and D = 17.65 m (bottom).

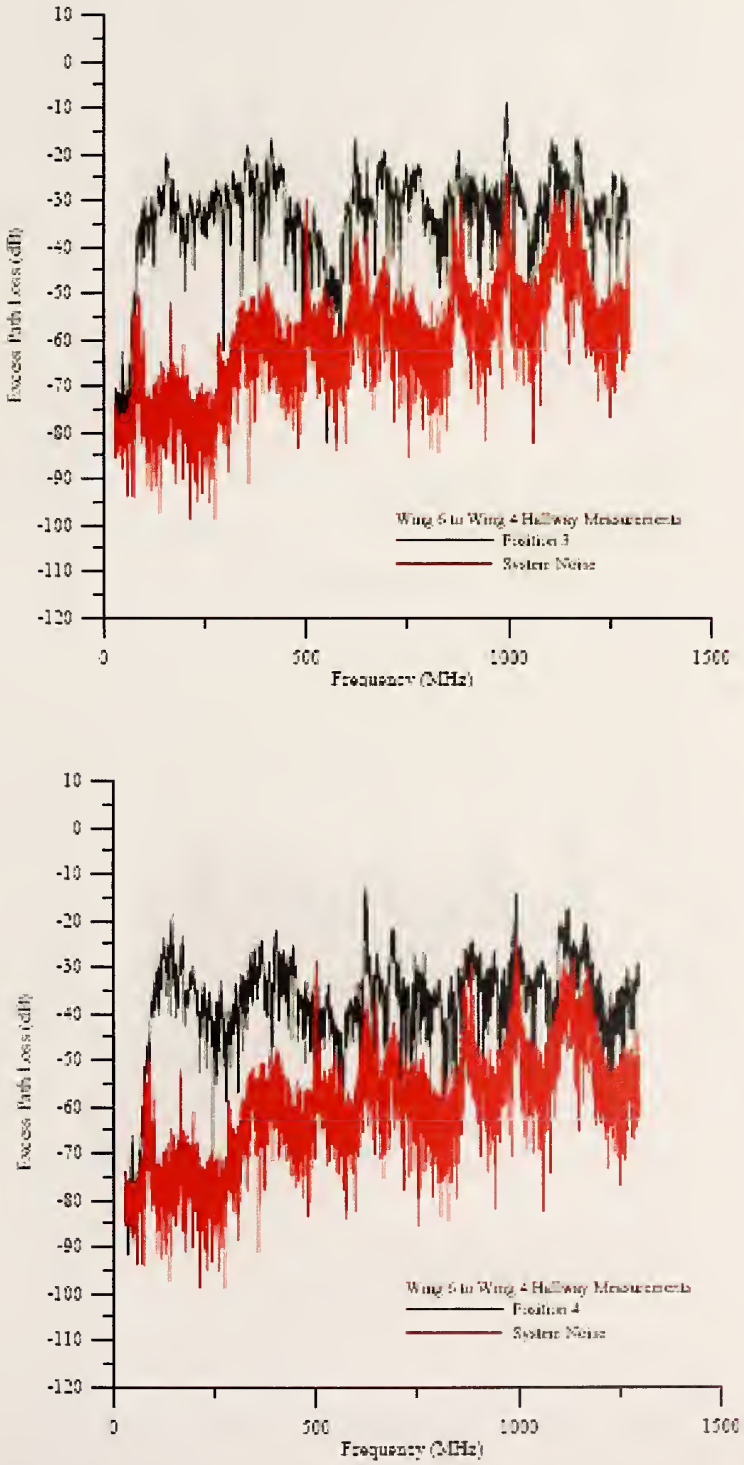

Figure 92. Excess path loss data from 25 MHz to 1.3 GHz for a path that includes building penetration obtained with data for the Wing 4 hallway. Omnidirectional antennas were used. Distance down the corridor is D = 32.90 m (top) and D = 48.15 m (bottom).

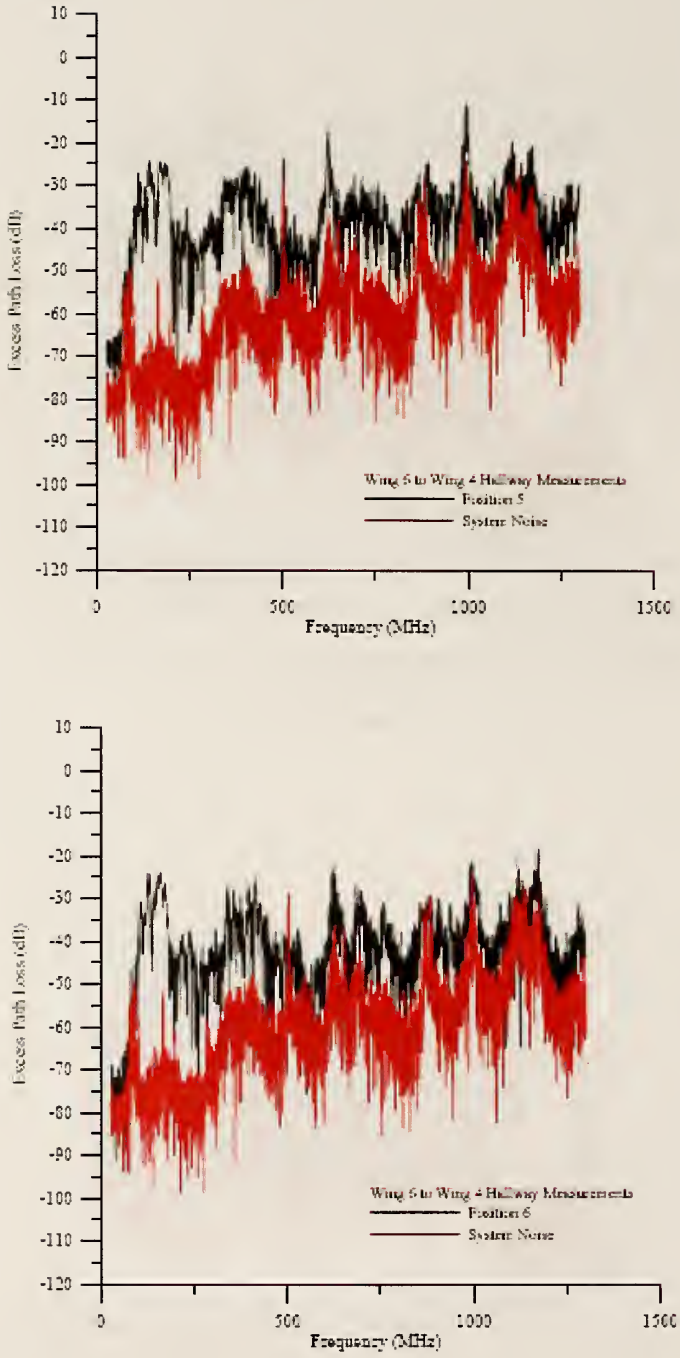

Figure 93. Excess path loss data from 25 MHz to 1.3 GHz for a path that includes building penetration obtained with data for the Wing 4 hallway. Omnidirectional antennas were used. Distance down the corridor is D = 63.40 m (top) and D = 78.65 m (bottom).

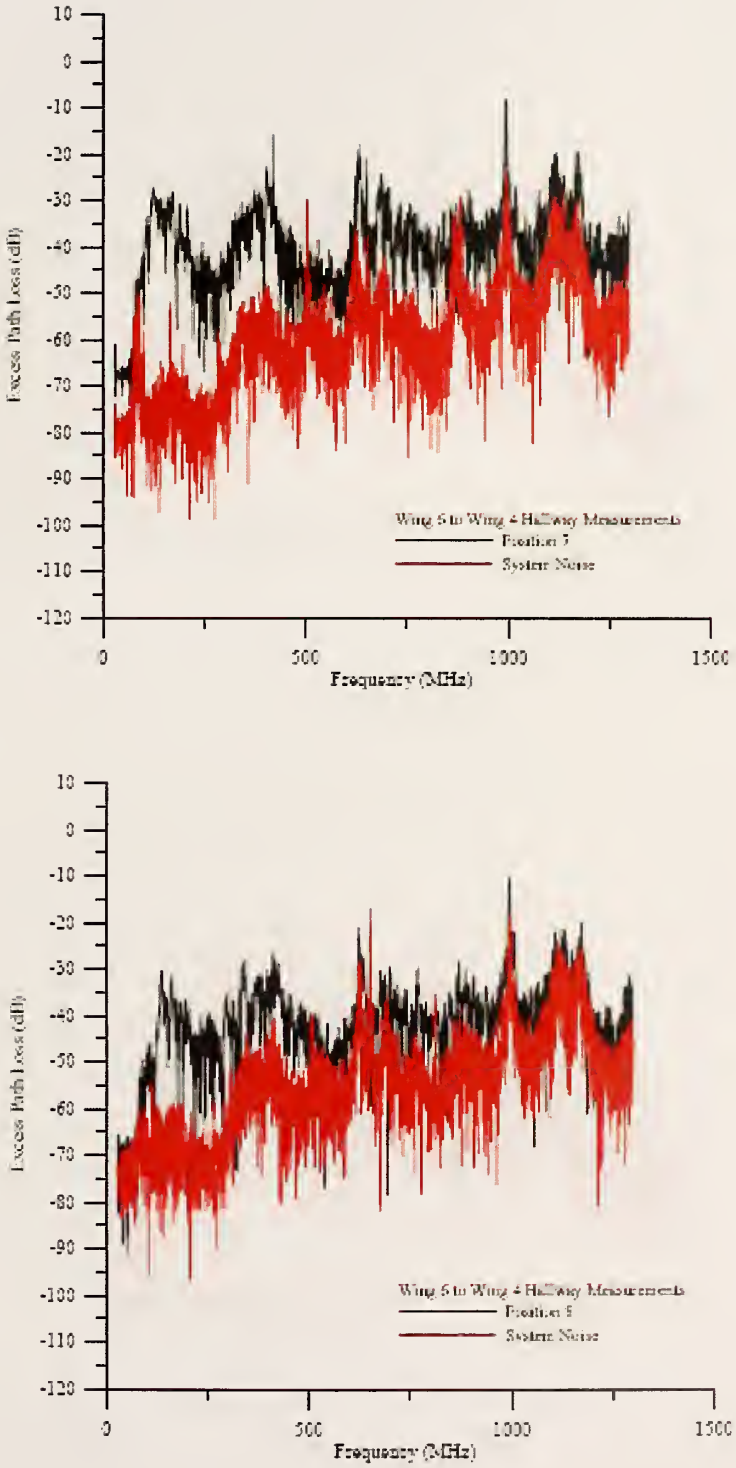

Figure 94. Excess path loss data from 25 MHz to 1.3 GHz for a path that includes building penetration obtained with data for the Wing 4 hallway. Omnidirectional antennas were used. Distance down the corridor is D = 93.90 m (top) and D = 109.15 m (bottom).

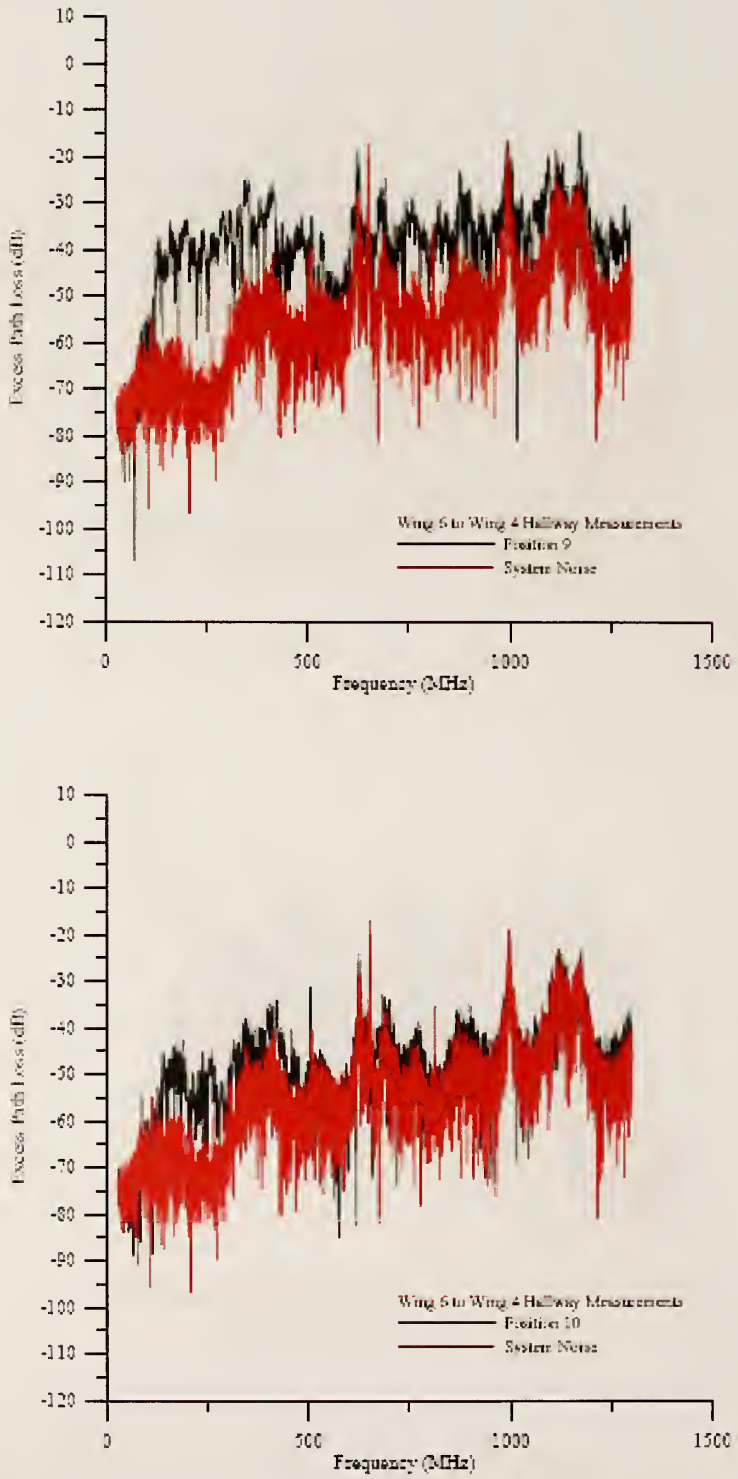

Figure 95. Excess path loss data from 25 MHz to 1.3 GHz for a path that includes building penetration obtained with data for the Wing 4 hallway. Omnidirectional antennas were used. Distance down the corridor is D = 124.4 m (top) and D = 139.65 m (bottom).

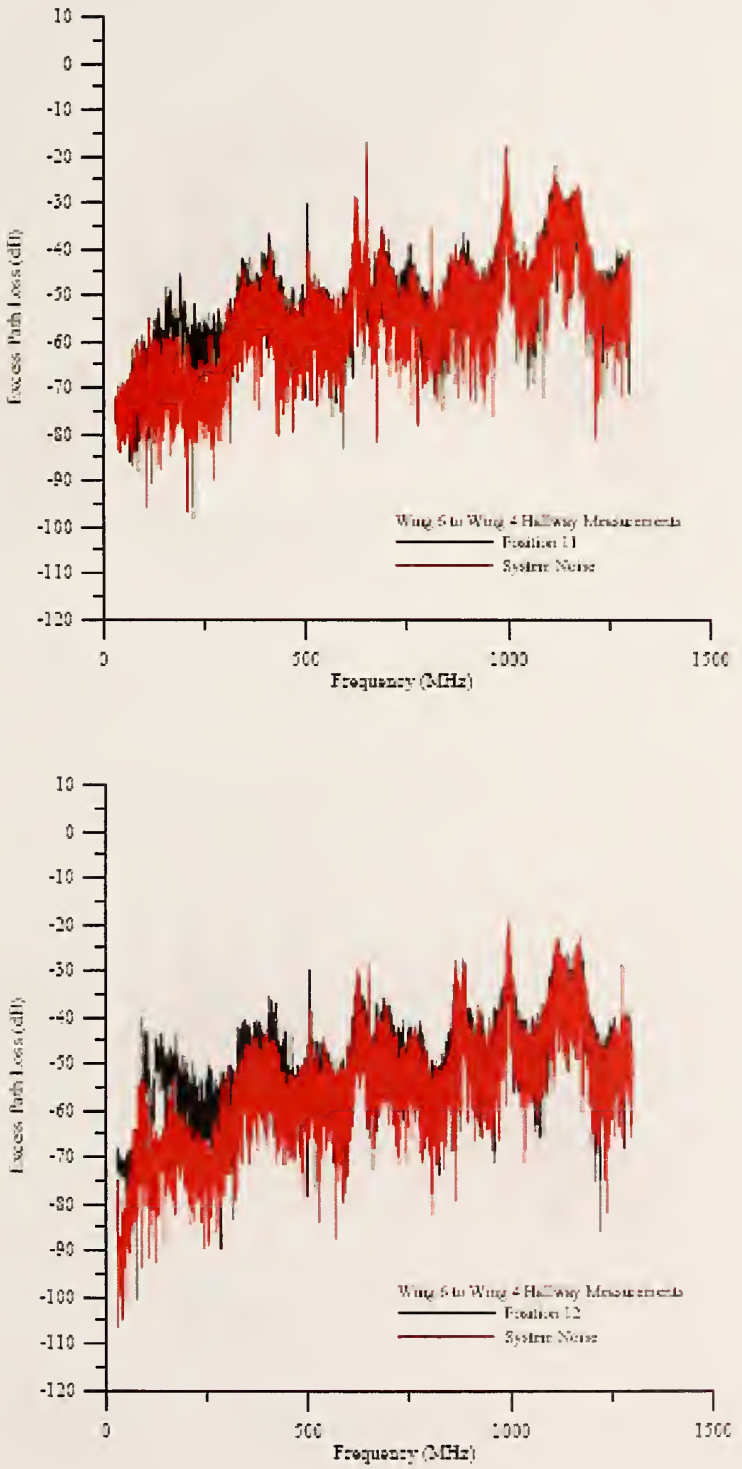

Figure 96. Excess path loss data from 25 MHz to 1.3 GHz for a path that includes building penetration obtained with data for the Wing 4 hallway. Omnidirectional antennas were used. Distance down the corridor is D = 154.9 m (top) and D = 170.15 m (bottom).

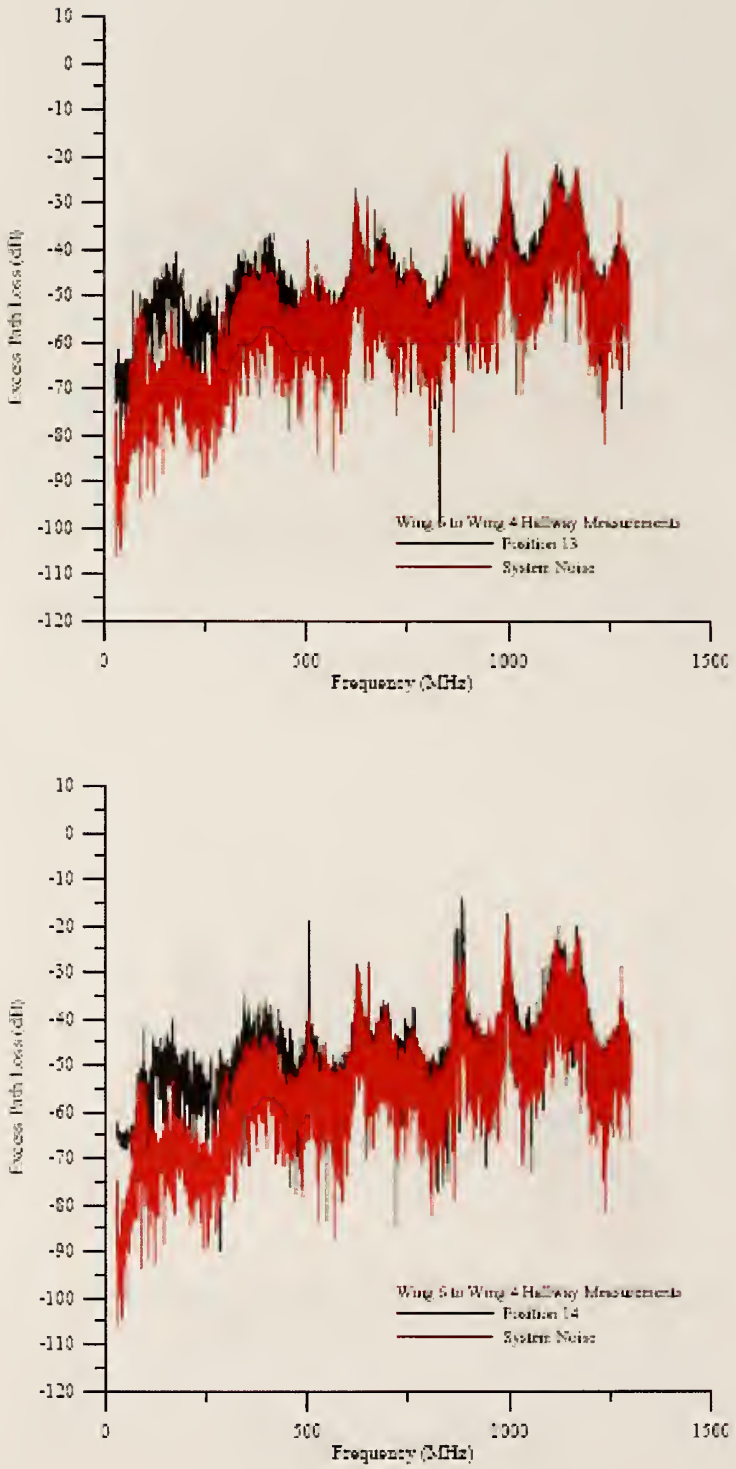

Figure 97. Excess path loss data from 25 MHz to 1.3 GHz for a path that includes building penetration obtained with data for the Wing 4 hallway. Omnidirectional antennas were used. Distance down the corridor is D = 185.40 m (top) and D = 200.65 m (bottom).

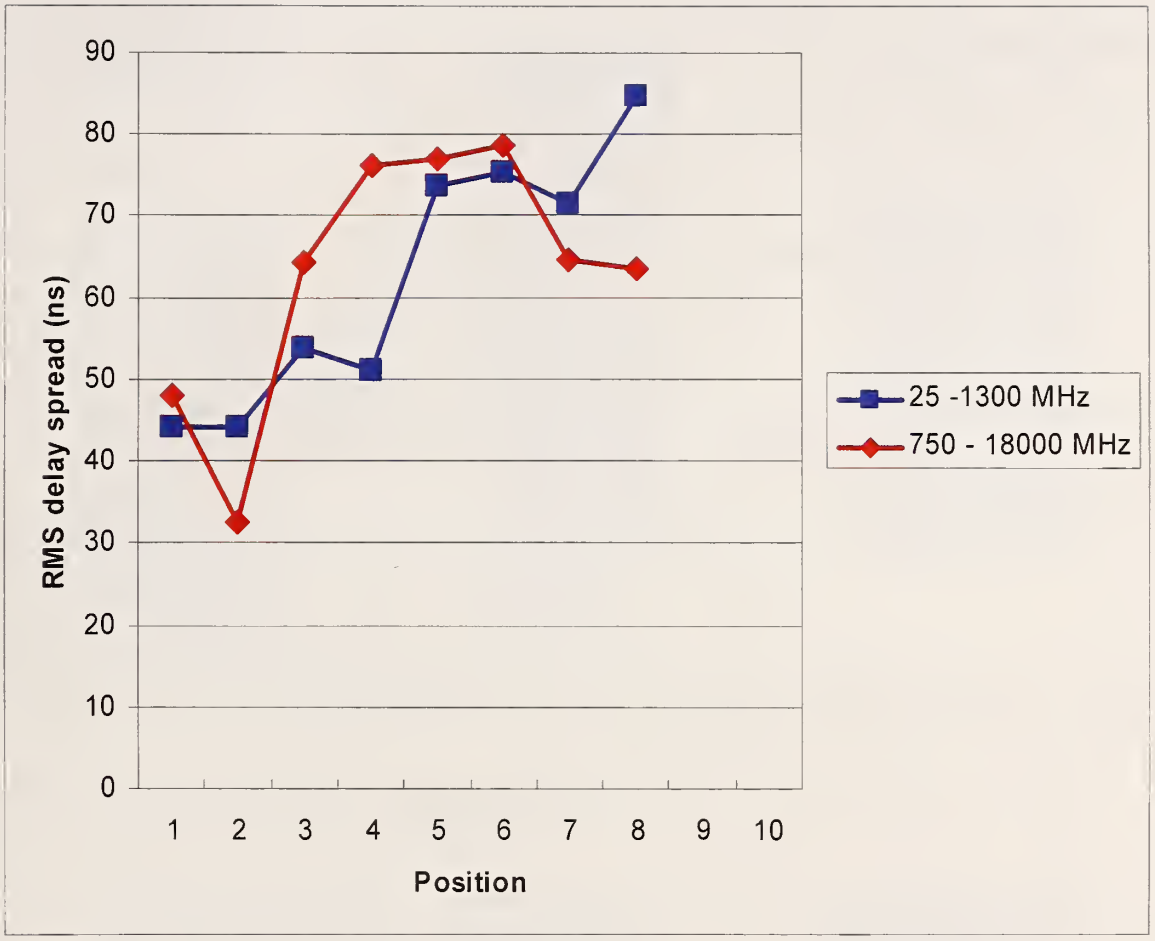

Figure 98. NIST Boulder Laboratory RMS delay spread versus position based on two different frequency bands.

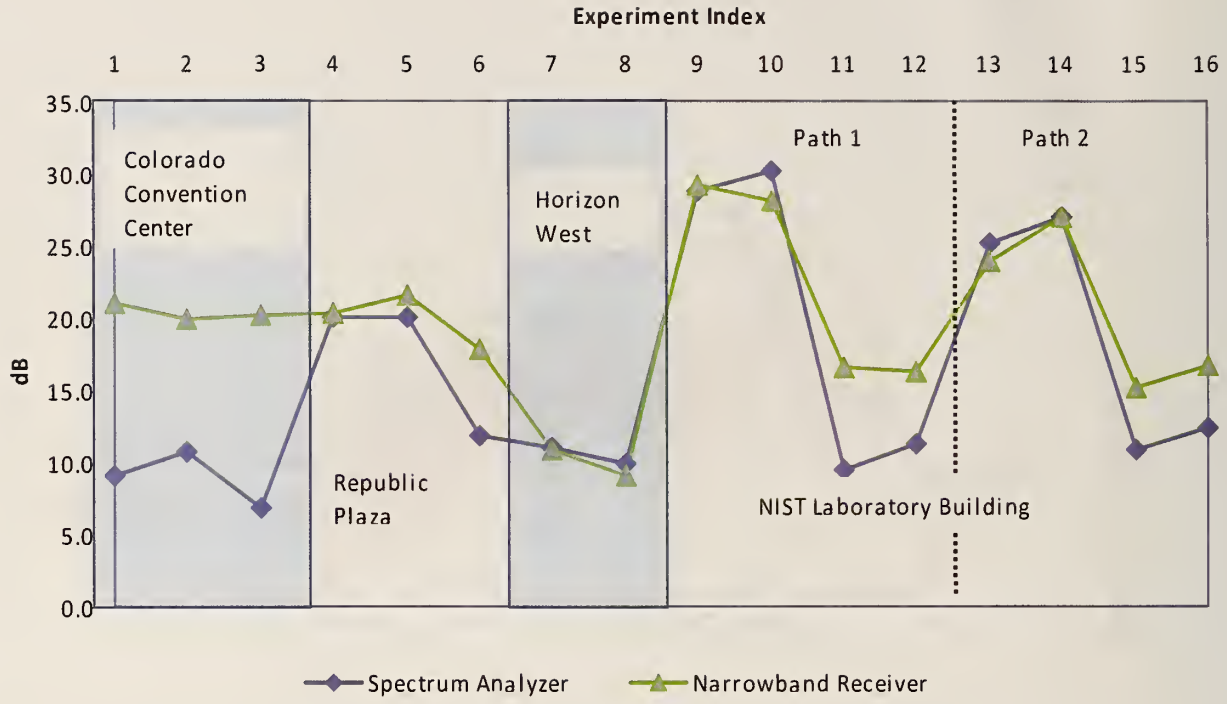

Figure 99. Comparison of the standard deviation for the normalized spectrum analyzer and narrowband receiver data across all the test locations.

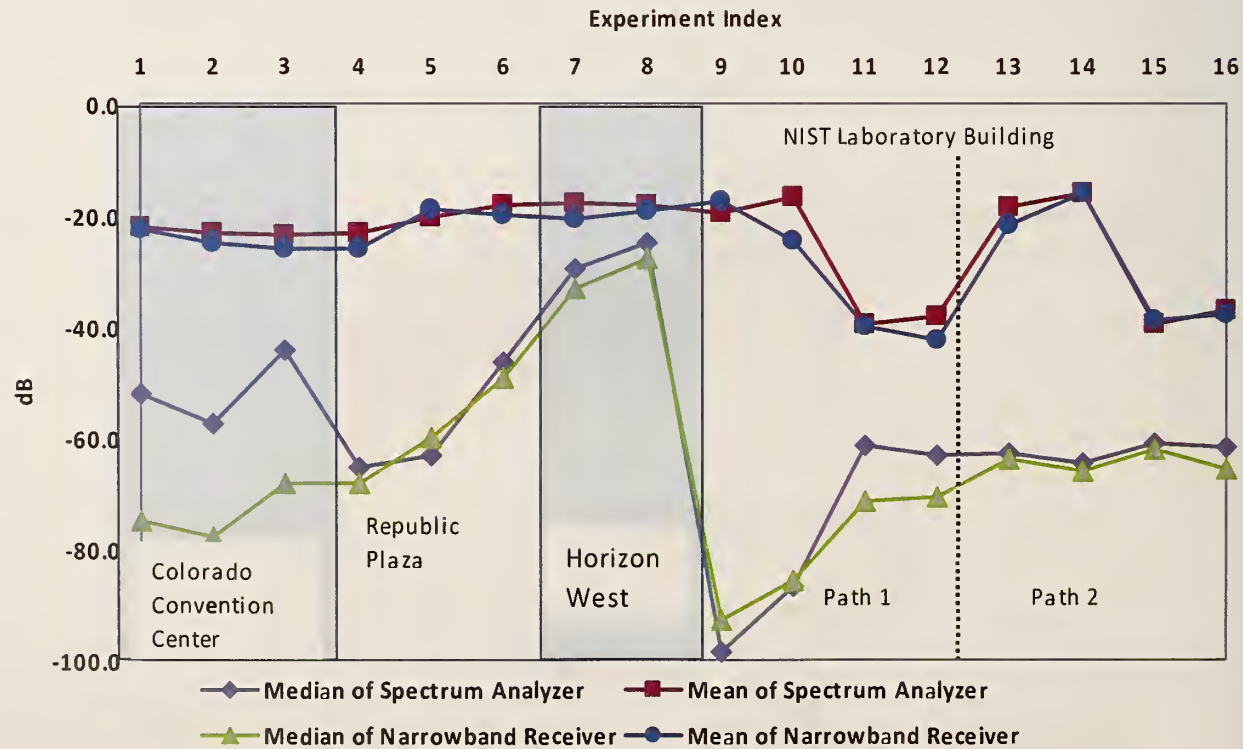

Figure 100. Comparison of median and mean values from the normalized spectrum analyzer and narrowband receiver data across all the test locations.

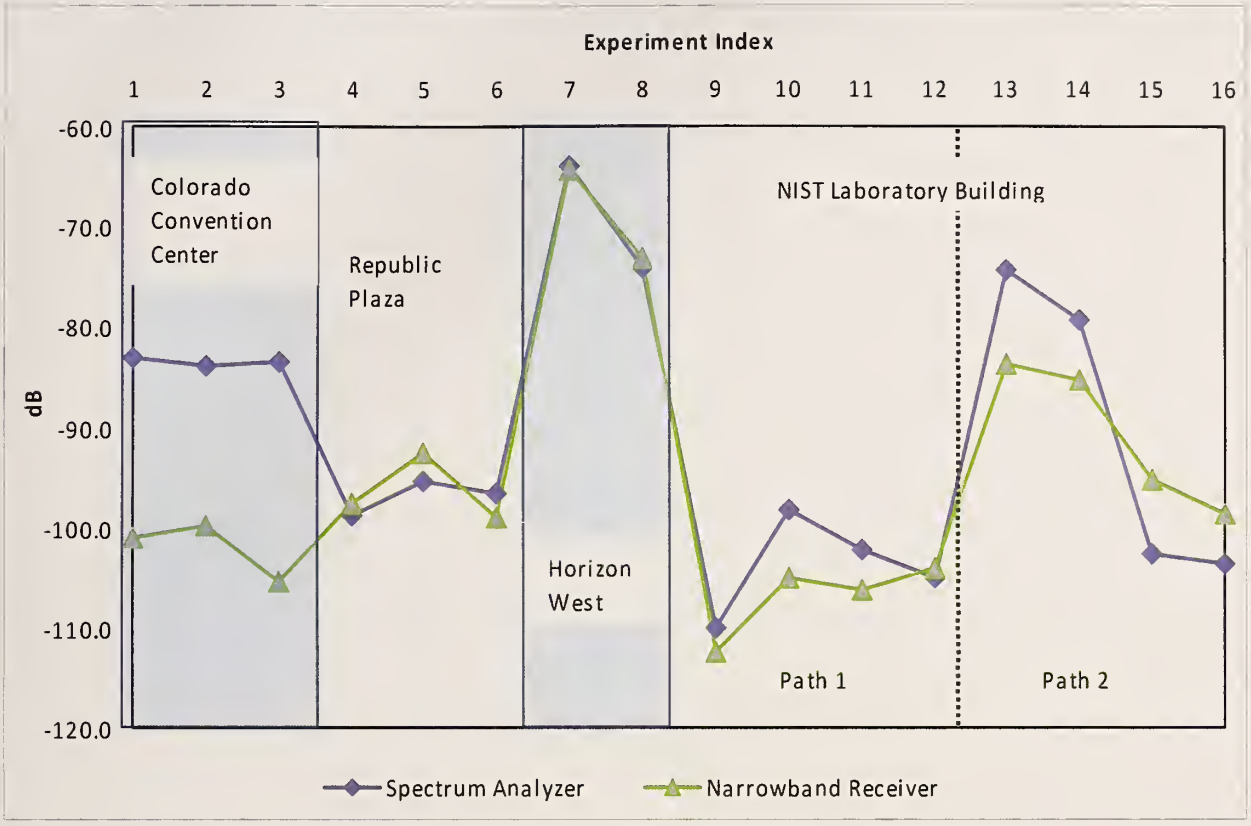

Figure 101. Comparison with the reference value added to the median values from the normalized spectrum analyzer and narrowband receiver data across all the test locations.

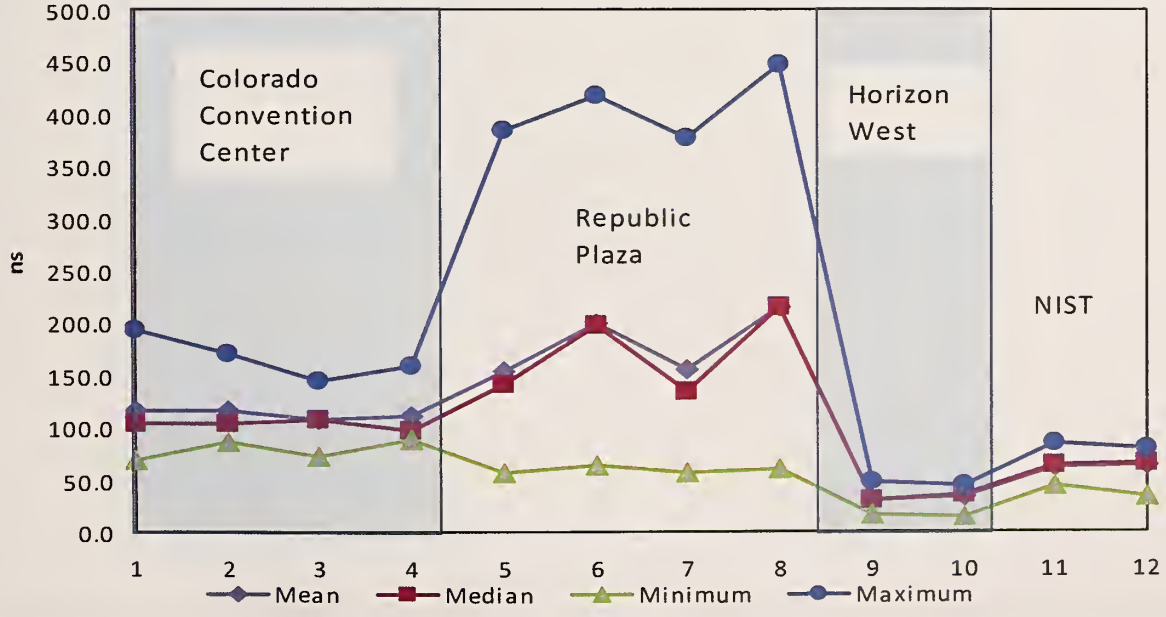

Figure 102. RMS delay spread statistics for the four buildings, indexed on the horizontal axis by the various frequency bands provided in Table 3.

GPO U.S. GOVERNMENT PRINTING OFFICE:2010 — 660-793

NIST Technical Publications

Periodical

Journal of Research of the National Institute of Standards and Technology–Reports NIST research and development in metrology and related fields of physical science, engineering, applied mathematics, statistics, biotechnology, and information technology. Papers cover a broad range of subjects, with major emphasis on measurement methodology and the basic technology underlying standardization. Also included from time to time are survey articles on topics closely related to the Institute's technical and scientific programs. Issued six times a year.

Nonperiodicals

Monographs–Major contributions to the technical literature on various subjects related to the Institute's scientific and technical activities.
Handbooks–Recommended codes of engineering and industrial practice (including safety codes) developed in cooperation with interested industries, professional organizations, and regulatory bodies.
Special Publications–Include proceedings of conferences sponsored by NIST, NIST annual reports, and other special publications appropriate to this grouping such as wall charts, pocket cards, and bibliographies.
National Standard Reference Data Series–Provides quantitative data on the physical and chemical properties of materials, compiled from the world's literature and critically evaluated. Developed under a worldwide program coordinated by NIST under the authority of the National Standard Data Act (Public Law 90-396). NOTE: The Journal of Physical and Chemical Reference Data (JPCRD) is published bimonthly for NIST by the American Institute of Physics (AIP). Subscription orders and renewals are available from AIP, P.O. Box 503284, St. Louis, MO 63150-3284.
Building Science Series–Disseminates technical information developed at the Institute on building materials, components, systems, and whole structures. The series presents research results, test methods, and performance criteria related to the structural and environmental functions and the durability and safety characteristics of building elements and systems.
Technical Notes–Studies or reports which are complete in themselves but restrictive in their treatment of a subject. Analogous to monographs but not so comprehensive in scope or definitive in treatment of the subject area. Often serve as a vehicle for final reports of work performed at NIST under the sponsorship of other government agencies.
Voluntary Product Standards–Developed under procedures published by the Department of Commerce in Part 10, Title 15, of the Code of Federal Regulations. The standards establish nationally recognized requirements for products, and provide all concerned interests with a basis for common understanding of the characteristics of the products. NIST administers this program in support of the efforts of private-sector standardizing organizations.

Order the following NIST publications–FIPS and NISTIRs–from the National Technical Information Service, Springfield, VA 22161.

Federal Information Processing Standards Publications (FIPS PUB)–Publications in this series collectively constitute the Federal Information Processing Standards Register. The Register serves as the official source of information in the Federal Government regarding standards issued by NIST pursuant to the Federal Property and Administrative Services Act of 1949 as amended, Public Law 89-306 (79 Stat. 1127), and as implemented by Executive Order 11717 (38 FR 12315, dated May 11,1973) and Part 6 of Title 15 CFR (Code of Federal Regulations).
NIST Interagency or Internal Reports (NISTIR)–The series includes interim or final reports on work performed by NIST for outside sponsors (both government and nongovernment). In general, initial distribution is handled by the sponsor; public distribution is handled by sales through the National Technical Information Service, Springfield, VA 22161, in hard copy, electronic media, or microfiche form. NISTIR's may also report results of NIST projects of transitory or limited interest, including those that will be published subsequently in more comprehensive form.

U.S. Department of Commerce
National Institute of Standards and Technology
325 Broadway
Boulder, CO 80305-3337